

Design and Development of an Anti-fouling Urinary Catheter

Utilizing Active Surface Deformation

by

Vrad Levering

Department of Biomedical Engineering
Duke University

Date: _____

Approved:

Gabriel P. López, Supervisor

Xuanhe Zhao

Bruce Klitzman

Howard Levinson

William Monty Reichert

Dissertation submitted in partial fulfillment of
the requirements for the degree of Doctor
of Philosophy in the Department of
Biomedical Engineering in the Graduate School
of Duke University

2015

ABSTRACT

Design and Development of an Anti-fouling Urinary Catheter

Utilizing Active Surface Deformation

by

Vrad Levering

Department of Biomedical Engineering
Duke University

Date: _____

Approved:

Gabriel P. López, Supervisor

Xuanhe Zhao

Bruce Klitzman

Howard Levinson

William Monty Reichert

An abstract of a dissertation submitted in partial
fulfillment of the requirements for the degree
of Doctor of Philosophy in the Department of
Biomedical Engineering in the Graduate School of
Duke University

2015

Copyright by
Vrad Wilson Levering
2015

Abstract

There are over 30 million Foley urinary catheters used annually in the USA, and the greatest problem with Foley catheters is catheter-associated urinary tract infections (CAUTIs). CAUTIs are the number one cause of hospital-acquired infections and make up to 40% of nosocomial infections. Biofilms on urinary catheters are critical to the progression of symptomatic CAUTIs, but are difficult to treat due to the protective effect of the biofilm matrix against antibiotics. The anti-fouling catheter technology proposed and demonstrated herein uses a mechanical, non-antibiotic approach to physically remove biofilms and thereby provide an appealing option for potentially stopping the progression of symptomatic infections. Additionally, because the anti-fouling technology is mechanical, it can circumvent the persistent failings of chemical and biological approaches that have failed to address catheter-associated urinary tract infections for the last 50+ years since Foley catheters were introduced.

We designed and optimized urinary catheter prototypes capable of on-demand removal of biofilms from the previously-inaccessible main drainage lumen of catheters. The concept uses pressure-actuated chambers in elastomer constructs to generate regio-selective strain and thereby remove biofilms. We first grew mature *Proteus mirabilis* crystalline biofilms on flat silicone elastomer substrates, and showed that application of strain to the substrate debonded the biofilm, and that increasing the strain rate increased

biofilm detachment. A quantitative relationship between the applied strain rate and biofilm debonding was found through an analysis of the biofilm segment length and the calculated driving force for debonding. We then constructed proof-of-concept prototypes of sections of anti-fouling catheter shafts using silicone and 3D printed reverse molding in methods akin to those used for soft robotics. The proof-of-concept prototypes demonstrated release of mature *P. mirabilis* crystalline biofilms from their strained surfaces, and prompted our development of more advanced multi-lumen prototypes. The multi-lumen prototypes were designed and optimized using successive rounds of finite element modeling to adjust the number and position of intra-wall inflation lumens. We then constructed prototypes based on the optimized design with clinically relevant dimensions and showed they were able to generate greater than 30% strain on the majority of the luminal surface, and along their full length. Those catheter prototypes were able to on-demand, and repeatedly, remove greater than 80% of a mixed community biofilm of *P. mirabilis* and *E. coli*. In summary, this study shows (1) strain in the elastomeric substrate actively debonds crystalline biofilms *in vitro* (2) modeling based on characterization of biofilm properties and understanding of substrate strain informs and facilitates prototype catheter design (3) urinary catheter prototypes utilizing inflation-induced substrate strain are capable of on-demand and repeatedly removing biofilms *in vitro*.

Dedication

I would like to dedicate this to my family. They have supported me through thick and thin, and words can never properly express my appreciation of their support and love. My mother and father, Jean and Joe Levering, have been there to listen to me and to support me through every stage of graduate school. My brother, Craig Levering, has kept me grounded and on track and has been my biggest cheerleader. My niece, Eva, and my nephew, Theo, are adorable sources of inspiration for working to benefit future generations.

Contents

Abstract	iv
List of Tables	xi
List of Figures	xii
Acknowledgements	xxii
1. Chapter 1: Background, significance, and specific aims.....	1
1.1 Background and significance	1
1.2 Unmet clinical need for infection control in urinary catheters	3
1.3 Unmet clinical need for biofilm control in urinary catheters.....	4
1.4 Urinary catheter background and pathogenesis.....	5
1.5 Healthy functioning bladder.....	7
1.6 Biofilm development in urinary catheters	8
1.7 Crystalline biofilm development.....	9
1.8 Current approaches on the market and their challenges.....	10
1.9 Urinary catheter regulatory documents.....	11
1.10 Recent approaches in biofilm control research and their challenges.....	11
1.11 Implications of biofilm removal	15
1.12 Innovation – Surface deformation to trigger biofilm debonding	15
1.13 Specific Aims.....	19
1.13.1 Specific Aim 1: <i>In vitro</i> active debonding of mature <i>Proteus mirabilis</i> crystalline biofilm on silicone substrates	19
Specific Aim 1 Hypotheses addressed:.....	20

1.13.2 Specific Aim 2: Urinary tract biofilm property characterization and urinary catheter inflation modeling for prototype design.....	20
Specific Aim 2 Hypotheses addressed:	21
1.13.3 Specific Aim 3: <i>In vitro</i> confirmation of a urinary catheter prototype for removing biofilm.	21
Specific Aim 3 Hypotheses addressed:	22
1.14 Organization of the dissertation.....	23
2. Chapter 2: Crystalline biofilm debonding and an on-demand fouling-release urinary catheter	24
2.1 Chapter synopsis	24
2.2 Chapter introduction	25
2.3 Methods and Materials	29
2.3.1 Bacteria strain and culture media	29
2.3.2 Preparation of silicone coupons:	30
2.3.3 Preparation of proof-of-concept prototypes.....	31
2.3.4 Biofilm growth.....	32
2.3.5 Strain and inflation testing.....	35
2.3.6 Rheology tests of biofilms and substrates.....	36
2.4 Results	37
2.4.1 Concept for urinary catheter with active fouling-release	37
2.4.2 Uniaxial strain debonds mature <i>P. mirabilis</i> crystalline biofilms	40
2.4.3 High strain and strain rate result in debonding of mature <i>P. mirabilis</i> crystalline biofilms.....	44

2.4.4 Development of a proof-of-concept prototype urinary catheter incorporating substrate deformation via intra-wall inflation	51
2.4.5 Proof-of-concept prototypes utilizing intra-wall inflation debond mature <i>P. mirabilis</i> biofilm	58
2.5. Chapter conclusions	62
2.6 Chapter acknowledgements	63
3. Chapter 3: Optimization of a design for a urinary catheter capable of repeated on-demand removal of infectious biofilms via active deformation	64
3.1 Chapter synopsis	64
3.2 Chapter introduction	65
3.3 Methods and Materials	70
3.3.1 Finite element modeling	70
3.3.2 Preparation of prototypes	72
3.3.3 Bacteria strain and culture media	74
3.3.4 Biofilm growth in catheter prototypes	74
3.3.5 Actuation testing	77
3.3.6 Preparation of flat silicone coupons:	79
3.3.7 Biofilm growth on flat silicone coupons:	79
3.3.7 Rheology of biofilms and substrates:	79
3.3.8 Adhesion testing of biofilms:	80
3.3.9 Statistical analysis	82
3.4 Results	82
3.4.1 Concept for urinary catheter with active fouling-release	82

3.4.2 Catheter fabrication.....	89
3.4.3 Biofilm debonding.....	95
3.4.4 Repeated biofilm debonding	99
3.4.5 Compressive strain of the substrate to debond biofilms	103
3.5 Chapter conclusions.....	105
3.6 Chapter acknowledgements	107
4. Chapter 4: Anti-fouling urinary catheters: Conclusions and Future Directions.....	108
4.1 Summary.....	108
4.2 Future directions.....	109
4.2.1 Coulter Translational Project Partnership	110
4.2.1.1 Coulter project summary	110
4.3 Conclusions and implications of this research.....	114
Appendix A.....	117
References	118
Biography	129

List of Tables

Table 1: Hydraulic inflation profile for proof-of-concept prototypes of urinary catheter sections.	58
---	----

List of Figures

Figure 1: Cross section of urinary catheter occluded by crystalline biofilm. Adapted from Stickler 1999 [14].....	4
Figure 2: Diagram of a bladder with a typical indwelling urinary catheter from Siddiq 2012 [7]. a) An eyelet allows drainage of urine from bladder. The reservoir balloon is filled with saline to secure catheter. b) Cross-section of commonly used double-lumen indwelling urinary catheter. c) Preconnected junction of indwelling catheter and drainage system. d) Port used to inflate the reservoir balloon with saline. e) Sampling port. f) Collection bag. g) Urine emptied via outlet valve.....	6
Figure 3: Typical progression of biofilm development within urinary catheters. 1) The catheter is coated with proteins and crystals. 2) Organisms are introduced. 3) Bacteria attach and begin to colonize. 4) Cell wall adhesion and proliferation. 5) Biofilm maturation. 6) At sufficient densities bacteria spontaneously detach to aid in dispersal for new colonies.	9
Figure 4: Commercial attempt at ultrasonic biofilm removal from NanoVibronix. Image from www.nanovibronix.com/uuroshield	13
Figure 5: Micropatterned surface commercially known as "Sharklet" used to delay biofilm formation [59].....	14
Figure 6: Diagram of how pneumatic inflation deforms a specified surface and increases strain. Adapted from Shivapooja 2013 [68].	16
Figure 7: Conventional catheter outcome. A conventional catheter eventually forms a biofilm, which promotes colonization and eventual symptomatic catheter-associated urinary tract infection.....	17
Figure 8: Side views of a conventional catheter and a proposed anti-fouling urinary catheter highlight the additional hub port for syringe actuation. The anti-fouling urinary catheter uses an additional hub port to provide access to inflate and deflate intra-wall inflation lumens.	17
Figure 9: Anti-fouling urinary catheter conceptual schematic. Upon insertion, the catheter appears like the top left panel and is free of biofilm. Biofilm gradually forms on the surface of the main urine drainage lumen. Actuation via inflation applies strain to the surface of the urine drainage lumen, thereby debonding the overlying biofilm. The	

debonded biofilm is then free-floating in the urine and is rinse out, thereby returning the catheter to its original state (free of biofilm) and thereby potentially reducing the risk of infection. 18

Figure 10: Growth and characterization of mature *P. mirabilis* crystalline biofilms on flat silicone substrates. (a) Schematic of the flow system. The silicone samples were submerged in (b) the modified drip flow reactor [80] and inoculated with a 4 hour culture of *P. mirabilis*. After allowing the bacteria to adhere for 1 hour, artificial urine with 1% tryptic soy broth was pumped at 0.5 mL min^{-1} through the drip flow reactor and over the flat silicone samples. The reactor was maintained at 37°C by mini-incubator. A mature crystalline biofilm grew over approximately 42 hours. (c) SEM of the resultant planar biofilm shows large crystals and microcrystal aggregates typical of mature *P. mirabilis* biofilms observed in catheters removed from infected patients.[39] 30

Figure 11: Construction of an active fouling release, proof-of-concept prototype of a section of silicone urinary catheter. (a) 3D printed mold patterns were generated using Solidworks 2011 and then printed on a Dimension sst 1200es 3D printer. Silicone (Dragon Skin 0020 or Ecoflex 0050) was poured into the mold and (b) resultant silicone prototypes were removed from the mold upon curing. "U" denotes the main urine drainage lumen, "I" denotes the inflation lumen, "i.w." denotes the inflation wall, and "e.w" denotes the external wall. The inflation lumen was sealed at the ends of the prototypes before experimentation. When using Dragon Skin 0020 silicone, the ratio of external wall to inflation wall thicknesses shown (approximately 3:1) was sufficient to direct inflation inwards. When using Ecoflex 0050 silicone, prototypes required an additional inelastic sheath to prevent bulging of the external wall. Ecoflex 0050 was chosen for *in vitro* biofilm testing due to its superior pour performance and consistently successful molding. Scale bar represents 1 cm. 31

Figure 12: Biofilm growth and testing setup for urinary catheter proof-of-concept prototypes. (a) Schematic of biofilm growth system that uses an "artificial bladder" [14] to supply infected urine to the proof-of-concept prototypes. The artificial bladder is a vessel modified with a glass tube penetrating the bottom and extending approximately 4 cm into the vessel, which thereby maintains a residual volume of 30 mL in the artificial bladder. The artificial bladder and prototypes were inoculated with a 4 hour culture of *P. mirabilis*. After allowing the bacteria to adhere for 1 hour, artificial urine with 1% tryptic soy broth was pumped at 0.5 mL min^{-1} into the artificial bladder and through the prototypes. As artificial urine media was fed into the artificial bladder the media overflowed into the glass tube, where it then fed down the main drainage lumen of the catheter prototypes. The bladder and prototypes were maintained at 37°C by mini-

incubator. A mature crystalline biofilm grew over approximately 42 hours. (b) Rinsing test setup for prototypes after biofilm growth. After carefully removing the prototypes from the biofilm growth system, a DI water rinse supplied at 4 mL min^{-1} flowed downward through the prototype main urine drainage lumen for 1 minute. Prototypes designated for actuation were hydraulically inflated 10 times at a rate of 0.1 s^{-1} approximately 30 seconds into the rinse. Hydraulic inflation was applied to the inflation lumen through an inflation port fixture on the bottom end of the prototype. The rinse effluent was collected for analysis and the prototype was then removed for inspection.³⁴

Figure 13: A conceptual schematic of the active fouling release urinary catheter and demonstration of proof-of-concept prototypes. (a) Cross section of urinary catheter before biofilm formation where R, U and I represent the restraint balloon lumen, main urine drainage lumen and inflation lumens. (b) Biofilm, denoted as B, forms on the drainage lumen. (c) Reversible actuation of the lumen via water inflation debonds the biofilm formed in the urine drainage lumen. (d) Debonded biofilm is carried away in the urine resulting in a cleared lumen thereby reducing risk of symptomatic infections. Optical images of proof-of-concept prototype cross sections (e) before biofilm growth, (f) after growth of a mature *P. mirabilis* crystalline biofilm (*P.m.*) in the drainage lumen, and (g) after actuation and a gentle rinse debonded and removed the biofilm 39

Figure 14: Debonding of mature *P. mirabilis* crystalline biofilms due to strain applied to flat silicone substrates. (a) Optical microscopy image of a crystalline biofilm on a flat silicone substrate. (b) Diagram (side view) illustrates tensile strain applied to the substrate causing biofilm debonding. Optical microscopy images of biofilm-covered silicone substrates (c) after rinsing and staining with crystal violet, or (d) after actuation to 35% strain 10 times (at 0.2 s^{-1}) before rinsing and staining. The arrow indicates an example residual island of stained biofilm that remained on the silicone substrate. (e) Image analysis of biofilm area coverage confirmed that 10 cycles of 35% substrate strain caused detachment of *P. mirabilis* biofilm. Data represents mean \pm standard error of the mean, N=3-4. 42

Figure 15: Increased debonding of mature *P. mirabilis* crystalline biofilms due to increased strain rate. (a) The percentage of biofilm area covering the substrate (see text for details) after straining (10 times) at various strain rates. Experiments were conducted for 2 - 4 replicates per condition. Dashed lines indicate strain testing using LRX tensile tester and solid lines indicate strain testing using modified syringe pump. Data represents mean \pm standard error of the mean. (b) Diagram of biofilm height, H, and segment length, L, used for (c) modeling the driving force for biofilm debonding as a function of L/H. Dashed vertical lines indicate normalized segment length for 0.01 and

0.4 s⁻¹ strain rates that were measured from optical images during 100% strain at (d) 0.01 s⁻¹ and (e) 0.4 s⁻¹. Arrows indicates examples of cracked biofilm or areas of silicone substrate exposed by debonded biofilm. Scale bars indicate 5 mm. 46

Figure 16: Storage modulus G' and loss modulus G'' of mature *P. mirabilis* crystalline biofilms and the silicone substrate as a function of frequency. (a) *P. mirabilis* crystalline biofilms appeared to demonstrate predominantly elastic properties; the storage modulus was higher than the loss modulus and was relatively constant over the frequency range tested.[90] (b) Storage and loss moduli of silicone substrate. 47

Figure 17: Segment length increases with increasing strain rate. Segment length from representative images at 100% strain (such as those in Figure 3 B and C). Five lines were drawn lengthwise (equally spaced along the width of the sample) on each image, and segment length was measured along the lines using ImageJ. Error bars provide the standard error of the mean of greater than 30 measurements per image. 50

Figure 18: Debonding of mature *P. mirabilis* crystalline biofilms via applied strain to silicone tubing substrates. (a) Representative image of crystalline biofilm occluding a portion of silicone tubing. Using similar growth methods to the flat configuration, mature crystalline biofilm was grown in silicone tubing (6.35mm inner diameter silicone tubing, VWR). Bar indicates 2.5 mm. (b) Diagram of how tensile strain applied to substrate debonds a biofilm within a tube. Unidirectional strain was applied axially. (c) Image of sliced tubing sample subjected to 50% strain 10 times (top) and unstrained control (bottom) after rinsing. Arrow indicates example of remaining islands of biofilm of partial-thickness. Strained samples were stretched at 1.7 cm s⁻¹ using a LRX tensile tester. Samples were then rinsed at 4 mL min⁻¹ before crystal violet staining. SEM comparison of flat and tubular silicone surfaces used for these experiments confirmed similar surface topographies. Scale bar indicates 5 mm. 52

Figure 19: Proof-of-concept prototype urinary catheters debonding mature *P. mirabilis* crystalline biofilms using inflation-generated strain at urinary lumen surface. (a) Schematic diagram of the prototype catheter (cross section). Increased pressure in intrawall, inflation lumen, I, causes wall to stretch into the urine drainage lumen. (b) Cross-sectional views of prototypes before and after inflation. Dashed red line outlines the inflated luminal surface. (c) Maximum principal strain at the luminal surface was calculated using finite element modeling. (d) Experimental and calculated luminal surface strain as a function of inflation pressure for Dragon Skin 0020 prototypes. Representative optical images from 3 - 4 replicates of (e) un-inflated control prototypes rinsed at 4 mL min⁻¹ for 1 min, and (f) prototypes inflated 10 times at 0.1 s⁻¹ during

rinsing demonstrate biofilm removal from actuated prototypes. Cross section of control (e) shows substantial biofilm coverage (*P.m.*) after rinsing. Prototypes were stained with crystal violet and sliced open, and biofilm was removed along the length of the inflated area of the luminal surface of actuated prototypes. Scale bar indicates 2.5 mm.54

Figure 20: (a) Nominal stress *vs.* strain curve of Dragon skin 0020 was fit to the Arrude-Boyce model, $\sigma = \mu s(\lambda - \lambda^{-2})(1 + 15n + 1112175n^2 + \dots)$, where σ and $\lambda = 1 + \epsilon$ are the nominal stress and stretch for uniaxial tension, $I = \lambda^2 + 2\lambda^{-1}$, and n is a parameter that accounts for the stiffening effect.[94] The fitted shear modulus is $\mu_s = 221$ kPa, and the exponent was fitted as $n = 0.27$. (b) Cycling test of Dragon skin 0020 shows negligible hysteresis after the first strain loading cycle. Silicone samples (flat and proof-of-concept prototypes) were prestrained or preactuated at least once prior to experimentation.56

Figure 21: Dramatic release of biofilm into the effluent from inflated proof-of-concept prototype urinary catheters. (a) Representative optical image of effluent from 3 prototypes each actuated 10x during rinsing (4 mL min⁻¹ through the prototype main urine drainage lumen for 1 minute); effluent contained visible biofilm debris. (b) Representative effluent from 2 un-actuated control prototypes had minimal biofilm debris, implying that control prototypes retained biofilm after rinsing alone. (c) The effluent was collected, centrifuged, and the excess liquid was aspirated. Figure shows hydrated mass of biofilm collected. Data represents mean \pm standard error of the mean.60

Figure 22: Microscopic observation of debonding of biofilm from the main urine drainage lumen of catheter section prototypes. (a) Microscope image of surface of control prototype main lumen covered with biofilm after rinsing and (b) Microscope image of inflated prototype main lumen with biofilm removed after inflation and rinsing. Note: Horizontal bars visible across the inflation wall are “ribs” around the lumen that are due to the 3D printing process used to form the mold. (c) ImageJ was used to analyze the images, and statistical comparison to the opposing side of the catheter lumen showed that inflation debonded the biofilm from the area of the luminal wall subjected to inflation. Comparison was statistically significant both with ($p < 0.006$) and without ($p < 0.0009$) rib artifacts removed from images. Data represents mean \pm standard error of the mean, N=4.....61

Figure 23: Nominal stress-strain curves for the final prototype materials obtained from uniaxial tensile testing. (a) Nominal stress-strain curves of (a) 35 durometer silicone shaft, (b) the 50 durometer silicone shaft and (c) the more “stiff” 65 durometer silicone sheath. All the curves were fit to the Neo-Hookean model. The shear moduli for the 35

durometer shaft, 50 durometer shaft and 65 durometer sheath materials are 0.52MPa, 0.68MPa and 2.44MPa, respectively.71

Figure 24: Schematic for the design of inflation hub and its configuration used in our experiments. (a) The mold fabricated by the 3D-printer (Dimension 1200es, Stratasys, USA). (b) Inflation hub fabricated with the mold in (a), and fit with a touhy borst connector. (c) Schematic of the configuration used for the inflation testing.73

Figure 25: The setup for biofilm-growth and debonding in urinary catheter prototypes. (a) Schematic of biofilm-growth system that uses an “artificial bladder” to supply infected urine to the catheter. The artificial bladder is a vessel modified to accept the distal, top tip of a catheter prototype penetrating the bottom and extending approximately 4 cm into the vessel, which thereby maintains a residual volume of 30 mL in the artificial bladder. (b) Optical image of artificial bladder with catheter prototype; the main urine drainage lumen of the catheter prototype drains into a collection manifold on the bottom end. The diameter of the catheter prototype shaft is 6.7 mm. The artificial bladder and prototypes were inoculated with 4 hour-cultures of *P. mirabilis* and *E. coli*. After allowing the bacteria to adhere for 1 hour, artificial urine media was pumped at 0.5 mL min⁻¹ into the artificial bladder and through the prototypes. The bladder and prototypes were maintained at 37°C in a mini-incubator. A mature biofilm grew over approximately 30 hours. (c) Setup for rinsing setup for testing debonding after biofilm growth. Artificial urine media supplied at 4 mL min⁻¹ flowed downward through the prototype’s main urine drainage lumen for 1 minute. Prototypes designated for actuation were hydraulically inflated through a hub port 10 times approximately 20 seconds into the rinse. Rinse effluent was collected, and the debonded biofilm (the white matter in the petri dish) was weighed. The prototype was then removed for inspection.75

Figure 26: Adhesion strength testing for the mixed community biofilm of *P. mirabilis* and *E. coli* biofilms. (a) Schematic of the experimental set-up for the adhesion testing using a custom designed scratch probe. (b) Sample of biofilms grown on the surface of silicone (Dragon Skin 0020®, Smooth-On Inc., USA) attached on an aluminum strip. (c) Optical image of the testing set-up. (d) Representative force-displacement curves obtained from the scratch tests. Rate=0.5mm/s..... 81

Figure 27: Schematic of a urinary catheter capable of on-demand removal of infectious biofilms via active deformation. (a) Cross-section of a conceptual design for a urinary catheter shaft with intra-wall inflation lumens. (b) Biofilm forms on the surface of urine drainage lumen after 1-2 days. (c) Actuation of inflation lumens by pumping air or water

to generate large mismatched strains between biofilm and the surface of main lumen to debond the biofilm from the urine drainage lumen. (d) The detached biofilm is removed by the flow of urine once the inflation lumens are deflated. Therefore, the catheter can be maintained free of mature biofilms for long-term use and thereby may reduce the risk of catheter-associated urinary tract infections. 84

Figure 28: Finite element models show that a four-inflation-lumen design for a urinary catheter shaft achieves higher levels of tensile strains along the urine luminal surface than a two-inflation-lumen design at the same inflation pressure. (a) Cross-section of catheter shaft with two intra-wall inflation lumens. (b) Predicted strain distribution over the cross section of the two-lumen catheter from finite element model when both inflation lumens are simultaneously inflated by a pressure of 60 kPa. (c) Predicted average strain along the urine luminal surface for the two-inflation-lumen configuration reaches a plateau after the inflation walls interact with each other. (d) Cross-section of catheter shaft with four inflation lumens. (e) Strain distribution of the four-lumen catheter when inflation pressure is 80 kPa. (f) Predicted average strain along the luminal surface of the four-lumen configuration; 30% strain is achieved at approximately 70 kPa. 86

Figure 29: Contour plot of nominal strains, and the resultant deformation profile, of the cross-section of a catheter with two lumens when one lumen is actuated to achieve an average strain of 30%. 88

Figure 30: FEM simulation and experimental data of a four-lumen catheter shaft made of 50 durometer silicone elastomer. (a) Schematic of cross section and FEM model (100kPa) of extruded silicone urinary catheter shaft. (b) Photographs of the cross-section and the inflated four-lumen catheter at 80 kPa inflation pressure. Scale bar indicates 1 mm. (c) The average strain of the urine luminal surface for the four-lumen configuration; 30% strain is achieved at approximately 93 kPa. (d) The change of the outer radius of the shaft as a function of applied pressure. 90

Figure 31: FEM simulation and experimental data of an extruded four-lumen catheter shaft made of 35 durometer silicone elastomer. (a) The average strain of the luminal surface for the four-lumen configuration; 30% strain is achieved at approximately 70 kPa. (d) The change of the outer radius of the shaft as a function of applied pressure.... 91

Figure 32: Experimental testing of a catheter shaft agrees well with the numerical prediction of strain of the central luminal surface as a function of inflation pressure. (a) Cross-section and FEM model for a silicone urinary catheter shaft with four inflation lumens. Strain contour plot from FEM model subjected to an inflation pressure of 80

kPa. (b) Digital photograph of the cross-section of a catheter shaft made of 35 durometer, low modulus silicone and constrained with a 65 durometer, high-modulus silicone sheath; and a representative image of its profile when inflated to 80 kPa. Scale bar indicates 1 mm. (c) Calculated and experimental average strain of the central luminal surface. 30% strain is achieved at approximately 70 kPa. (d) The increase in the outer radius of the shaft as a function of applied inflation pressure. 92

Figure 33: Deformation profiles from FEM simulation of an extruded four-lumen catheter shaft made of 35 durometer silicone shaft and with a 65 durometer silicone sheath when it is subjected to a range of pressures. Deformation profiles predicted at the following pressures: (a) 0 kPa, (b) 20 kPa, (c) 40 kPa, (d) 60 kPa, (e) 80 kPa and (f) 100 kPa. 94

Figure 34: Prototype fouling-release urinary catheter debonds mixed community *P. mirabilis* and *E. coli* biofilm. Representative optical images of the cross sections of urinary catheter shafts with biofilm intact on main lumen of (a) control (uninflated) and removed from the main lumen of (b) inflated prototypes. All catheters were rinsed at 4 mL min⁻¹ with artificial urine for 1 minute. Catheters designated for inflation were inflated to 80 kPa (approximately 35% strain) 10 times. Sections of the catheter shaft were removed and stained with crystal violet to enhance biofilm visualization. (c) Inflation removed a significant fraction of *P. mirabilis* and *E. coli* biofilm mass as determined by weight of biofilm in the rinse effluent normalized to the weight of biofilm grown in each run. N=3 replicates, “****” indicates p<0.005. Scale bar indicates 1 mm.... 96

Figure 35: Storage modulus, G' , and loss modulus, G'' , of the co-biofilm of *P. mirabilis* and *E. coli* and the silicone substrate as a function of frequency. Moduli of (a) the co-biofilm of *P. mirabilis* and *E. coli* and (b) the silicone substrate. In both cases, the storage modulus is much higher than the loss modulus. Thus, these two kinds of materials are both apparently elastic dominant [127]. 98

Figure 36: Prototype urinary catheter repeatedly debonded biofilms with mixed communities of *P. mirabilis* and *E. coli*. Biofilms were re-grown on samples that had undergone actuation. Samples were rinsed at 4 mL min⁻¹ of artificial urine for 1 minute. Catheters designated for inflation were inflated to 100 kPa (approximately 40% average strain) for 10 times. Sections of the catheter shaft were removed and imaged, and select sections were crystal violet stained to enhance biofilm visualization. (a) Representative optical images from control samples (no inflation); both (i) cross section and (ii) sliced open samples show thorough biofilm coverage. Scale bar indicates 1 mm. (b) Representative optical images from inflated samples; (i) both cross section and (ii) sliced

open samples show substantial biofilm removal. (c) Inflation removed a significant fraction of re-grown *P. mirabilis* and *E. coli* biofilm mass as determined by weight of biofilm in the rinse effluent normalized to the weight of biofilm grown in each run. N=4 replicates, “****” indicates $p < 0.001$ 100

Figure 37: Prototype urinary catheters debond biofilms with mixed communities of *P. mirabilis* and *E. coli* along the full length of the catheter shaft. Representative optical images of the cross sections from (a) control catheter (no inflation), (b) first round of inflation after 30 h of growth of biofilm, and (c) second round of debonding after re-growing the biofilm for another 24 h. (d) Sections were taken from the prototypes at the following locations: (i) bottom, (ii) middle, (iii) top, and (iv) distal tip. Blue coloring in intra-wall inflation lumens is an artifact of residual colored water used for inflation. Scale bars indicate 1 mm. 102

Figure 38: Compressive strain along luminal surface also debonds biofilm. (a) Contour plot of FEM-calculated nominal strains (absolute values of compressive and tensile strains) along luminal surface during inflation mapped onto undeformed surface. Compressive strain is generated in the luminal surface over the connecting walls due to the compression derived from the squeezing of adjacent inflation lumens during inflation. Lower absolute values of strain appear at the edge of inflation lumens due to the transition from tensile to compressive strain at the connecting walls. (b) Optical image of sliced-open crystal violet stained section of a catheter shaft that experienced two rounds of biofilm growth and debonding. Red, dashed box highlights the region on the luminal surface overlying a connecting wall between inflation lumens that has substantial biofilm removal due to compressive strain. (c) Optical image of luminal surface excised from catheter and flattened. Scale bars indicate 1 mm. (d) Optical microscopic image of luminal surface overlying the boundary between the wall and the inflation lumen. Dashed line shows area overlying connection wall. Biofilm is visible at edge of inflation area, where low levels of strain were predicted by FEM calculations. Scale bar indicates 500 μm 104

Figure 39: Side view of the prototype anti-fouling urinary catheter designed in collaboration with the third-party catheter manufacturer. 114

Figure 40: Adhesion force of mature *P. mirabilis* crystalline biofilm measured via modified scratch test A) Diagram of scratch test B) Representative run of scratch test. Rate=0.5mm/s. We measured the bulk adhesion using a method established in Chen *et al.* [123], to measure an adhesion strength ranging from 1.25 to 4 J m^{-2} for stretching rates

0.5 – 20 mm/s. Mature *P. mirabilis* crystalline biofilm was grown on flat silicone elastomer substrate using the methods described in Chapter 2..... 117

Acknowledgements

I thank Dr. Gabriel Lopez for providing the opportunity to earn a PhD at Duke University, providing the vision for a rewarding and fulfilling project, trusting my ability to contribute in a field new to me, supplying truly impressive writing tutelage, and giving me the chance to own a project and take it to completion. Gabriel taught me the power of science and reignited my love of learning just when I needed it most. It has been a tremendous journey taking this project from a sketch on a whiteboard to a functioning prototype, and I thank Gabriel for one of the most rewarding experiences of my life. I would like to thank Dr. Xuanhe Zhao for teaching me to look beyond the next most obvious experiment, and to try to “leapfrog” ahead to the next generation of concepts and technology. Dr. Howie Levinson has been an unflagging voice of support for the commercial application of this research, and his irrepressible enthusiasm for the project has kept me going when the times got tough. Without Howie’s prodding, we would not have won the Coulter grant which has been fundamental for moving the project towards commercial application. I thank Dr. Bruce Klitzman for his calm and thoughtful feedback and for providing translational inspiration. Dr. Monty Reichert has been a voice of insight and powerful motivation since the day he became my department advisor, and I treasure his friendly and eloquent support for changing labs and improving PhD Plus. I would absolutely like to thank Dr. George Truskey for

bringing me to Duke and teaching me a tremendous amount about cell therapies and the way to get experiments done. Dr. Neil Freedman, Dr. Lisheng Zhang, and Leigh Brian were instrumental in conducting, and teaching me about, *in vivo* experiments and the compelling power of beautiful images to present data. I especially appreciate Dr. Qiming Wang and Dr. Changyong Cao as great collaborators that greatly expanded the scope and impact of my research. I would also like to thank the many undergraduate and masters student researchers that contributed to the advancement of this research.

The mentorship and support of my peers and coworkers has also been crucial to my learning and development during the PhD. Writing a dissertation while going through a divorce is not an easy process, and I could not have made it to the end without the support of my friends and cohort. Alex Jantzen was the best and most supportive “lab spouse” and friend a person could ask for, and her support along with that of Peter Hollender, Devin Bridgen, Suzana Vallejo-Heligon, Mike Nichols, and Tyler Gibson got me through. The incoming Biomedical Engineering PhD cohort of 2009 proved to be an exceptionally tight-knit and capable group that was always supportive of each other, and I look forward to their amazing contributions to science over the coming years. Though we are now apart, I also appreciate Shelley Alonso-Marsden for the support over the years and helping me learn about communication and values. The people of the Lopez lab were tremendously welcoming, and their hard work and happy attitude contributed to both my scientific success and to making the PhD an enjoyable

experience. Phanindhar Shivapooja especially deserves thanks; he welcomed me into the biofilm realm and became my teammate for combatting the evils of biofilm.

1. Chapter 1: Background, significance, and specific aims.

This dissertation will be publicly available after the two year embargo period.

1.1 Background and significance

Biofilm infection in urinary catheters is a pervasive and challenging issue in healthcare. There are over 30,000,000 Foley urinary catheters used annually in the USA to treat urine retention and urinary incontinence. Although urinary catheters are typically associated with the elderly, urinary catheters are also correctly used for short-term surgical procedures as well as long-term conditions requiring kidney dialysis or time in intensive care [1-3]. Approximately 1 in 5 people admitted to the hospital will receive a urinary catheter, and many of those will be either mistakenly prescribed or left in-dwelling longer than the appropriate time. Unfortunately, catheter-associated urinary tract infections (CAUTIs) are the most common cause of hospital-acquired infections, and more than 50% of those microbial infections will have associated biofilms [1-3]. Biofilms not only promote aggressive infections but may also grow to thicknesses sufficient to occlude the urine lumen, causing trauma, leakage, pyelonephritis, septicemia, and shock, all of which could lead to dangerous and expensive emergency treatments [4]. Additionally, there is a significant financial motivation within the healthcare industry to reduce infection rates because each infection costs the hospital money; CAUTIs are on the nonpayment list and are nonreimbursable [5]. Current

commercially available catheters attempt to either kill or prevent adhesion of bacteria through non-fouling surface treatment or antibiotic elution, but at best they simply delay bacterial adherence for several days [6]. Thus, there exists a need to develop a catheter that resists or debonds biofilms, as well as reduces the occurrence of catheter-associated urinary tract infections.

The technology presented in this document avoids the pitfalls of previous chemical or biological approaches because it uses a mechanical approach – active surface deformation of the elastomeric substrate that triggers the on-demand release of overlying biofilms. Biofilms have multi-faceted chemical resistance, but the anti-fouling catheter design circumvents that resistance by actively deforming the surface of the drainage lumen to physically detach the biofilm. We have confirmed that this technology detaches infectious biofilms from materials common to urinary catheters, and that anti-fouling urinary catheters utilizing this active surface deformation can remove the majority of the biofilm from the previously inaccessible luminal surface. This document presents research data that establishes the efficacy of the catheter technology as well as elucidates the methodology behind its design. The effective anti-biofilm technology integrated into the anti-fouling urinary catheters is well suited to provide a potential solution to the ubiquitous problem of CAUTIs.

1.2 Unmet clinical need for infection control in urinary catheters

There are over 30 million Foley urinary catheters used annually to treat urinary incontinence and urine retention, and urinary tract infections following catheterization are the most common cause of hospital acquired infections [6, 7]. Catheter-associated urinary tract infections (CAUTIs) account for 30-40% of all hospital infections [1, 5]. More than 50% of microbial infections will have associated biofilms that consist of bacteria and exopolysaccharides produced by those bacteria [8]. These biofilms protect the resident bacteria and encourage additional infection; biofilm-protected bacteria often require over 100x the typical antibiotic concentration (vs. planktonic phenotype) [9], and facile gene transfer between cells within the biofilm allow enhanced development of antibiotic resistance [10]. As stated by Siddiq et al., in his thorough 2012 *Nature Reviews Urology*, “Biofilm formation is crucial for the development and progression of CAUTI” [7].

In addition to the public health implications of antibiotic resistance and individual patient concerns about infection-related pain, hospitals are faced with a financial burden related to CAUTIs [5]. Approximately 20% of patients admitted to a hospital in the US receive a urinary catheter, and over 400,000 infections occur each year, each costing between \$600 and \$1,000 (not including those that cause sepsis) [1, 11]. Medicare has moved CAUTIs to the “nonpayment list” and CSM (the single largest healthcare payer in the US) has termed CAUTIs a “never event” and withholds reimbursement [5]. Hospitals lose money with each CAUTI [5], and thus the

development of an effective antibiofilm strategy for urinary catheters represents not only a significant societal need but also a huge potential commercial opportunity.

1.3 Unmet clinical need for biofilm control in urinary catheters

The biofilm not only promotes infections; it can grow in thickness sufficient to occlude the urine lumen (see Figure 1) causing possible trauma, leakage, pyelonephritis, septicemia, and shock, which can lead to dangerous and expensive emergency treatments [2, 12]. Scientific efforts to eliminate catheter infections and biofilms have been underway since the 1950's, but have had very limited success; almost 100% of patients that undergo catheterization longer than 28 days will suffer a CAUTI [13].

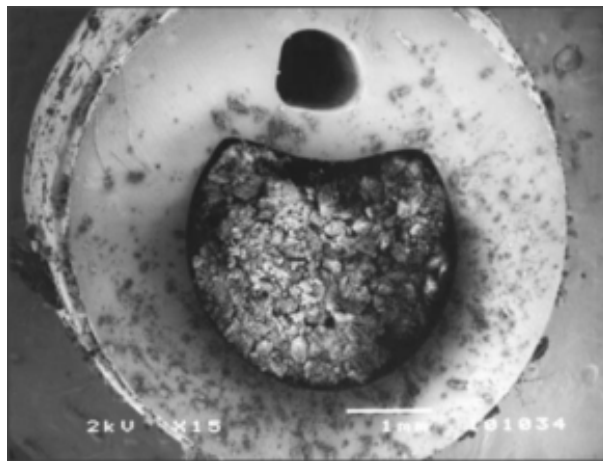


Figure 1: Cross section of urinary catheter occluded by crystalline biofilm. Adapted from Stickler 1999 [14].

1.4 Urinary catheter background and pathogenesis

Urinary catheters are used to treat urinary incontinence and urine retention, and can be indwelling short or long term depending on the associated condition. Foley catheters are typically used for longer term implants and have a reservoir balloon that is inflated after the catheter is inserted up the urethra into the bladder (see Figure 2) [7]. Once inflated, the reservoir balloon is left inflated and secures the tip of the catheter inside the bladder. An eyelet hole at the tip of the catheter allows drainage through the main lumen of the catheter [15]. The catheter is attached to a drainage bag; ideally it is pre-attached to preserve sterility. The drainage bag can then be opened via valve by the patient or caregiver. However, the indwelling catheter can result in a continuous low flow stream of urine (low urine flow rate low 2 mL hr^{-1} to high $4\text{-}200 \text{ mL hr}^{-1}$) [4] (vs intermittent voiding) that does not flush bacteria from the urethra [16]. Additionally, urine pools around the balloon, below the eyehole, or even around “airlocks” due to patient movement of the catheter [15]. The catheter shaft also exerts pressure radially on the urethra, which impairs mucosal blood flow and function while decreasing mucin secretion from the periurethral glands [16].

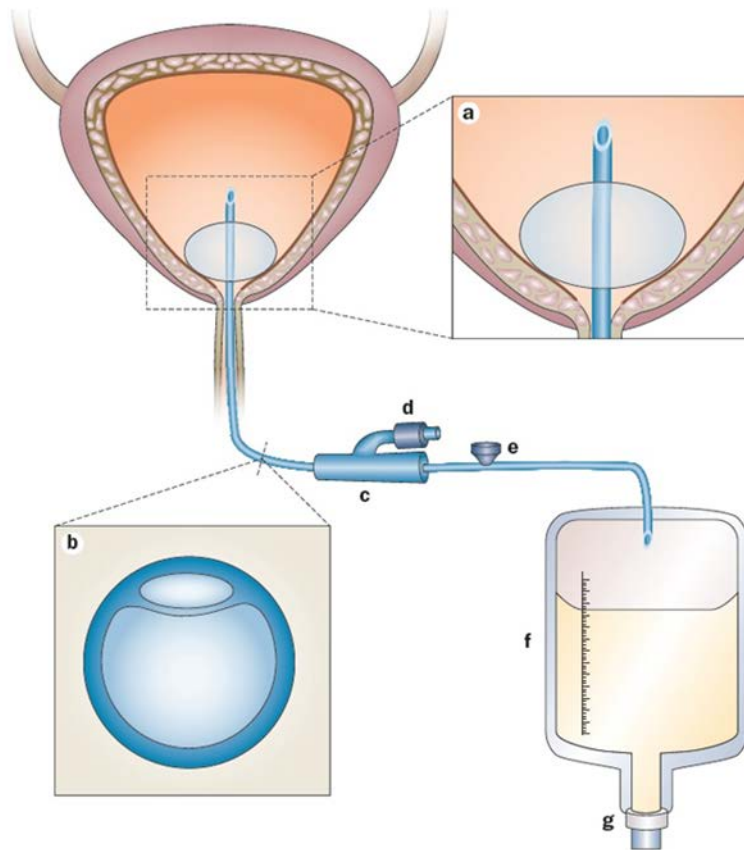


Figure 2: Diagram of a bladder with a typical indwelling urinary catheter from Siddiq 2012 [7]. a) An eyelet allows drainage of urine from bladder. The reservoir balloon is filled with saline to secure catheter. b) Cross-section of commonly used double-lumen indwelling urinary catheter. c) Preconnected junction of indwelling catheter and drainage system. d) Port used to inflate the reservoir balloon with saline. e) Sampling port. f) Collection bag. g) Urine emptied via outlet valve.

Bacteria can enter the urinary tract either extraluminally (on the outside of the catheter) or intraluminally, and gram-negative infections (such as *P. mirabilis*) occurred equally between the two routes [17-19]. Intraluminal bacterial entry can occur when urine refluxes or goes upstream from the drainage bag, or if there is a break in the collection system [17]. Although the patient's own perineal or skin flora are the most

common causes of CAUTIs, bacteria from the hands of health care workers are occasionally responsible as well [20-22]. Transitory bacteria originating from hospital workers may represent antibiotic-resistant nosocomial strains which increase the difficulty of treatment. Although the exact ranking of bacteria causing catheter biofilms varies depending on the study, *Enterobacteriaceae* such as *Escherichia coli* are the predominant pathogen isolated from CAUTIs, and the top four bacterial species are *Pseudomonas aeruginosa*, *Enterococcus faecalis*, *Escherichia coli*, and *Proteus mirabilis* [4, 11, 23].

1.5 Healthy functioning bladder

The healthy bladder is distended passively by the inflow of urine via the ureters from the kidney. Pressure builds within the bladder until it reaches a threshold that signals your bladder is full at approximately 250 mL, although the bladder can continue to fill until a maximum of approximately 400-500 mL [24]. Once the bladder feels full, the urge to urinate will grow as the bladder volume continues to fill based on stretch receptors in the bladder wall, and an involuntary reflex is initiated. However, voiding still requires a voluntary or conscious action to open the urethral sphincter, at which point the bladder voids and achieves near-complete emptying [24]. The flushing of the urethra and the emptying of the bladder combine to prevent the ascent by bacteria of the urethra and subsequent colonization [25]. The voiding of the bladder has been

measured as a range of release flows (varies with age and sex, average ranges from 9 – 17 mL s⁻¹) [26-28].

1.6 Biofilm development in urinary catheters

Biofilm formation begins with an initial layer of crystals and proteins attaching, which then facilitate the attachment of the planktonic phase (aquatic, free floating) of bacteria to the catheter surface (see Figure 3) [9]. Pilli help form stable attachment, a thin basal layer forms, and the bacteria multiply [9]. The bacterial attachment activates genes for synthesis of exopolysaccharide matrix. Unfortunately, the biofilm matrix has a protective effect for the bacteria, often requiring over 100 times the concentration of antibiotic to kill the bacteria (vs planktonic swimming phenotype) [9, 29].

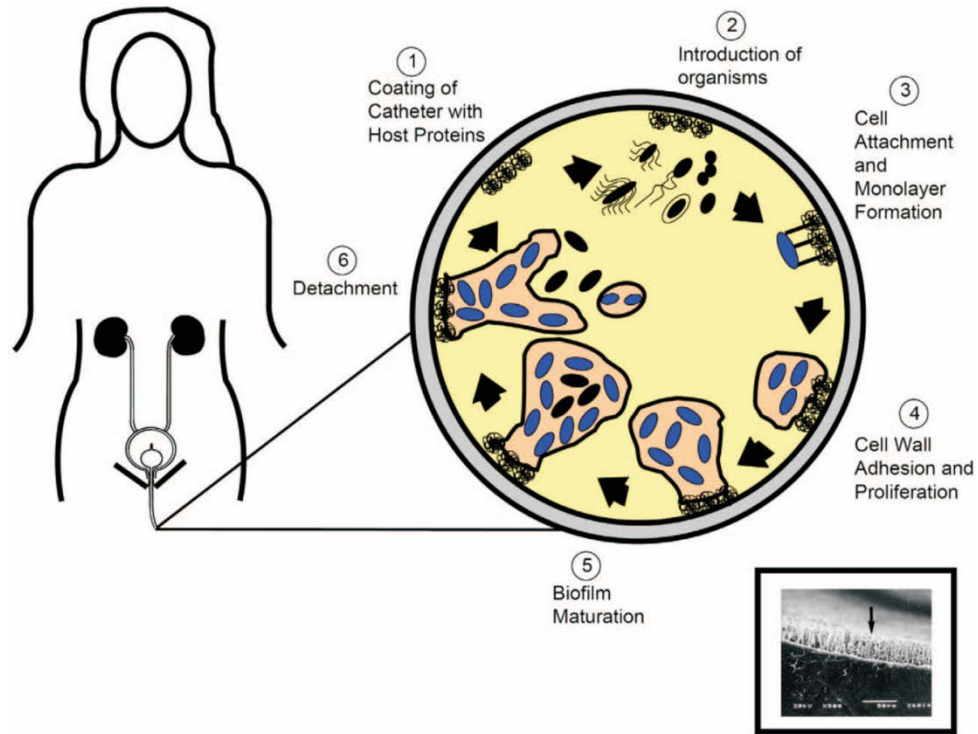


Figure 3: Typical progression of biofilm development within urinary catheters. 1) The catheter is coated with proteins and crystals. 2) Organisms are introduced. 3) Bacteria attach and begin to colonize. 4) Cell wall adhesion and proliferation. 5) Biofilm maturation. 6) At sufficient densities bacteria spontaneously detach to aid in dispersal for new colonies.

1.7 Crystalline biofilm development

Proteus mirabilis is a particularly problematic and common variety of bacteria that causes crystalline biofilm encrustation [4, 13, 30]. *P. mirabilis* is a urease-producing bacterium that creates an alkaline environment, thus causing precipitation of calcium and magnesium phosphates from urea. The resultant biofilm incorporates crystals of ammonium magnesium phosphate hexahydrate and the poorly crystalline form of

calcium phosphate [31]. The reaction produces nitrogen for the bacteria while also creating a protective crystalline biofilm [32]. The bacterium also possesses several other potent virulence factors. *P. mirabilis* has bacterial appendages with adhesive proteins at the tip, which are referred to as fimbriae. *P. mirabilis* has at least 5 fimbrial types, and has 17 fimbrial operons (the most of any species thus far encoded) [33]. *P. mirabilis* also demonstrates a distinctive swarming motility, which is thought to be triggered by contact with a solid surface. While in suspension, *P. mirabilis* cells appear as 1 – 2 μm rods, but on surfaces they differentiate into multinucleated 20 - 50 fold elongated swarm cells with thousands of flagella [32, 34]. The swarming motility is distinctly helpful for migrating across catheters as well as for gaining entry to the urinary tract [15]. The swarm cells can later dedifferentiate and consolidate, although the crystalline biofilm still contains protruding swarm cells [16, 35].

1.8 Current approaches on the market and their challenges

The common approaches to prevent bacterial growth and adhesion on the market use passive catheter surfaces or chemical means. Examples include (i) hydrogel coatings – which still suffer from attachment and biofilm formation in less than 7 days; (ii) antibiotic-releasing luminal materials – which prevent biofilm formation for, at most, 7 days; and (iii) silver-impregnated luminal biomaterials –the silver ions do not elute in sufficient quantities to prevent biofilm formation long-term [4, 6]. There is currently no

effective method on the market to stop crystalline biofilm encrustations, and only limited methods to slow biofilm formation [9, 36-39]. An expert panel from the Infectious Diseases Society of America eventually concluded that clinical studies don't demonstrate sufficient effect, and that the best way to reduce the occurrence of CAUTIs was to limit the use of catheters and remove them as soon as possible [40].

1.9 Urinary catheter regulatory documents

ASTM F-623-99 "Standard Performance Specification for Foley Catheter" defines the performance testing specific to most urinary catheters. Biocompatibility requirements for implantable devices are defined in ISO 10993; and sterilization requirements in ISO 11135.

1.10 Recent approaches in biofilm control research and their challenges

Antimicrobial coating and impregnation using liposomes and polymers, silver coatings, bacteriophages, nanoparticles and iontophoresis, and other more typical antimicrobials such as triclosan have all been attempted with limited success [7]. Hydrogel coatings on their own, or impregnated with a variety of active moieties, have been experimented with for years and several varieties are currently on the market. As stated before, at best they delay biofilm formation for a matter of days [6, 41]. A recent

promising approach was using quorum-sensing inhibitors such as furanones to prevent biofilm formation; quorum sensing molecules are how bacteria regulate their biofilm formation [42-44]. Over 200 furanones have been identified but more research is required to select the most suitable for translation [45]. Thus far the results have been mixed and a study by Baveja et al., determined that the furanones had no significant effect [44, 46].

Vibroacoustic stimulation is an appealing concept and utilizes acoustic waves at the catheter surface to cause chaotic microstreaming or cavitation to prevent bacterial attachment, and has even been proven in a rabbit model [47-49]. However, it typically requires local piezo elements that need to be constantly on to prevent bacterial attachment, and any mis-tuning of the acoustic frequency can actually enhance bacterial attachment [47].



Figure 4: Commercial attempt at ultrasonic biofilm removal from NanoVibronix. Image from www.nanovibronix.com/uroshield.

Bacterial interference is the term for antagonism between bacterial species, and it has been used as an approach to selectively introduce nonpathogenic bacteria to prevent pathogenic biofilm formation [50]. Although apparently effective, the clinical implementation would require the challenging maintenance of and introduction of specific bacteria in the hospital setting since catheters must be sterilized before packaging [7]. NO-impregnated silicones and NO-releasing carbon layers showed some success but have not been pursued further [51, 52]. Light-activated antimicrobial agents (LAAAs) are chemicals that emit reactive oxygen species deleterious to bacteria when excited with the appropriate light wavelength, and recently have been integrated into

common catheter materials without causing material degradation [53, 54]. However, the actual introduction of the appropriate light into an indwelling catheter remains problematic. Recent approaches using PEG and zwitterionic brushes for temperature-triggered active release of biofilms are still under development, but are likely insufficient for established or occlusive encrustation formation [55-57]. There has even been development of catheters with integrated pH sensors to warn of impending crystalline encrustation [58]. Perhaps the most well-publicized recent approach is the use of micropatterned surfaces by companies such as Sharklet Technologies [59]. The micropatterned surfaces mimic those of bacteria-resistant surfaces such as shark skin and has been effective in small *in vitro* studies, but the technology is likely hindered by the difficulty in manufacturing large quantities [59].

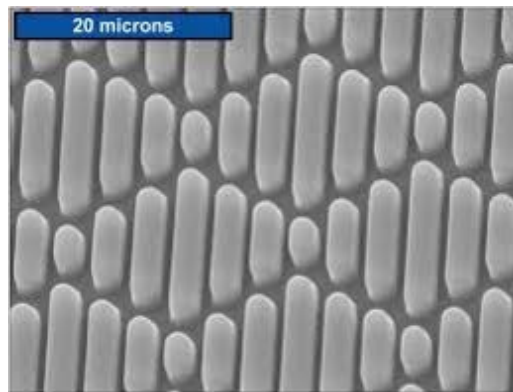


Figure 5: Micropatterned surface commercially known as "Sharklet" used to delay biofilm formation [59].

1.11 Implications of biofilm removal

Although biofilm formation is considered crucial for the development and progression of CAUTI's [7], there is a paucity of studies examining the influence of *in situ* biofilm removal on urinary catheter associated infections. A handful of studies have assessed *in vitro* medically-relevant biofilm removal and declared successful biofilm removal at 60-94% removal [60-64]. Removal of biofilm in combination with antibiotic therapy has been shown to prevent infection recurrence in a variety of indwelling devices when previous antibiotic therapies were ineffective [65, 66]. Additionally, one study showed that removal of biofilm-laden urinary catheters in patients (i.e. assuming 100% removal of catheter-associated biofilm mass) combined with immediate antibiotic therapy: almost tripled the number of patients that avoided polymicrobial bacteriuria, doubled the number of patients with a shorter time to afebrile status, and tripled the number of patients that avoided a symptomatic relapse [67].

1.12 Innovation – Surface deformation to trigger biofilm debonding

The anti-fouling catheter technology uses surface deformation of elastomeric substrates to trigger the active release of biofilms. The concept was recently demonstrated by the Lopez and Zhao labs at Duke University on mucoid, "slimy", biofilms typical of marine environments as well as biofilms generated by infectious bacteria such as *E. coli*.

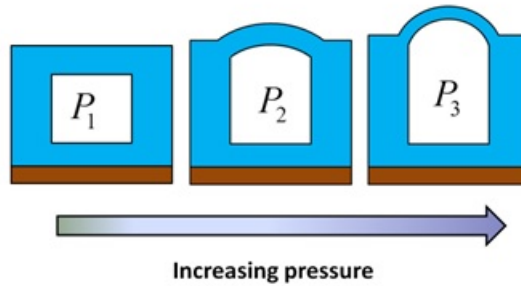


Figure 6: Diagram of how pneumatic inflation deforms a specified surface and increases strain. Adapted from Shivapooja 2013 [68].

Practical implementations of this concept included use of a pneumatic network (multiple, connected inflation chambers) to stretch the elastomer substrate (silicone, Ecoflex 010 from Smoothon Inc.), thereby detaching > 95% of the mature *E. coli* biofilm from the substrate (see Figure 6).

We discovered that debonding occurs when the elastic energy of the biofilm exceeds the adhesion energy between the biofilm and polymer [68]. This research study took advantage of a clinically relevant yet unexplored scientific research area to develop a catheter prototype concept. Conventional catheters form biofilms that are crucial for the development and progression of catheter associated urinary tract infections (Figure 7) [7]. If that biofilm can be removed, then presumably the progression to infection could be interrupted and the chance of infection reduced.

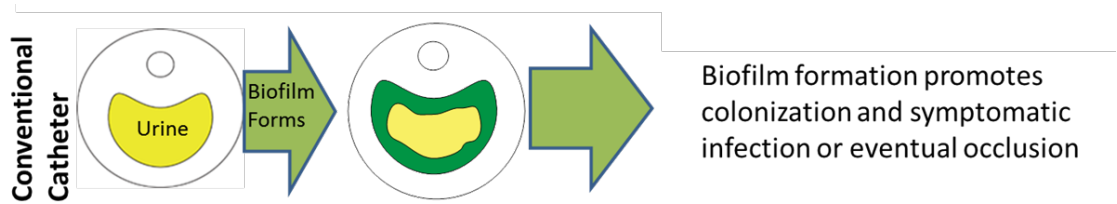


Figure 7: Conventional catheter outcome. A conventional catheter eventually forms a biofilm, which promotes colonization and eventual symptomatic catheter-associated urinary tract infection.

This concept incorporates an intra-wall inflation lumen that can be actuated via an additional hub port and a temporarily-attached syringe (Figure 8).

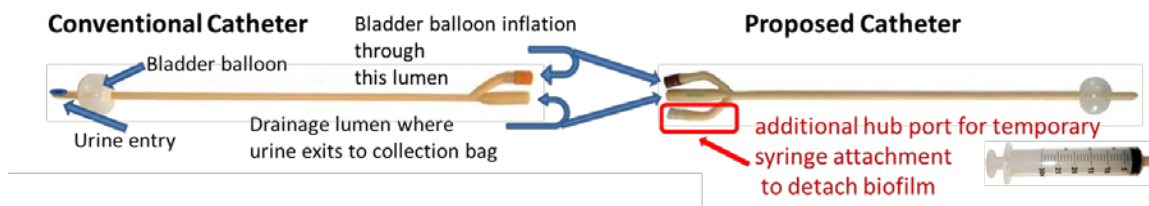


Figure 8: Side views of a conventional catheter and a proposed anti-fouling urinary catheter highlight the additional hub port for syringe actuation. The anti-fouling urinary catheter uses an additional hub port to provide access to inflate and deflate intra-wall inflation lumens.

The translational approach demonstrated in this document uses the biofilm-detaching technology in a urinary catheter by incorporating an inflation system along the length of the catheter shaft, and inflating *inwards* to detach luminal biofilms, as shown in Figure 9. We used “hydraulic” inflation applied manually using a saline-filled syringe (Figure 8).

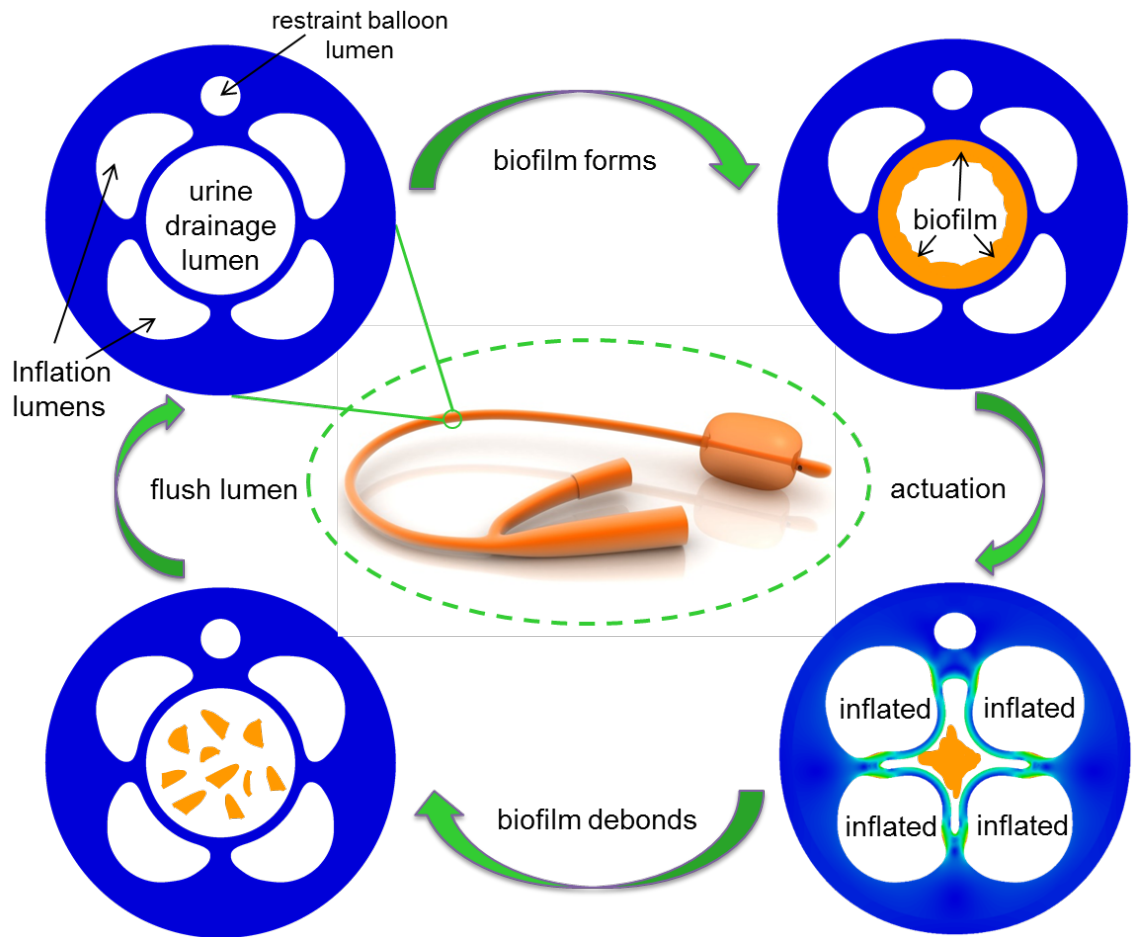


Figure 9: Anti-fouling urinary catheter conceptual schematic. Upon insertion, the catheter appears like the top left panel and is free of biofilm. Biofilm gradually forms on the surface of the main urine drainage lumen. Actuation via inflation applies strain to the surface of the urine drainage lumen, thereby debonding the overlying biofilm. The debonded biofilm is then free-floating in the urine and is rinse out, thereby returning the catheter to its original state (free of biofilm) and thereby potentially reducing the risk of infection.

1.13 Specific Aims

Aim 1 addressed our initial hypothesis that we would be able to use surface deformation to debond crystalline biofilms. Aim 2 modeled prototype and biofilm properties to aid in design and optimization of a prototype anti-fouling urinary catheter. Aim 3 presents data demonstrating that single-channel proof-of-concept prototypes and more advanced multi-inflation lumen prototypes remove biofilm from their luminal surfaces.

1.13.1 Specific Aim 1: *In vitro* active debonding of mature *Proteus mirabilis* crystalline biofilm on silicone substrates

Aim 1 was structured to expand fundamental understanding of substrate strain as a method for debonding biofilms, specifically crystalline biofilms. We grew crystalline biofilms on flat silicone surfaces to allow focused study of the influence of substrate strain, and thereby remove the influence of surface deformation associated with the Lopez lab's other efforts with inflation-actuated debonding. Although *P. mirabilis* forms one of the most aggressive infectious crystalline biofilms, and is also one of the most useful crystalline biofilms for *in vitro* study; there was no established method for growing a crystalline biofilm on a flat silicone surface. We first established a growth method for cultivating a mature crystalline biofilm on a flat silicone substrate. We then used the mature crystalline biofilm to establish that strain applied to the silicone substrate debonds biofilm in a similar manner to that observed with *E. coli* [69]. Once

we established that substrate strain debonds crystalline biofilms, we then examined the influence of substrate strain rate on the debonding and showed that decreasing the strain rate decreased debonding.

Specific Aim 1 Hypotheses addressed:

(1) The active surface distortion via unidirectional strain will facilitate debonding of encrustation by crystalline urinary biofilms *in vitro*.

(2) Strain rate will influence the percentage of biofilm debonding.

1.13.2 Specific Aim 2: Urinary tract biofilm property characterization and urinary catheter inflation modeling for prototype design.

The ability of substrate strain to debond the overlying biofilm is partially dependent upon the biofilm mechanical properties, however the properties of crystalline biofilms that are often found in urinary catheters had never been characterized [70]. We characterized the mechanical properties of a mature crystalline biofilm formed by *P. mirabilis*, and similarly characterized a mature mixed community biofilm of *P. mirabilis* and *E. coli*. We tested the complex visco-elastic modulus of the biofilms and found that both biofilms demonstrated properties that were predominantly elastic with a constant storage modulus that was 1 – 3 orders of magnitude greater than other clinically relevant biofilms. During our experimentation on the influence of strain rate upon debonding in Aim 1, we observed a relationship between strain rate and segment length (distance between cracks formed while the substrate is subjected to strain). We used that observation and the biofilm mechanical properties to develop a macro-scale

quantitative relationship between applied strain rate and biofilm debonding through an analysis of biofilm segment length and the driving force for debonding. Finally, we used finite element modeling to understand the strain within the elastomeric substrate of prototype catheters during inflation, and then used successive rounds of modeling to thereby optimize the design of an anti-fouling urinary catheter with multiple intra-wall inflation lumens.

Specific Aim 2 Hypotheses addressed:

(1) The crystalline component of mature crystalline biofilms will influence the biofilm's mechanical properties.

(2) Computational modeling will inform catheter prototype design by facilitating predictions of the substrate strain generated at the catheter main luminal surface when the number and position of intra-wall inflation lumens of the catheter shaft are adjusted.

1.13.3 Specific Aim 3: *In vitro* confirmation of a urinary catheter prototype for removing biofilm.

The overall goal of this study was to demonstrate *in vitro* that urinary catheter prototypes were capable of successful controlled detachment of mature crystalline and mixed community biofilms. We completed that task in two formats: first with proof-of-concept prototypes with a single intra-wall inflation lumen, and second with a more advanced prototype with four intra-wall inflation lumens. The proof-of-concept prototypes were short, large diameter, sections of the shaft of the conceptualized active, fouling-release catheters. The proof-of-concept prototypes were constructed using 3D-

printed reverse molds and pourable silicone in a technique inspired by soft robotics. The proof-of-concept prototypes demonstrated release of the majority of mature *P. mirabilis* crystalline biofilms (e.g., ≈90%) from their strained luminal surfaces. We therefore proceeded to design and construct prototypes with clinically relevant dimensions that could apply strain to a majority of their luminal surface. We utilized the optimized design from Aim 2 and constructed prototypes with clinically relevant dimensions using a combination of extrusion and 3D printed reversed-mold fabrication techniques. The catheter prototypes were able to on-demand remove greater than 80% of a mixed community biofilm of *P. mirabilis* and *E. coli* from the majority of their luminal surfaces. We regrew the biofilm, and the prototypes were again able to remove the regrown biofilm. Finally, analysis of the luminal surfaces of the prototypes after biofilm-debonding showed that biofilm was removed from substrate surfaces that had undergone compressive strain. The fouling-release catheter offers the potential for a non-biologic, non-antibiotic method to remove biofilms and thereby for impacting the thus far intractable problem of catheter-associated infections.

Specific Aim 3 Hypotheses addressed:

(1) Active surface distortion via inflation-generated strain will facilitate luminal debonding of encrustation by crystalline urinary biofilms in an *in vitro* prototype model.

(2) Adjusting the number and position of intra-wall inflation lumens will allow inflation to generate sufficient tensile strain to debond a mixed community biofilm *in vitro* over the majority of the internal lumen perimeter.

(3) Active surface distortion via inflation-generated strain will facilitate luminal debonding of a mixed community biofilm in an *in vitro* prototype model after the biofilm has regrown after previous debonding.

(4) Compressive strain in the substrate will debond the overlying biofilm in a similar manner to tensile strain.

1.14 Organization of the dissertation

The goals of this project were broken down into three specific aims as described above, and those aims were addressed in two major research efforts. Although those efforts were originally planned to be described in three or four publications, the bulk of those two research efforts were documented in two publications in order to increase the impact of the research. The two publications are presented in chapters 2 and 3 in order to provide a parallel narrative to the publications.

2. Chapter 2: Crystalline biofilm debonding and an on-demand fouling-release urinary catheter

Sections of the text and figures included in Chapter 2 were published in *Advanced Healthcare Materials*. The full citation for the article is: Vrad Levering, Qiming Wang, Phanindhar Shivapooja, Xuanhe Zhao, and Gabriel P. López. 2014. Soft Robotic Concepts in Catheter Design: an On-demand Fouling-release Urinary Catheter. *Advanced Healthcare Materials*, 25 MAR 2014; 3:1588-96. John Wiley & Sons Ltd. does not require permission for authors to reuse their own articles, but an optional grant of license will be obtained as soon as one is available.

Please note that this manuscript described the work for Specific Aim 1 and parts of Aim 2 that were originally intended to be two separate manuscripts, but were combined for a more compelling narrative for submission to *Advanced Healthcare Materials*. Vrad Levering was the lead author and drove the experimentation, conception and documentation, however this work represents a collaboration with Qiming Wang who supplied mechanical engineering and materials science input as a co-first author.

2.1 Chapter synopsis

Infectious biofilms are problematic in many healthcare-related devices, and are especially challenging and ubiquitous in urinary catheters. This report presents an on-

demand fouling-release methodology to mechanically disrupt and remove biofilms, and proposes this method for the active removal of infectious biofilms from the previously-inaccessible main drainage lumen of urinary catheters. Mature *Proteus mirabilis* crystalline biofilms detach from silicone elastomer substrates upon application of strain to the substrate, and increasing the strain rate increases biofilm detachment. The study presents a quantitative relationship between applied strain rate and biofilm debonding through an analysis of biofilm segment length and the driving force for debonding. Based on this mechanism, hydraulic and pneumatic elastomer actuation was used to achieve surface strain selectively within the lumen of prototypes of sections of a fouling-release urinary catheter. Proof-of-concept prototypes of sections of active, fouling-release catheters were constructed using techniques typical to soft robotics including 3D printing and replica molding, and those prototypes demonstrate release of mature *P. mirabilis* crystalline biofilms (e.g., $\approx 90\%$) from strained surfaces. These results provide a basis for the development of a new urinary catheter technology in which infectious biofilms are effectively managed through new methods that are entirely complementary to existing approaches.

2.2 Chapter introduction

Infection of urinary catheters with bacterial biofilms is a pervasive and challenging issue in healthcare. In the U.S. alone, over 30 million Foley urinary catheters

are used annually to treat urine retention during short-term surgical procedures as well as longer-term conditions requiring kidney dialysis, time in intensive care, or time in assisted-living facilities.[2, 3] Catheter-associated urinary tract infections (CAUTIs) are the most common type of nosocomial infections and account for 30-40% of all hospital infections.[71] The unavoidable formation of asymptomatic biofilms in urinary catheters promotes development of symptomatic CAUTIs, and nearly 100% of patients that undergo catheterization for longer than 28 days will suffer some form of infection.[7] A biofilm can harbor bacteria for persistent infections, and can also grow in thickness sufficiently to block urine flow causing trauma, leakage, pyelonephritis, septicemia, and shock, which lead to dangerous and expensive emergency treatments.[4] These infections are a concern for individual patients and for the public due to the implications of antibiotic resistance, and catheter-associated urinary tract infections can represent a significant financial burden to hospitals.[5]

Biofilm formation begins with an initial layer of proteins attaching, which then facilitate the attachment of aquatic (planktonic) bacterial cells to the catheter surface.[9] Pili often help stabilize attachment, a thin basal layer forms, and the bacteria multiply.[9] Bacterial attachment activates genes for synthesis of exopolysaccharide matrix, which has a protective effect for the bacteria, often requiring over 100 times the concentration of antibiotic to kill the bacteria compared to the liquid-borne phenotype.[9] In the case of *Proteus mirabilis*, a particularly problematic bacteria

commonly associated with CAUTIs, attachment also results in the production of urease, which causes *crystalline* biofilm encrustation akin to that of better-known kidney stones.[4, 13, 72] The urease that *P. mirabilis* generates leads to an alkaline environment, and the biofilm then incorporates calcium and magnesium phosphate crystals precipitated from the urine.[31]

Current commercially available catheters attempt to either kill or prevent adhesion of bacteria through elution of antibiotics or through incorporation of non-fouling surface treatments, but at best these measures simply delay bacterial adherence for several days. Examples of extant commercial approaches include hydrogel coatings – which still suffer from attachment and biofilm formation in less than 7 days;[4, 7, 37, 73, 74] and antibiotic-releasing or silver-ion-releasing luminal materials – which prevent biofilm formation for, at most, 7 days.[4, 6, 7, 36, 73, 74] Indeed, Pickard’s recent and thorough multi-center randomized trial conclusively determined that silver alloy-catheters did not effectively reduce the incidence of symptomatic CAUTIs.[75] No effective method exists on the current market to stop crystalline biofilm encrustations, and commercially available methods meant to slow biofilm formation show only limited efficacy.[7, 36-39, 73, 74]

Here, we present a new concept for a urinary catheter capable of on-demand fouling-release, a new approach that is different from all antifouling methods used in current catheters. The new design is based on active deformation of the inner surfaces of

elastomeric catheters in response to external stimuli. The mechanism employed to achieve active surface deformation is similar to that reported by Whitesides and coworkers who actuated the appendages of soft robots pneumatically.[76, 77] In our work, we hypothesized that active surface deformation of elastomers [69] can significantly facilitate the release of encrustation by crystalline urinary biofilms. To test the hypothesis, we first developed a method to grow mature crystalline biofilms *in vitro*, on flat silicone substrates. We applied strains on the silicone substrates at various strain rates, and then examined the detachment of biofilms. We found that the applied strain and strain rate both have significant effects on biofilm detachment: when the applied strain rate is relatively low, biofilms will not debond from the substrates even under very high strains; instead, the biofilms are fractured into small segments that remain attached to the substrates. On the other hand, when the applied strain rate is relatively high, biofilms can be readily detached as large pieces, once the applied strain reaches a critical value. We quantified the mechanical properties of biofilms formed by *P. mirabilis* and developed a theoretical model to account for the effects of applied strain and strain rate on biofilm detachment. The model can be used to interpret the experimental phenomena, offering a potential design tool in future design of active surfaces for antifouling applications. We then used prototype fabrication techniques established for soft robotics [76, 78] to develop models of segments of urinary catheters that utilized substrate deformation by hydraulic actuation to debond *P. mirabilis* biofilms *in vitro*.

Crystalline biofilms were effectively debonded from these prototypes, suggesting a promising option for development of a new approach to control of catheter-associated biofilms and UTIs that can augment, as well as circumvent the limitations of, current antifouling approaches used in catheter technology.

2.3 Methods and Materials

2.3.1 Bacteria strain and culture media

Proteus mirabilis 2573 (ATCC 49565) was thawed from frozen stock and cultivated overnight at 37°C on a tryptone soya broth agar slant which was stored at 4°C and used for up to 2 weeks. Artificial urine was prepared per the recipe originally described in Griffith and modified by Ciach and was composed of calcium chloride 0.49 g/L, magnesium chloride hexahydrate 0.65 g/L, sodium chloride 4.6 g/L, disodium sulfate 2.3 g/L, trisodium citrate dihydrate 0.65 g/L, disodium oxalate 0.02 g/L, potassium dihydrogen phosphate 2.8 g/L, potassium chloride 1.6 g/L, ammonium chloride 1.0 g/L, urea 25 g/L, and gelatin 5.0 g/L in deionized water [79]. The medium was adjusted to a pH of 6.1 and then sterilized. Tryptone soya broth was prepared separately, sterilized, and added to the artificial urine to a final concentration of 1.0 g/L; this made the total artificial urine media (AUM). A colony of *P. mirabilis* was inoculated into 75 mL of AUM and grown for 4 hours at 37°C on a shaker at 240 rpm.

2.3.2 Preparation of silicone coupons:

Flat silicone samples (Dragon Skin 0020, Smooth-On, Inc.) were manufactured by pouring 10 mL of silicone into a 90 mm diameter petri dish (VWR) generating a 1.7mm thick silicone layer. Coupons were trimmed into 24 mm x 75 mm dimensions that would fit in a drip flow reactor (Figure 10). The coupons were removed from the petri dishes in the biosafety cabinet after rinsing with 95% ethanol and sterilized water.



Figure 10: Growth and characterization of mature *P. mirabilis* crystalline biofilms on flat silicone substrates. (a) Schematic of the flow system. The silicone samples were submerged in (b) the modified drip flow reactor [80] and inoculated with a 4 hour culture of *P. mirabilis*. After allowing the bacteria to adhere for 1 hour, artificial urine with 1% tryptic soy broth was pumped at 0.5 mL min^{-1} through the drip flow reactor and over the flat silicone samples. The reactor was maintained at 37°C by mini-incubator. A mature crystalline biofilm grew over approximately 42 hours. (c) SEM of the resultant planar biofilm shows large crystals and microcrystal aggregates typical of mature *P. mirabilis* biofilms observed in catheters removed from infected patients.[39]

2.3.3 Preparation of proof-of-concept prototypes

Silicone prototype samples (Dragon Skin 0020 and Ecoflex 0050, Smooth-On, Inc.) were prepared by pouring approximately 10 mL of silicone into a mold prepared by a 3D printer (Dimension sst 1200es, with patterns generated using Solidworks 2011, Figure 11).

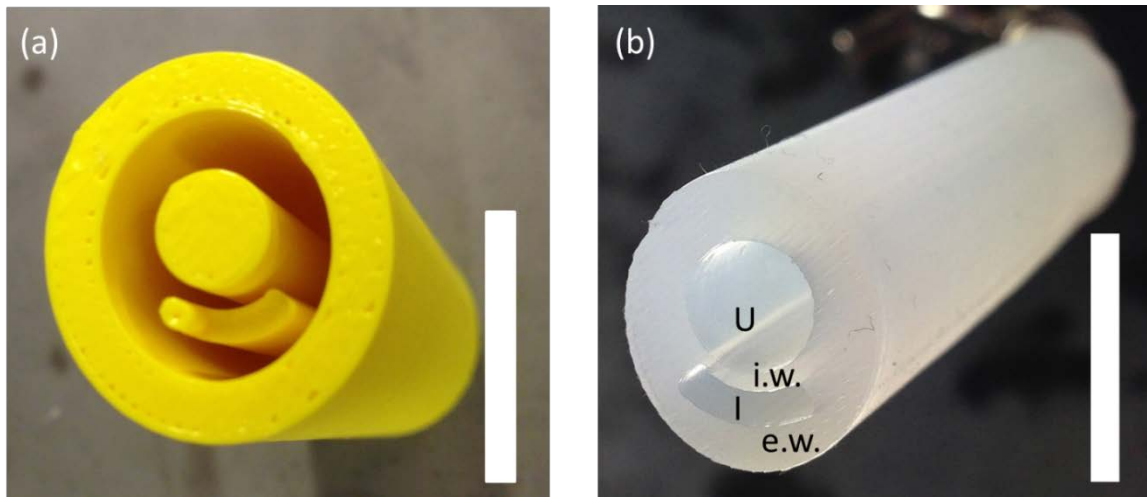


Figure 11: Construction of an active fouling release, proof-of-concept prototype of a section of silicone urinary catheter. (a) 3D printed mold patterns were generated using Solidworks 2011 and then printed on a Dimension sst 1200es 3D printer. Silicone (Dragon Skin 0020 or Ecoflex 0050) was poured into the mold and (b) resultant silicone prototypes were removed from the mold upon curing. “U” denotes the main urine drainage lumen, “I” denotes the inflation lumen, “i.w.” denotes the inflation wall, and “e.w.” denotes the external wall. The inflation lumen was sealed at the ends of the prototypes before experimentation. When using Dragon Skin 0020 silicone, the ratio of external wall to inflation wall thicknesses shown (approximately 3:1) was sufficient to direct inflation inwards. When using Ecoflex 0050 silicone, prototypes required an additional inelastic sheath to prevent bulging of the external wall. Ecoflex 0050 was chosen for *in vitro* biofilm testing due to its superior pour performance and consistently successful molding. Scale bar represents 1 cm.

Silicone was degassed for three minutes prior to pour. Once cured, prototypes were removed from the molds and then the inflation lumens were sealed with additional silicone. Dragon Skin 0020 silicone prototypes were used for modeling and initial characterization including video and image analysis of inflation profiles in combination with pressure and volume measurements. Ecoflex 0050 silicone samples were also characterized, and then used for biofilm growth due to Ecoflex 0050's superior pour performance and more consistently successful molding. Before biofilm growth, the samples were sterilized in a biosafety cabinet by rinsing with 95% ethanol and sterilized water.

2.3.4 Biofilm growth

The drain of a drip flow reactor (BioSurface Technologies Corporation) was modified to keep flat silicone coupons submerged in 0.3 – 0.6 cm media while under flow (Figure 10). The reactor and all associated supply and drain tubing were sterilized and placed in a Class II biosafety cabinet. The reactor was maintained at 37°C by placing it in a mini-incubator. AUM was introduced using a peristaltic pump to prime the flow system. The samples in the reactor were infected with 10 mL of the 4 hour *P. mirabilis* culture and the infected culture was left for 1 hour to allow bacterial attachment before the media supply was resumed. The model was run continuously at a flow rate of 0.5 mL min⁻¹ until the desired time point, or a system blockage occurred.

Biofilms on proof-of-concept prototypes were grown using the same flow loop and method, but the drip flow reactor was replaced with a manifold of four artificial bladders in a vertical orientation (Figure 12). The bladders were maintained at 37°C by a mini-incubator. The bladders each held a 30 mL reservoir of infected media that would overflow into glass tubing and then drip-feed through the prototypes as fresh media was added to the bladder. Again, the model was run continuously at a flow rate of 0.5 mL min⁻¹ until the desired time point, or a system blockage occurred.

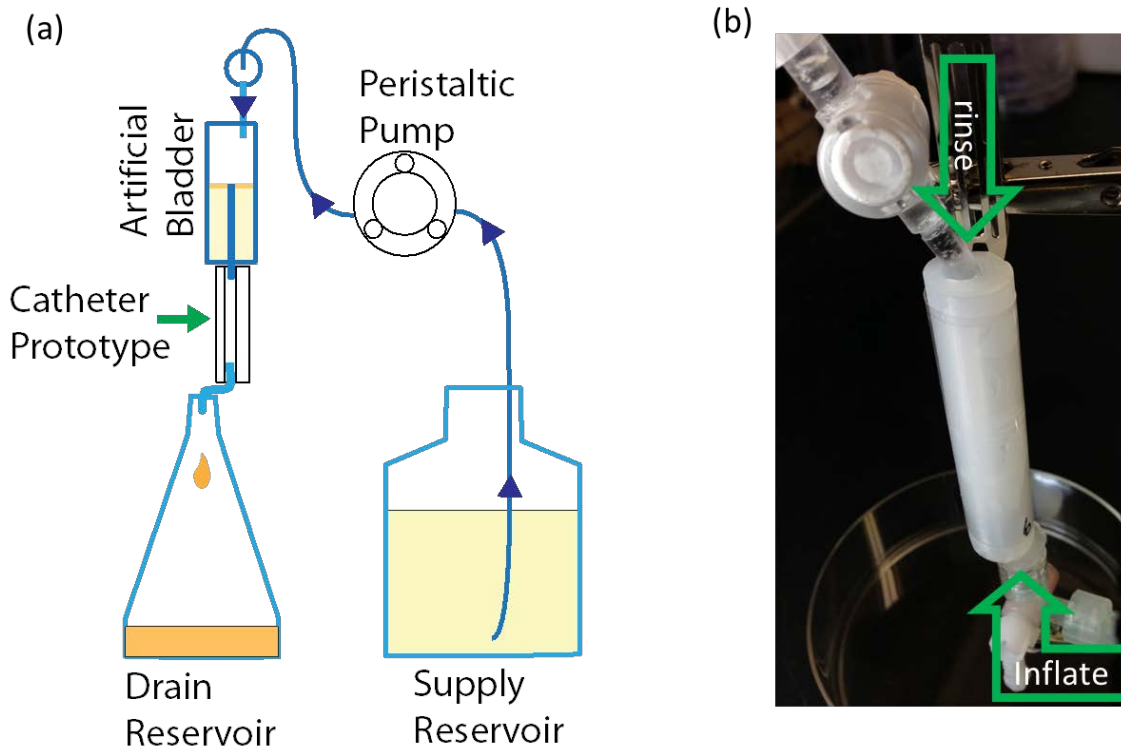


Figure 12: Biofilm growth and testing setup for urinary catheter proof-of-concept prototypes. (a) Schematic of biofilm growth system that uses an “artificial bladder” [14] to supply infected urine to the proof-of-concept prototypes. The artificial bladder is a vessel modified with a glass tube penetrating the bottom and extending approximately 4 cm into the vessel, which thereby maintains a residual volume of 30 mL in the artificial bladder. The artificial bladder and prototypes were inoculated with a 4 hour culture of *P. mirabilis*. After allowing the bacteria to adhere for 1 hour, artificial urine with 1% tryptic soy broth was pumped at 0.5 mL min^{-1} into the artificial bladder and through the prototypes. As artificial urine media was fed into the artificial bladder the media overflowed into the glass tube, where it then fed down the main drainage lumen of the catheter prototypes. The bladder and prototypes were maintained at 37°C by mini-incubator. A mature crystalline biofilm grew over approximately 42 hours. (b) Rinsing test setup for prototypes after biofilm growth. After carefully removing the prototypes from the biofilm growth system, a DI water rinse supplied at 4 mL min^{-1} flowed downward through the prototype main urine drainage lumen for 1 minute. Prototypes designated for actuation were hydraulically inflated 10 times at a rate of 0.1 s^{-1} approximately 30 seconds into the rinse. Hydraulic inflation was applied to the inflation lumen

through an inflation port fixture on the bottom end of the prototype. The rinse effluent was collected for analysis and the prototype was then removed for inspection.

2.3.5 Strain and inflation testing

Biofilm-covered silicone coupons were removed from the reactor and kept covered in a hydrated state. The coupons were carefully sliced longitudinally to bisect the coupon (12mm x 75mm) while avoiding disturbance of the biofilm. Resultant samples were stretched to the desired strain percentage at controlled strain rates; samples were spritzed with DI water to maintain hydration during strain testing. The gauge length was 5 cm, and the sample was 1.2 cm wide. Samples were subjected to 10 strain cycles and representative videos and images were captured during testing. Two different stretchers were required to apply strains across the range of strain rates. A tensile tester with grips oriented vertically (LRX Model 400c) was used for strain rates of 0.01 and 0.2 s⁻¹ (velocities of 0.2 and 1 cm s⁻¹); while a syringe pump modified with additional clamps was used for the slowest and fastest strain rates 0.04 and 0.4 s⁻¹ (velocities 0.05 and 2 cm s⁻¹) due to speed limitations of the LRX tensile tester (see dashed and solid lines, respectively, in Figure 15).

Once strain tested, samples were immediately submerged in DI water and subjected to 4 mL min⁻¹ flow for 1 minute. Samples were then stained with 0.01% crystal

violet for 10-15 minutes and rinsed 3 times with DI water. Each sample was imaged at least 6 times (at center of sample to eliminate edge effects), and each image was analyzed using ImageJ version 1.43u (<http://rsbweb.nih.gov/ij/>). ImageJ's threshold function was used to render each greyscale image into a binary image with distinct areas with and without biofilm. The images were then each measured for biofilm area coverage, and the images' area coverage was averaged for each sample.

Proof-of-concept prototype samples were removed from the reactor and kept covered in a hydrated state. The samples were mounted vertically, and DI water was introduced from the upper end at 4 mL min⁻¹ flow for 1 minute (Figure 12). Samples intended for inflation were inflated 10 times at 0.1 s⁻¹ to 35% strain approximately 30 seconds into the 1 minute rinse. Inflation was conducted hydraulically using a syringe-delivered pre-determined volume of water. Control and inflated samples were stained with crystal violet, rinsed with DI water at 4 mL min⁻¹ flow for thirty seconds and then filleted open for examination.

2.3.6 Rheology tests of biofilms and substrates

Circular pieces (8 mm) were punched out of biofilm-covered silicone coupons and sweep tested on a flat-plate rheometer (Rheology Advantage Instrument ARG2, USA). During the tests, the applied strain was controlled to oscillate from 0 to 0.02. Bare silicone pieces (without biofilm covering) were separately tested as controls; their

storage and loss modulus values were subtracted from the biofilm-covered samples to isolate biofilm storage and loss modulus values. The modulus of biofilms and the substrates are presented in Figure 16.

2.4 Results

2.4.1 Concept for urinary catheter with active fouling-release

As shown in Figure 13, we conceived a urinary catheter that uses regio-selective actuation of soft elastomers to actively debond biofilms from its inner surfaces (Figure 13a-c). The debonded biofilm can then be removed by a minimal flow (e.g., of urine), thereby removing any biofilm obstructions and clearing the urine drainage lumen. We grew crystalline biofilms on proof-of-concept prototypes and actuated the prototypes to debond and remove the biofilm (Figure 13f, g). While multiple inflation lumens are feasible for urinary catheter manufacturing (Figure 13a-d), we used a single intra-wall lumen to demonstrate the concept (Figure 13e-g). The actuation was achieved on the luminal surface through inflation of an intra-wall lumen that is separated from the main drainage lumen by a thin wall. When sufficient pressure is applied to the intra-wall lumen(s), the thin wall stretches and generates strain on the luminal surface (Figure 13c; see also additional actuation description in Section 2.4). We first experimentally and theoretically explored the substrate-strain induced debonding of an infectious crystalline

biofilm, and then used that understanding to develop a proof-of-concept prototype of a section of an active, fouling-releasing catheter.

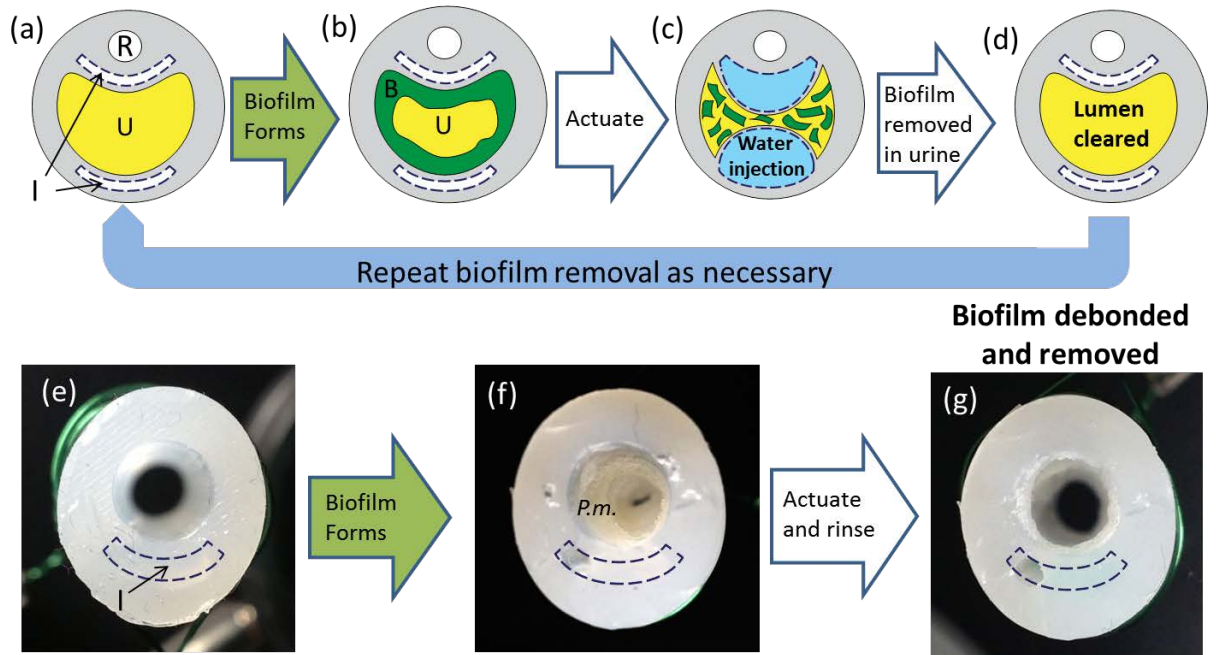


Figure 13: A conceptual schematic of the active fouling release urinary catheter and demonstration of proof-of-concept prototypes. (a) Cross section of urinary catheter before biofilm formation where R, U and I represent the restraint balloon lumen, main urine drainage lumen and inflation lumens. (b) Biofilm, denoted as B, forms on the drainage lumen. (c) Reversible actuation of the lumen via water inflation debonds the biofilm formed in the urine drainage lumen. (d) Debonded biofilm is carried away in the urine resulting in a cleared lumen thereby reducing risk of symptomatic infections. Optical images of proof-of-concept prototype cross sections (e) before biofilm growth, (f) after growth of a mature *P. mirabilis* crystalline biofilm (*P.m.*) in the drainage lumen, and (g) after actuation and a gentle rinse debonded and removed the biofilm

2.4.2 Uniaxial strain debonds mature *P. mirabilis* crystalline biofilms

Before the implementation of the design in a model of a catheter, we first tested the hypothesis that active surface deformation can effectively detach crystalline urinary biofilms using flat elastomer coupons. We developed an *in vitro*, flat, biofilm-growth configuration to facilitate quantitative measurement of the biofilm area coverage and mechanical properties. *Proteus mirabilis* was grown on silicone substrates in a modified drip flow reactor [81] where the silicone substrate was submerged to simulate physiological conditions in a conventional silicone urinary catheter (Figure 10a, b).

We chose DragonSkin20 silicone (Smooth on, USA) to fabricate the flat silicone substrate coupons due to the similarity in mechanical properties (tensile modulus approximate 0.2 MPa) to those in commercial all-silicone catheters.[79] Artificial urine supplemented with 1% tryptic soy broth was peristaltically pumped through the reactor at 0.5 mL min^{-1} for 48 hours, or until the drainage tubing occluded (average time: 42 hours). The resultant biofilm included crystal deposition typical of the mature crystalline biofilms observed in occluded catheters removed from patients (Figure 14a, Figure 10c). SEM analysis revealed the large crystals and microcrystalline aggregates that are similar to struvite and apatite crystals typically seen on SEM images of cross sections of occluded catheters (Figure 10c).[39] The biofilm thickness ($0.57 \pm 0.07 \text{ mm}$) was measured by quantifying microscope height adjustment as the focus was adjusted from the substrate to the top of the biofilm. It was comparable to the thickness required

to block catheters in previous *in vitro* studies.[27, 82, 83] To our knowledge, this study presents the first growth model for a mature crystalline biofilm in a flat configuration, which was then used to study biofilm debonding and biofilm mechanical properties.

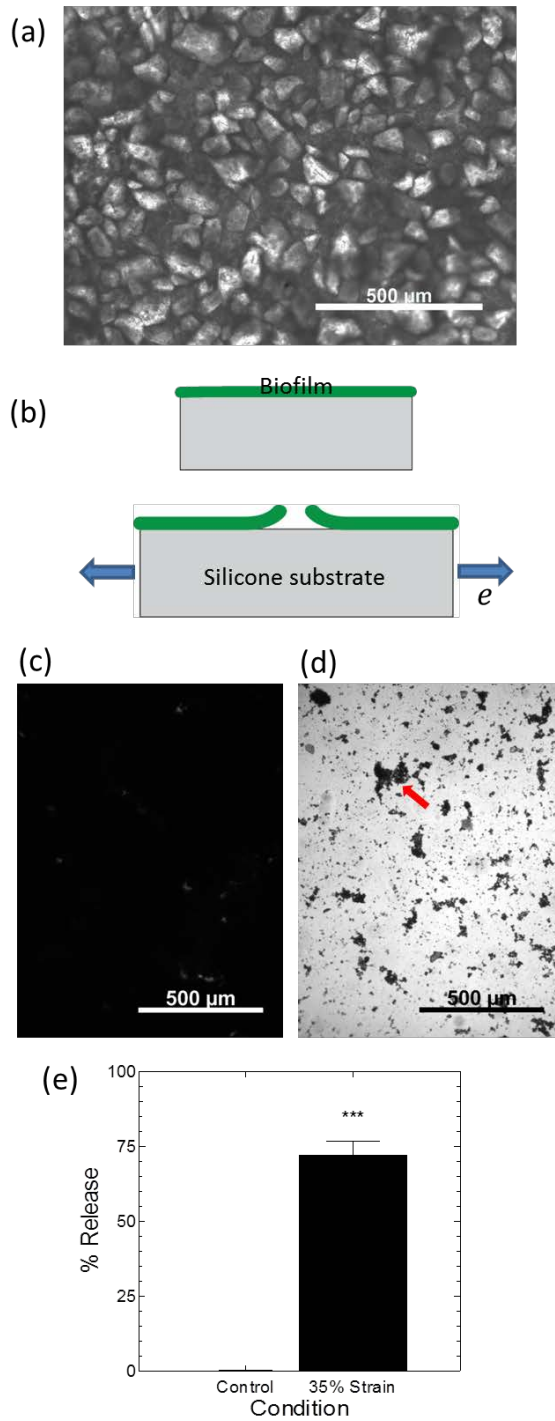


Figure 14: Debonding of mature *P. mirabilis* crystalline biofilms due to strain applied to flat silicone substrates. (a) Optical microscopy image of a crystalline biofilm on a flat silicone substrate. (b) Diagram (side view) illustrates tensile strain

applied to the substrate causing biofilm debonding. Optical microscopy images of biofilm-covered silicone substrates (c) after rinsing and staining with crystal violet, or (d) after actuation to 35% strain 10 times (at 0.2 s^{-1}) before rinsing and staining. The arrow indicates an example residual island of stained biofilm that remained on the silicone substrate. (e) Image analysis of biofilm area coverage confirmed that 10 cycles of 35% substrate strain caused detachment of *P. mirabilis* biofilm. Data represents mean \pm standard error of the mean, N=3-4.

We carefully removed the flat silicone samples from the reactor to avoid disturbing the integrity of the crystalline biofilm. Uniaxial strain was applied to the silicone substrates using methods similar to those established in our previous study.[69] We clamped the silicone at both longitudinal ends on a horizontal mechanical stretcher (Figure 14b), and applied strain to the silicone substrate at a rate of 0.2 s^{-1} . The samples were stretched to 35% strain 10 times, unclamped, submerged in DI water and rinsed at 4 mL min^{-1} for 1 minute. We removed the samples from the DI water and then crystal violet stained (0.1%) the biofilm for 10-15 minutes before two additional water rinses.[84] Crystal violet effectively stained and allowed quantitative assessment of the area coverage of the biofilms (Figure 14c, d).[85] The samples were imaged along the longitudinal midline, and the images were characterized for biofilm area coverage by use of image analysis to estimate the fraction of pixels in the image corresponding to crystal violet stained biofilm. We note that in the discussion here and below, the term “biofilm area coverage” is a conservative indicator of the actual amount of biofilm debonded from the sample surface because local cohesive failure of the biofilm can

result in the bulk of the material being shed from the surface while small amounts of stainable biofilm are retained at the substrate surface. The 35% straining regimen applied to the substrate resulted in a reduction in the biofilm area coverage of the silicone surface of 72% (Figure 14c, d and e). These data suggest that at least 72% of the crystalline biofilm detached from the samples, and we emphasize again here that this number is a conservative indication of the amount of biofilm removed (especially when considering the > 0.5 mm thickness of the initial biofilm). These results are consistent with our previous studies which showed that straining of an elastomer can result in detachment of mucoid biofilms formed by *Escherichia coli* and *Cobetia marina*, a marine bacterium.[69] Interestingly, Limbert *et al.* recently conducted finite element analysis predicting biofilm debonding due to substrate micromotion caused by tension, torsion, or bending but did not provide experimental results to confirm their predictions.[86] The current work represents the first experimental observation of active debonding of a mature, crystalline biofilm (>24 hrs old) by strain applied to an elastomeric substrate.

2.4.3 High strain and strain rate result in debonding of mature *P. mirabilis* crystalline biofilms

We next studied the effects of applied strain and strain rate on the debonding of *P. mirabilis* crystalline biofilms from flat silicone substrates. For strains ranging from 0 to 100%, the strain rate was varied across a wide range, from 0.01 – 0.4 s⁻¹; each sample was strained 10 times at its designated strain rate. As shown in Figure 15a, both the applied

strain and the strain rate are important in eliciting the debonding of crystalline biofilms. At relatively high strain rates (i.e., 0.2 and 0.4 s⁻¹), significant amounts of biofilm are debonded (i.e., over 70%, measured using crystal violet staining as described above) as the applied strain reaches critical values (e.g., 20% - 30%). However, at relatively low strain rates (i.e., 0.01 and 0.04 s⁻¹), the debonded biofilm area is insignificant (i.e. less than 10%), even when the substrate is under strains up to 100%.

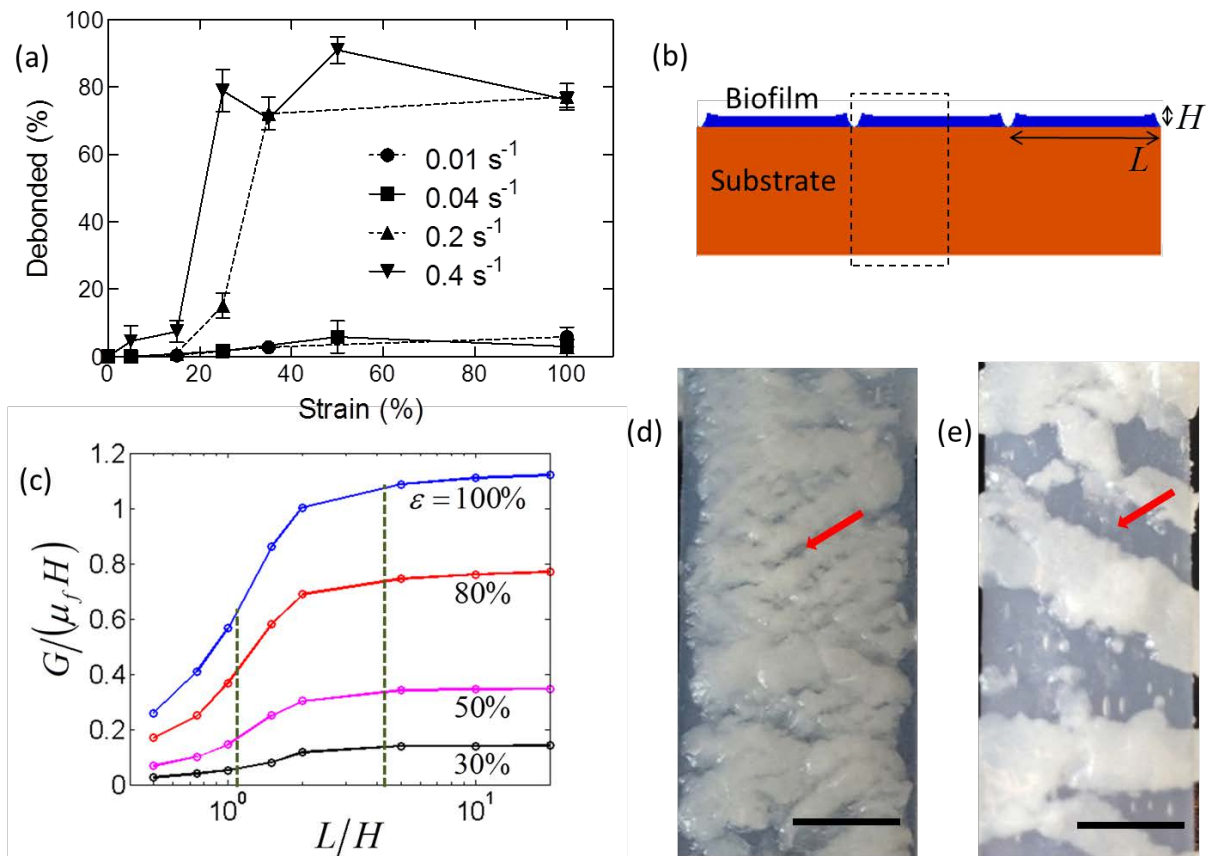


Figure 15: Increased debonding of mature *P. mirabilis* crystalline biofilms due to increased strain rate. (a) The percentage of biofilm area covering the substrate (see text for details) after straining (10 times) at various strain rates. Experiments were conducted for 2 - 4 replicates per condition. Dashed lines indicate strain testing using LRX tensile tester and solid lines indicate strain testing using modified syringe pump. Data represents mean \pm standard error of the mean. (b) Diagram of biofilm height, H , and segment length, L , used for (c) modeling the driving force for biofilm debonding as a function of L/H . Dashed vertical lines indicate normalized segment length for 0.01 s^{-1} and 0.4 s^{-1} strain rates that were measured from optical images during 100% strain at (d) 0.01 s^{-1} and (e) 0.4 s^{-1} . Arrows indicates examples of cracked biofilm or areas of silicone substrate exposed by debonded biofilm. Scale bars indicate 5 mm.

We measured the storage and loss moduli of the crystalline biofilms with a frequency sweep rheometer. Although biofilms are typically viscoelastic,[87, 88] we found that the mature crystalline biofilms generated by *P. mirabilis in vitro* appeared to be predominantly elastic (Figure 16a), with a constant storage modulus G' of approximately $1.5 \times 10^4 Pa$ for low sweep frequencies (0.1 – 6 Hz) that was also higher than the loss modulus (approximately $4.5 \times 10^3 Pa$).[89]

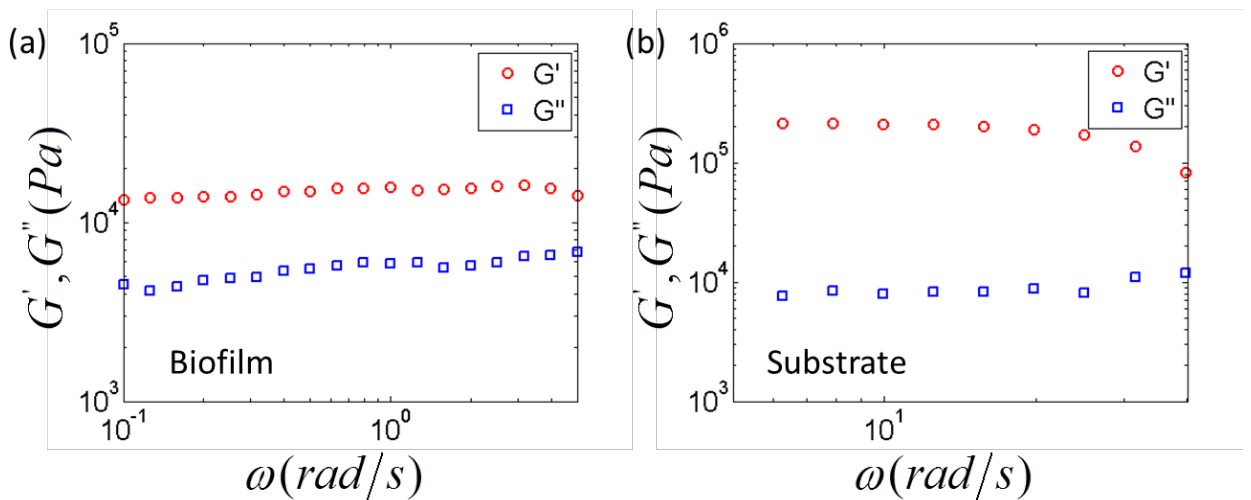


Figure 16: Storage modulus G' and loss modulus G'' of mature *P. mirabilis* crystalline biofilms and the silicone substrate as a function of frequency. (a) *P. mirabilis* crystalline biofilms appeared to demonstrate predominantly elastic properties; the storage modulus was higher than the loss modulus and was relatively constant over the frequency range tested.[90] (b) Storage and loss moduli of silicone substrate.

Pseudomonas auregenosa biofilms have demonstrated similar predominantly elastic properties within the same frequency range,[89, 91] but the storage modulus of

mature *P. mirabilis* crystalline biofilms ($\approx 1.5 \times 10^4 \text{ Pa}$) was higher than that measured by Lahaye *et al.* for *P. mirabilis* biofilms (G' of $0.9 - 1.0 \times 10^3 \text{ Pa}$).[92] The higher storage modulus is likely due to the integration of rigid crystals in the biofilms; similar phenomena of modulus enhancement have been observed in rigid particle filled polymers.[93, 94] Lahaye and coworkers only tested the proteinaceous component of *P. mirabilis* biofilms and did not use growth media that would support crystal generation.[92] While a wide range of viscoelastic properties for biofilms have been reported, overall the storage modulus of mature crystalline *P. mirabilis* biofilms is 1 – 3 orders of magnitude greater than other clinically relevant biofilms.[90, 95]

To better understand the effects of applied strain rates on the debonding of biofilms, we then developed a theoretical model that relates the fracture of biofilms into segments to the segments' subsequent debonding from the substrate. With a mature biofilm attached on the substrate, we stretched the substrate at a specified rate. Upon stretching, the biofilm first formed channel-like cracks, which then branched to form fragmented segments of biofilm with an average length, L . [96] Upon deformation of the substrate, cracks nucleated at the bottom of each segment, propagated through the interface between the biofilm and the substrate, and eventually debonded the biofilm from the substrate. We constructed a simplified, 2D, plane-strain model of the system of biofilm segments on the elastomer substrate as illustrated in Figure 17b. The biofilm and substrate were modeled as Neo-Hookean materials; the shear moduli (μ_f for the

biofilm and μ_s for the substrate) were extracted from the measured storage moduli at near-zero frequency (Figure 16).[97] The thickness of the substrate was taken to be much larger (>20 times) than that of the biofilms, H . Considering the periodicity and symmetry of the model, only half of one biofilm segment was analyzed, as indicated in the dashed box in Figure 3b. The energy release rate G (not to be confused with G' and G'' storage and loss moduli) was computed by a commercial finite element package Abaqus 6.10.1 (SIMULIA, USA). The modelling results suggest that the average segment length L plays a critical role in the biofilm debonding process.

As shown in Figure 17, the normalized energy release rate, $G/(\mu_f H)$, which is the driving force for biofilm debonding,[98] increases with the normalized segment length, L/H , for various applied strains in the substrate. These curves can be qualitatively understood as follows: if the biofilm segment length is very small, the segments can be regarded as tall plates vertically attached on the substrate, which result in a relatively low energy release rate.[99] When $L/H \rightarrow 0$, the driving force for biofilm debonding $G/(\mu_f H) \rightarrow 0$. On the other hand, if the biofilm segment is infinitely long, it can be regarded as a film attached on the substrate. Therefore, when $L/H \gg 1$, the driving force for biofilm debonding approaches its maximum, i.e., $G/(\mu_f H) = [(1 + \varepsilon)^2 + (1 + \varepsilon)^{-2} - 2]/2$.[69, 100] Therefore, the driving force for biofilm debonding increases with biofilm segment length, from 0 for very narrow segments to a plateau of $[(1 + \varepsilon)^2 + (1 + \varepsilon)^{-2} - 2]/2$ for very wide segments.

We noted that images gathered during strain testing revealed differences in typical segment length (Figure 17d, e) that correlated to strain rate. Actuation with low strain rates (i.e., 0.01 and 0.04 s⁻¹) tended to fracture the biofilm into small segments that maintained attachment on substrates (Figure 15e), while high strain rates (i.e., 0.2 and 0.4 s⁻¹) resulted in relatively large pieces of biofilms that were easily detached (Figure 15d, e; both samples at 100% strain). We quantified the segment length at 100% strain for different loading rates from representative images (Figure 17), which confirmed that segment length increased monotonically as strain rate increased over the conditions studied.

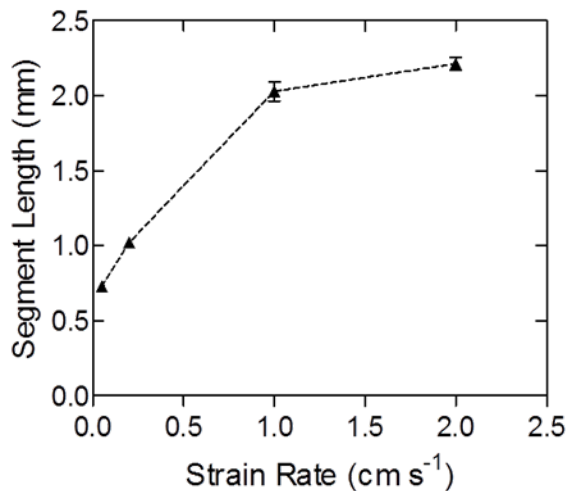


Figure 17: Segment length increases with increasing strain rate. Segment length from representative images at 100% strain (such as those in Figure 3 B and C). Five lines were drawn lengthwise (equally spaced along the width of the sample) on each image, and segment length was measured along the lines using ImageJ. Error bars provide the standard error of the mean of greater than 30 measurements per image.

In Figure 15c, the dashed lines are the measured segment lengths for highest and lowest strain rates at 100% strain. The larger segment length ($L/H \approx 4.2$), given by the highest strain rate, correlates to a sufficiently high driving force to debond most of the biofilm from the substrate. Conversely, the smaller segment width ($L/H \approx 1$) for the lowest strain rate correlates to a low driving force for debonding that is not large enough to detach the biofilms from the substrate. As a result, the high strain rates lead to a higher percentage of debonded biofilm, while low strain rates debond low percentages of biofilm. The current study gives the first demonstration that the rate of the strain applied to the substrate significantly influences biofilm debonding, and the calculated relationship of segment length to debonding driving force represents a macro-scale interpretation of the effect of strain rate.

2.4.4 Development of a proof-of-concept prototype urinary catheter incorporating substrate deformation via intra-wall inflation

Our interest in debonding crystalline biofilms was motivated by the desire to translate the active biofouling management method [69] into tubular devices such as urinary catheters. We first applied strain axially to tubular silicone substrates to debond crystalline biofilms that were grown within their lumens (Figure 18).

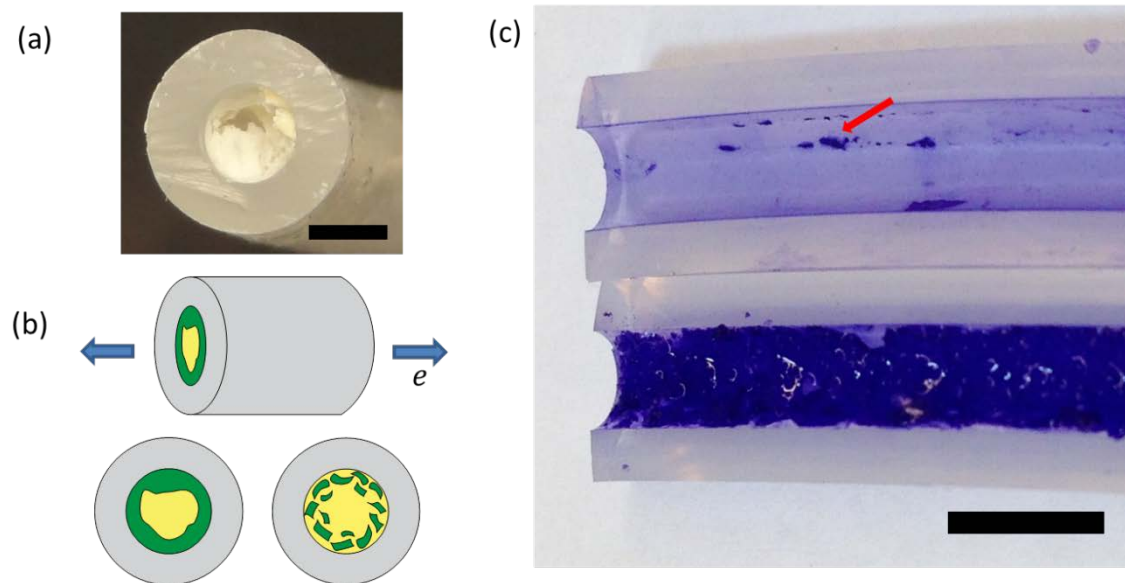


Figure 18: Debonding of mature *P. mirabilis* crystalline biofilms via applied strain to silicone tubing substrates. (a) Representative image of crystalline biofilm occluding a portion of silicone tubing. Using similar growth methods to the flat configuration, mature crystalline biofilm was grown in silicone tubing (6.35mm inner diameter silicone tubing, VWR). Bar indicates 2.5 mm. (b) Diagram of how tensile strain applied to substrate debonds a biofilm within a tube. Unidirectional strain was applied axially. (c) Image of sliced tubing sample subjected to 50% strain 10 times (top) and unstrained control (bottom) after rinsing. Arrow indicates example of remaining islands of biofilm of partial-thickness. Strained samples were stretched at 1.7 cm s^{-1} using a LRX tensile tester. Samples were then rinsed at 4 mL min^{-1} before crystal violet staining. SEM comparison of flat and tubular silicone surfaces used for these experiments confirmed similar surface topographies. Scale bar indicates 5 mm.

Application of an axial strain (50% strain at a rate of 1.7 cm s^{-1}) effectively debonded the intra-luminal crystalline biofilms (Figure 18c). While this result demonstrates effective biofilm debonding, applying strain axially by extending the length of a catheter might not be practical in a point-of-care setting.

In order to incorporate our methods for biofilm release into technologies suitable for implementation in healthcare settings, we suggest another catheter design capable of actively debonding urinary biofilms by applying hydraulic actuation within a catheter. We conceptualized a method, similar to those used in the implementation of pneumatic networks for soft robotics,[76] to apply strain to the catheter solely along its luminal walls, where the strain would debond urinary biofilms on the luminal surfaces without affecting the external dimensions of the catheter. Figure 19 shows a schematic of a proof-of-concept prototype catheter cross section with an *intra-wall* lumen separated by a thin wall from the main, urine drainage lumen. As pressure is increased in the intra-wall lumen, it inflates and the thin wall deforms and the main luminal surface strains, until it impinges on the opposite wall of main lumen (Figure 19b).

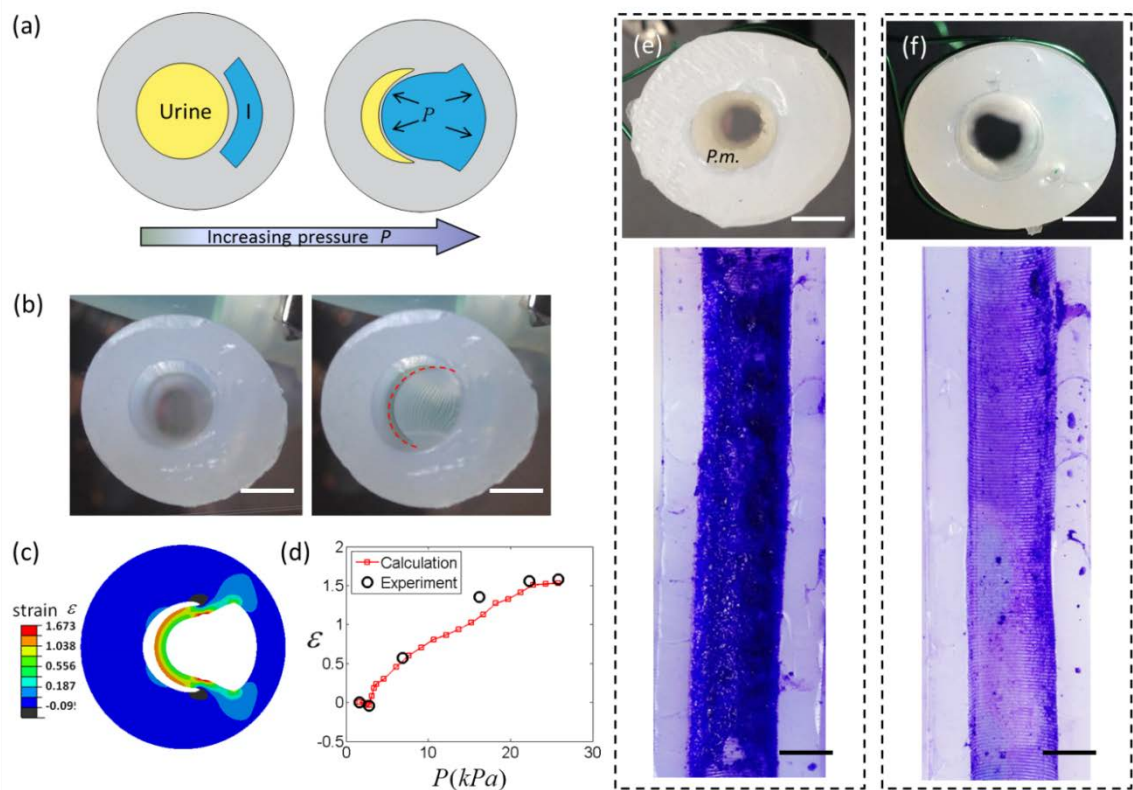


Figure 19: Proof-of-concept prototype urinary catheters debonding mature *P. mirabilis* crystalline biofilms using inflation-generated strain at urinary lumen surface. (a) Schematic diagram of the prototype catheter (cross section). Increased pressure in intrawall, inflation lumen, I, causes wall to stretch into the urine drainage lumen. (b) Cross-sectional views of prototypes before and after inflation. Dashed red line outlines the inflated luminal surface. (c) Maximum principal strain at the luminal surface was calculated using finite element modeling. (d) Experimental and calculated luminal surface strain as a function of inflation pressure for Dragon Skin 0020 prototypes. Representative optical images from 3 - 4 replicates of (e) un-inflated control prototypes rinsed at 4 mL min^{-1} for 1 min, and (f) prototypes inflated 10 times at 0.1 s^{-1} during rinsing demonstrate biofilm removal from actuated prototypes. Cross section of control (e) shows substantial biofilm coverage (*P.m.*) after rinsing. Prototypes were stained with crystal violet and sliced open, and biofilm was removed along the length of the inflated area of the luminal surface of actuated prototypes. Scale bar indicates 2.5 mm.

To make physical, proof-of-concept models (herein referred to as prototypes) of sections of such a urinary catheter, we constructed molds for pourable silicone using 3D printing (Figure 11) which allowed rapid, iterative prototype development. Our early proof-of-concept prototyping efforts varied intra-wall luminal shape and position, and confirmed that using circular intra-wall lumens or crescent intra-wall lumens positioned too far from the main lumen resulted in non-specific wall deformation. We achieved preferential deformation of the wall between the inflation and main lumen into the main lumen by constructing thicker external walls. Figure 19b shows uninflated and pneumatically inflated prototypes. We then numerically calculated the strain within the cross-section of the prototypes using the finite element package Abaqus, while assuming the silicone was an Arrude-Boyce material [94] with a shear modulus μ_s of 221 kPa (Figure 20).

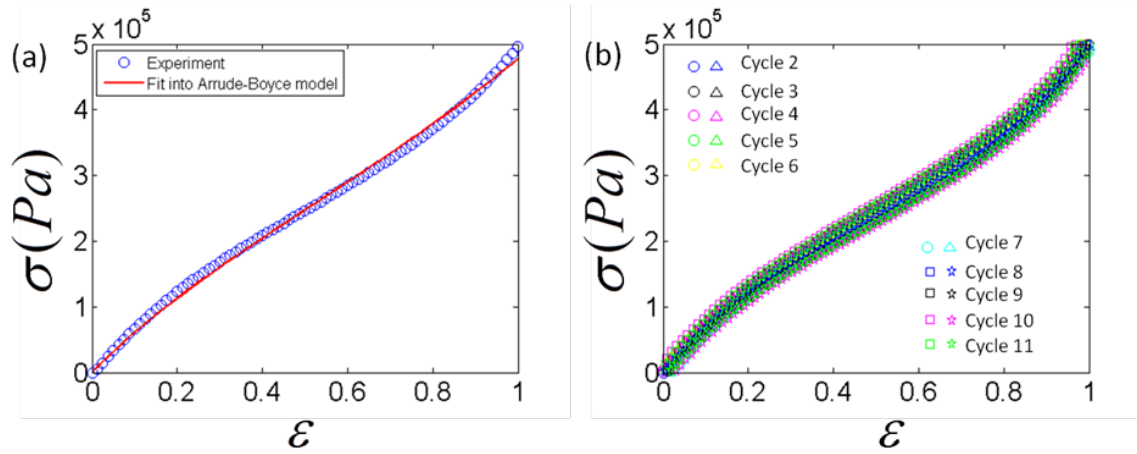


Figure 20: (a) Nominal stress *vs.* strain curve of Dragon skin 0020 was fit to the Arrude-Boyce model, $\sigma = \mu_s(\lambda - \lambda^{-2})(1 + \frac{I}{5n} + \frac{11I^2}{175n^2} + \dots)$, where σ and $\lambda = 1 + \epsilon$ are the nominal stress and stretch for uniaxial tension, $I = \lambda^2 + 2\lambda^{-1}$, and n is a parameter that accounts for the stiffening effect.[94] The fitted shear modulus is $\mu_s = 221$ kPa, and the exponent was fitted as $n = 0.27$. (b) Cycling test of Dragon skin 0020 shows negligible hysteresis after the first strain loading cycle. Silicone samples (flat and proof-of-concept prototypes) were prestrained or preactuated at least once prior to experimentation.

Model results confirmed that the inflated wall can easily achieve substrate strains sufficient to debond crystalline biofilms (e.g., greater than 30% strain, Figure 3a) over an area corresponding to approximately 40% of the perimeter of the main lumen of the prototype (Figure 19c). We again used Abaqus to calculate the inflation pressures necessary to achieve given amounts of wall strain, and the model matched well with experimental data (Figure 19d). Inflation occurred along approximately 70% of the length of the prototype catheter sections, and was limited by our methods for sealing the inflation lumen of the prototypes. No prototypes experienced failure due to wall-tears

and no hysteresis was observed (Figure 20). We were able to attain complete inflation and deflation within 1 second. Prototypes were easily inflated pneumatically or hydraulically, and strain was controllable through pressure or volume control (Figure 19d and Table 1).

Table 1: Hydraulic inflation profile for proof-of-concept prototypes of urinary catheter sections.

Inflation Volume (mL water)	Strain (%)
0	0.0
1	13.0
1.3	34.7
1.6	38.8
1.7	39.1

2.4.5 Proof-of-concept prototypes utilizing intra-wall inflation debond mature *P. mirabilis* biofilm

We modified the artificial bladder biofilm growth model pioneered by Stickler and coworkers [14] to feed infected artificial urine downward through prototypes (Figure 12 for flow schematic) at a rate of 0.5 mL min^{-1} , and after approximately 42 hours achieved uniform biofilm distribution around the perimeter and down the length of the main lumen (see Figure 19e for control sample).

We switched to the artificial bladder growth system from the drip flow reactor system because the drip flow reactor mounting fixtures caused bubble formation and subsequent non-uniform biofilm growth in the prototypes. Once a mature biofilm formed on the prototypes, we carefully removed the prototypes from the growth model before rinsing them at 4 mL min^{-1} for 1 minute (Figure 12b). We note that, although urine voiding reaches quite high flow rates, catheters are always “open”, and therefore flow rates are dominated by urine *production* rates. Normal urine production rates vary from $0.5 - 1.7 \text{ mL min}^{-1}$, but oral water loads of $8 - 12 \text{ mL kg}^{-1}$ (i.e., $560 - 840 \text{ mL}$ for a 70 kg individual) can cause urine production rates in excess of 10 mL min^{-1} . [101] A rinse rate of 4 mL min^{-1} is well within the urine production rates achievable through oral loading.

Thirty seconds into the rinse, prototypes designated for inflation were inflated 10 times to 35% strain at approximately 0.1 s^{-1} . The 10x inflation cycles, quite dramatically, produced visible biofilm debris in the effluent (Figure 21a and Video S1) and subsequent examination of the cross section showed that a large portion of the biofilm was removed (see Figure 19f for a representative cross section).

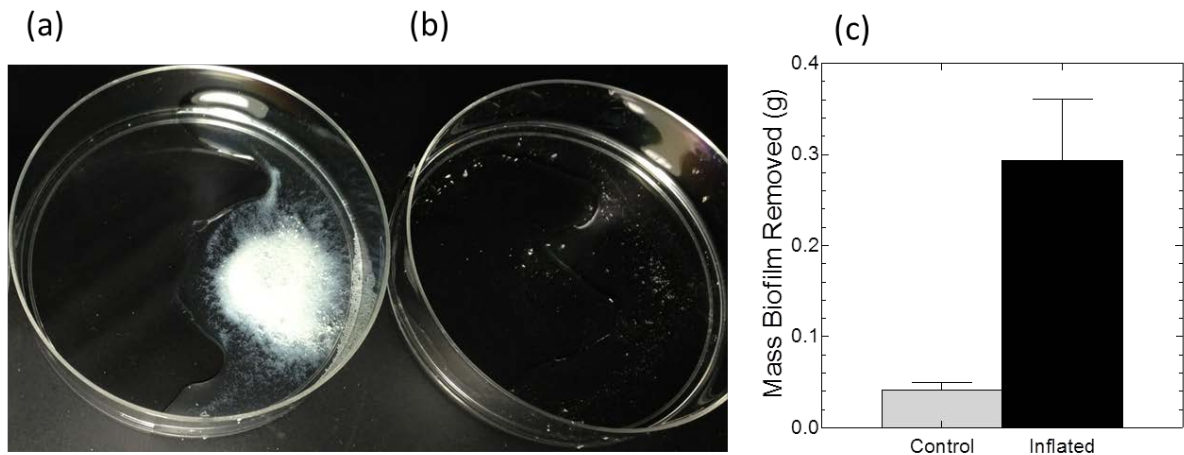


Figure 21: Dramatic release of biofilm into the effluent from inflated proof-of-concept prototype urinary catheters. (a) Representative optical image of effluent from 3 prototypes each actuated 10x during rinsing (4 mL min^{-1} through the prototype main urine drainage lumen for 1 minute); effluent contained visible biofilm debris. (b) Representative effluent from 2 un-actuated control prototypes had minimal biofilm debris, implying that control prototypes retained biofilm after rinsing alone. (c) The effluent was collected, centrifuged, and the excess liquid was aspirated. Figure shows hydrated mass of biofilm collected. Data represents mean \pm standard error of the mean.

No “backflow” was observed (i.e., the inflation did not cause fluid to eject/flow out the top of the prototype). Biofilms in control and inflated prototypes were stained with crystal violet before the prototypes were sliced open. We confirmed that biofilm had been removed from strained areas (Figure 19f) while biofilm remained bonded to the unstrained areas. We then analyzed microscopic images of the biofilm area coverage using ImageJ and confirmed significant biofilm removal (approximately 84% of the biofilm removed from strained areas of the lumen vs. 7% removed from unstrained areas; Figure 22).

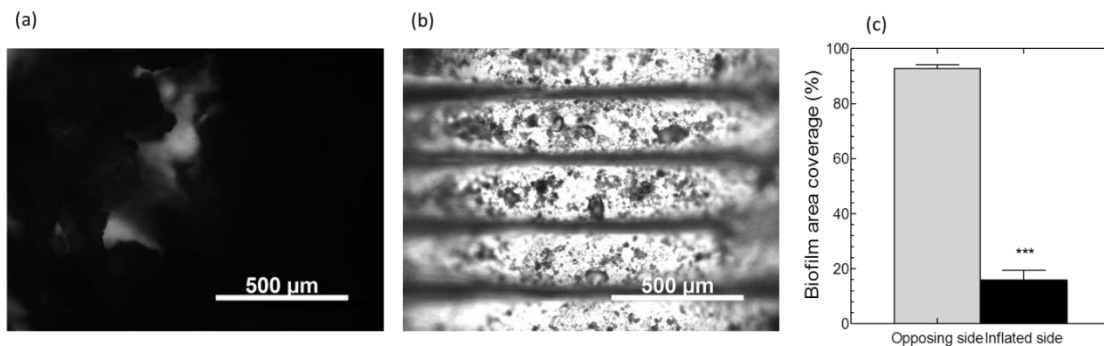


Figure 22: Microscopic observation of debonding of biofilm from the main urine drainage lumen of catheter section prototypes. (a) Microscope image of surface of control prototype main lumen covered with biofilm after rinsing and (b) Microscope image of inflated prototype main lumen with biofilm removed after inflation and rinsing. Note: Horizontal bars visible across the inflation wall are “ribs” around the lumen that are due to the 3D printing process used to form the mold. (c) ImageJ was used to analyze the images, and statistical comparison to the opposing side of the catheter lumen showed that inflation debonded the biofilm from the area of the luminal wall subjected to inflation. Comparison was statistically significant both with ($p < 0.006$) and without ($p < 0.0009$) rib artifacts removed from images. Data represents mean \pm standard error of the mean, $N=4$.

Again, area coverage measurements appeared to understate the magnitude of biofilm removal, so the effluent collected during the rinse/inflation test was assessed for biofilm mass (Figure 21c). An average of 0.29 g was removed from three inflated prototypes, which when compared to the total mass of biofilm in a control prototype (0.6 g) suggests that greater than 90% of the biofilm mass was removed from the inflated side of the sample.

2.5. Chapter conclusions

We showed that surface deformation can result in debonding of crystalline biofilms and developed the first macro-scale quantitative relationship between strain rate, biofilm segment length, and biofilm debonding. We then extrapolated from actuation techniques used in soft robotics to develop a method for on-demand removal of biofilms from catheters that can be applied in the previously-inaccessible main lumen.[102] The mechanical biofilm-removal method circumvents the many chemical and biological issues with previous approaches to biofouling control in catheters [32, 87, 102] and is complementary to bactericidal and physico-chemical approaches towards biofilm-resistant surfaces.[69, 102] This active biofouling removal method presents a promising and affordable infection control option for urinary catheters, inexpensive devices relatively unchanged for 50 years due to the complexity and expense of previous infection control efforts.[4, 7] A urinary catheter with on-demand biofouling release would be valuable to the subset of patients dealing with serial, occlusive catheter blockages,[36] but even more beneficial to society if used to proactively remove asymptomatic biofilms that lead to symptomatic catheter associated urinary tract infections.[4, 7, 39] Existing extrusion techniques are thoroughly capable of adding an intrawall inflation lumen, or even multiple inflation lumens, to catheter shafts without affecting the shafts' external dimensions. Multiple inflation lumens would allow actuation of the entire luminal surface, and inflation lumen(s) could be inflated via an

additional hub port for actuation. Finally, the combination of this work with previous demonstrations of mucoid *E. coli* and *C. marina* biofilm debonding provides compelling evidence of the utility of a substrate-strain biofilm debonding method in a variety of applications.

2.6 Chapter acknowledgements

V.L. and Q.W. contributed equally to this work. Funding for this work was provided by the NSF's Research Triangle Materials Research Science and Engineering Center (DMR-1121107), the Office of Naval Research (N0014-13-1-0828), and NIH Training Grant #5T32GM008555-18. The authors would like to thank Howard Levinson, M.D. for sharing his clinical perspective and Johan Adami for his assistance with 3D printing.

3. Chapter 3: Optimization of a design for a urinary catheter capable of repeated on-demand removal of infectious biofilms via active deformation

Sections of the text and figures included in Chapter 3 will be submitted to be published in the journal *Biomaterials*. As such, this article does not yet have a publication date; however, Elsevier does not require permission for authors to reuse their own articles, but an optional grant of license will be obtained as soon as one is available. This manuscript describes the work for Specific Aim 2 and parts of Aim 3 and was combined into one chapter to provide a complete narrative for the experiments described below.

Vrad Levering was the lead author and drove the experimentation, conception and documentation, however this work represents a collaboration with Changyong Cao who supplied mechanical engineering and materials science input as a co-first author.

3.1 Chapter synopsis

Biofilm removal from biomaterials is of fundamental importance, and is especially relevant when considering the problematic and deleterious impact of biofilm infections on the inner surfaces of urinary catheters. Catheter-associated urinary tract infections are the most common cause of hospital-acquired infections and there are over 30 million Foley urinary catheters used annually in the USA. In this paper, we present the design and optimization of urinary catheter prototypes capable of on-demand

removal of biofilms from the inner luminal surface of catheters. The urinary catheters utilize 4 intra-wall inflation lumens that are pressure-actuated to generate regio-selective strain in the elastomeric urine lumen, and thereby remove overlying biofilms. Successive rounds of finite element modeling and prototype fabrication were used to optimize the catheter design to generate greater than 30% strain in the majority of the luminal surface when subjected to pressure. The catheter prototypes are able to remove greater than 80% of a mixed community biofilm of *P. mirabilis* and *E. coli* on-demand, and furthermore are able to remove the biofilm repeatedly. Additionally, experiments with the prototypes demonstrate that biofilm debonding can be achieved upon application of compressive strain. The fouling-release catheter offers the potential for a non-biologic, non-antibiotic method to remove biofilms and thereby for impacting the thus far intractable problem of catheter-associated infections.

3.2 Chapter introduction

Infection associated with the use of urinary catheters is a pervasive and challenging issue in healthcare [37, 38, 59, 103-105]. There are over 30 million urinary catheters used annually in the USA and catheter-associated urinary tract infections (CAUTIs) are the most common type of nosocomial infections, which account for 30–40% of all hospital infections and lead to over 50,000 deaths each year [6, 7]. Microbes such as bacteria are able to colonize the surface of urinary catheters very quickly and

often form biofilms in the drainage lumen of catheters [2, 41, 88, 106-109]. The formation of asymptomatic biofilms in urinary catheters promotes development of symptomatic CAUTIs [7], and nearly all patients that undergo catheterization for longer than 28 days will suffer some form of infection [7]. In addition, CAUTIs also contribute to the alarming general increase in antibiotic resistance due to horizontal gene transfer between bacteria within biofilms, and the frequent use of antibiotics in their treatment [6, 110-112].

Current commercially marketed strategies, such as killing bacteria or delaying bacterial attachment [41, 64, 113], to reduce infection induced by urinary catheters have been unsuccessful in the long-term prevention of biofilm formation which ultimately leads to CAUTIs [6, 7]. Although recent research on techniques to prevent catheter infection such as bacterial interference [114] and phage delivery [61] show some promise, they are effective only against specific bacterial strains which prohibitively increases the difficulty of their implementation. Identification of the infecting strain(s) is not a typical clinical procedure, and even more challenging is the huge variety of infectious microbes, both bacterial and fungal [41]. Indeed, even the most recently discovered new antibiotic is only effective on Gram positive bacteria [115]. Microtopography [59, 116, 117], permanently attached silicone oils [118, 119], hydrogels [4, 7, 73], polymer brushes [57, 120], and ultrasound [47] are other promising non-strain-specific strategies, but again they only delay biofilm formation for a short period and

eventually a biofilm still forms. Moreover, the possible large cost to implement them will prevent their routine implementation in clinical settings. Urinary catheters are essentially commodity devices that cost on the order of 10 US dollars; any additional technology that costs more than pennies to implement would face a high barrier to enter the urinary catheter market. Therefore, it is both practically important and fundamentally interesting to propose a new kind of antifouling or fouling release method capable of maintaining catheters free of infection-promoting biofilm at minimal additional cost.

With this consideration, we recently proposed an active control approach, adapted from our work on marine biofilms, which uses inflation-generated strain of the elastomeric substrate to debond the overlying biofilms [69, 121]. We found that increasing the strain in the substrate increases the energy release rate and thereby increases the driving force for debonding of the biofilm. We then used 3D printing to fabricate proof-of-concept (POC) urinary catheter prototypes that generate enough strain to successfully debond and remove mature *P. mirabilis* biofilm from their interior [121]. However, the POC prototypes left multiple questions of practical significance unresolved. The POC prototypes were less than 7 cm long and over 1.4 cm diameter, which is much shorter and stouter than the standard urinary catheter (25-42 cm long and 5 – 10 mm in diameter). Additionally the POC prototypes had only one intra-wall inflation lumen, resulting in straining and debonding of the biofilm from only part of

the surface (about 35% of the perimeter). These limitations raise the following questions: does the active control approach work well for the length scales of a standard urinary catheter, in particular, with a small diameter catheter, e.g., around 6 mm? Is it possible to remove biofilm from the full perimeter of the urine lumen? Finally, although our pilot study demonstrated that strain applied on the substrate debonded a range of biofilms [69, 121], the technique has never been demonstrated with a mixed community biofilm. Moreover, we did not yet know whether the substrate strain would debond biofilms repeatedly to allow long term use.

Here we present the design and a prototype of a urinary catheter capable of repeated on-demand biofilm removal. We hypothesized that adjusting the number and position of intra-wall inflation lumens would allow inflation to generate sufficient tensile strain to debond biofilms over the majority of the internal lumen perimeter. We used successive rounds of finite element modeling to optimize the predicted strain of catheter cross sectional profiles to ensure the design fell within the fabrication capability of an industrial catheter manufacturer. We then constructed prototypes with clinically relevant dimensions using a combination of extrusion and 3D printed reversed-mold fabrication techniques. Different materials for the prototype catheter shaft were compared to determine the ideal operational parameters for clinicians to manually inflate our prototype. We further characterized the prototypes and compared their inflation performance against our finite element models. The prototype catheter, less

than 7 mm in diameter with four intra-wall inflation lumens, was able to achieve substrate strain over most of the perimeter of the main drainage lumen, as well as along the full length of the device. We hypothesized that prototypes would debond a mixed community biofilm of *E. coli* and *P. mirabilis*, two of the most common bacteria found in CAUTIs, and we developed an artificial bladder flow system to grow mature biofilms inside the main drainage lumen of prototype catheters. Upon on-demand, inflation-generated actuation, the prototypes dramatically removed the vast majority of the biofilm along the full length of the catheter. After that first successful biofilm removal, we then regrew biofilm within the catheter and demonstrated that inflation-induced strain would indeed repeatedly remove biofilm in the catheter. Interestingly, upon dissection of the catheters, we observed that areas that underwent compressive strain, as predicted by the finite element modeling, debonded biofilm similarly to areas that underwent tensile strain. In total, using currently available manufacturing techniques from a catheter manufacturer, we developed a urinary catheter that allows the repeated and thorough removal of infectious biofilms from its interior; we are thus poised to impact the long-stagnant urinary catheter technology market.

3.3 Methods and Materials

3.3.1 Finite element modeling

Since catheters are relatively long compared to their cross-section dimensions, we simplified our design analysis to a plane-strain problem. In our analysis, the proposed catheter designs were modeled with the hybrid quadratic elements (CPE8MH) under plane-strain deformation using the software package, ABAQUS 6.12. Pressure was applied along the inner surfaces of the inflation lumens while a free boundary condition was used along the outer surface of the catheter to predict its radial displacements. Mesh density was determined by a convergence study and 10,441 CPE8MH elements were used for the whole model. A nonlinear solution method and geometric nonlinearity were adopted in the analysis. We used a 0.2 mm thick wall between the inflation lumen and the main lumen for models used for selecting the number of inflation lumens. Finite element models of the fabricated tubing used a 0.27 mm thick wall to reflect the actual dimensions achieved by the extrusion vendor. Three different materials are used for the catheters: 50 durometer silicone elastomer, 35 durometer silicone elastomer, and a more rigid sheath 65 durometer silicone elastomer (all durometers defined per the type A scale), which were tested using a tensile tester (MSA Inc., USA) and fitted using the Neo-Hookean model with shear modulus of 0.69 MPa, 0.52 MPa, and 2.44 MPa, respectively (Figure 23). The strains along the internal

surface of the drainage lumens and the average radial displacement along the outer surface were calculated by the finite element model for comparison.

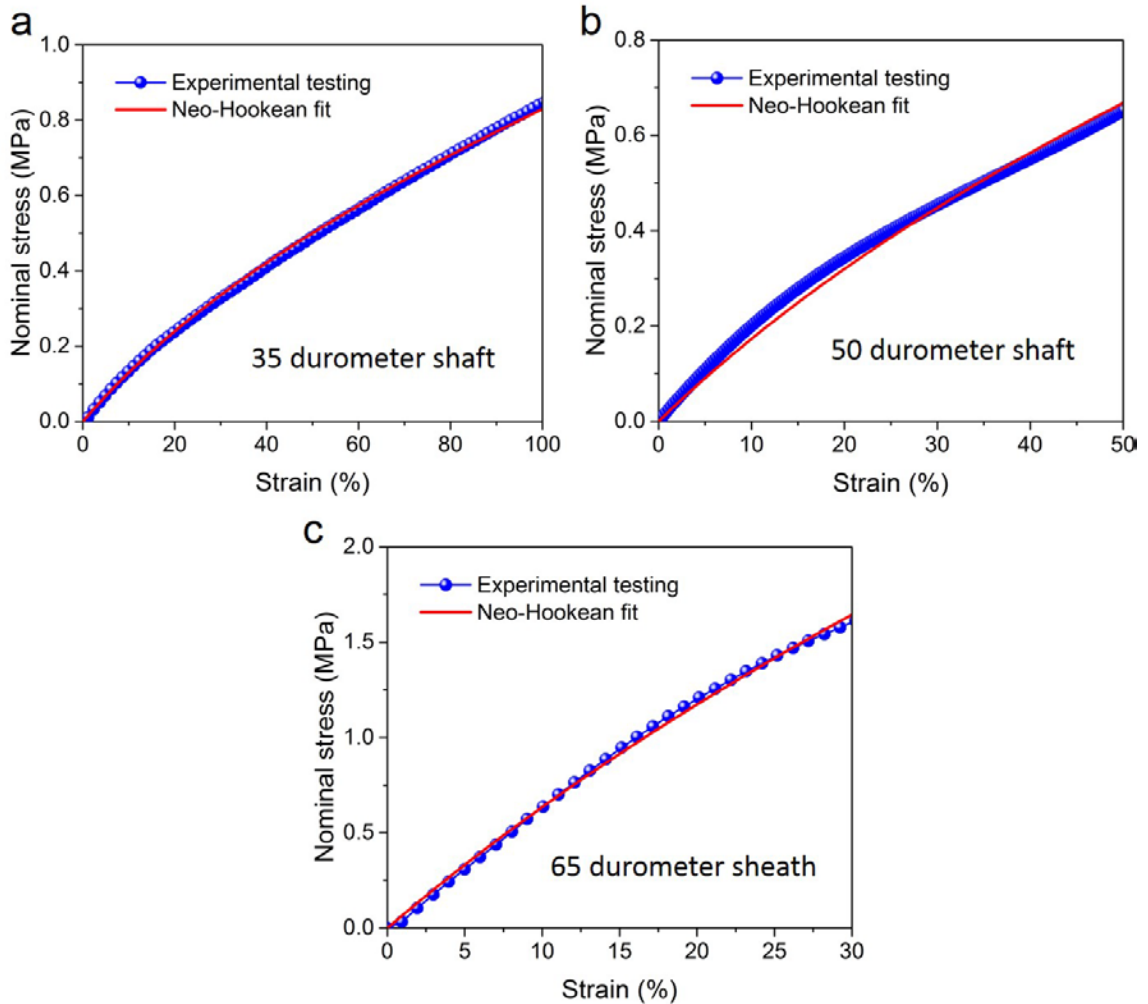


Figure 23: Nominal stress-strain curves for the final prototype materials obtained from uniaxial tensile testing. (a) Nominal stress-strain curves of (a) 35 durometer silicone shaft, (b) the 50 durometer silicone shaft and (c) the more “stiff” 65 durometer silicone sheath. All the curves were fit to the Neo-Hookean model. The shear moduli for the 35 durometer shaft, 50 durometer shaft and 65 durometer sheath materials are 0.52MPa, 0.68MPa and 2.44MPa, respectively.

3.3.2 Preparation of prototypes

Vesta Inc. (Lanham, Maryland, USA) extruded silicone catheter shaft components according to our specifications using Dow Corning two-part, platinum-catalyzed Class VI silicone feedstock. Vesta Inc. varied the silicone feedstock to achieve 35 and 50 durometer multi-lumen silicone main shafts and the 65 durometer silicone sheath (all durometers defined per the type A scale). In instances where a sheath was used, we slip-fit the sheath over the main shaft using isopropyl alcohol. The inflation lumens were then sealed at each end of the main shaft using Sil-Poxy® silicone adhesive (Smooth-on Inc., USA). We then skived 2 mm long holes out of the outer walls of the inflation lumen approximately 1 cm from the designated hub end of the shaft. Hub manifolds were prepared by pouring silicone (Dragon Skin 0020®, Smooth-On Inc., USA) into a mold prepared by a 3D printer (Dimension SST 1200ES, with patterns generated using Solidworks 20131, Figure 24).

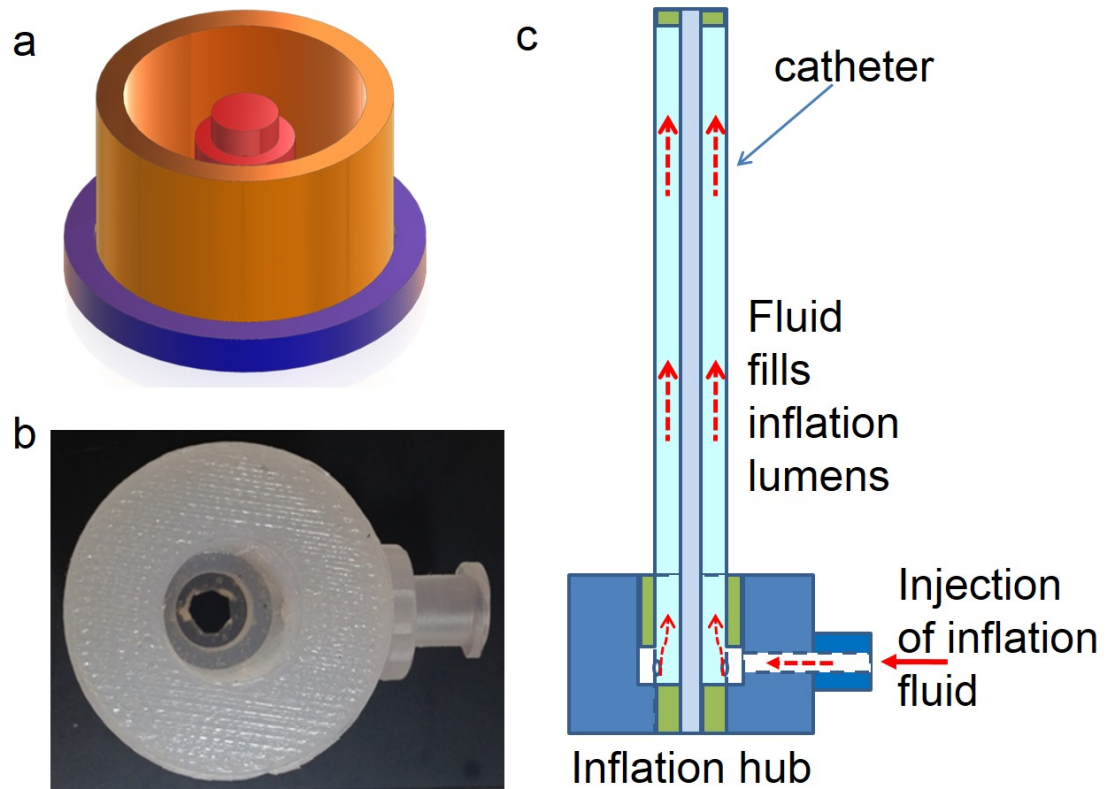


Figure 24: Schematic for the design of inflation hub and its configuration used in our experiments. (a) The mold fabricated by the 3D-printer (Dimension 1200es, Stratasys, USA). (b) Inflation hub fabricated with the mold in (a), and fit with a touhy borst connector. (c) Schematic of the configuration used for the inflation testing.

The inner diameter of hubs was approximately 0.5 mm greater than the shaft in order to create a manifold to allow simultaneous inflation of all four lumens. Once cured, the hubs were removed from the molds and then pierced and fit with a male touhy borst connector to be used for inflation. We fit the hubs over the designated hub end of the shaft and carefully glued the hub in place without occluding the skived holes in the inflation lumens, thus allowing simultaneous inflation of all four lumens via the

to uhy borst connector. Prototype performance was examined using optical video of on-end and side-views of inflation. We then analyzed still images from the video using ImageJ (<http://rsbweb.nih.gov/ij/>) to characterize strain and dimensional parameters as a function of inflation pressure.

3.3.3 Bacteria strain and culture media

Proteus mirabilis 2573 (ATCC 49565) and *Escherichia coli* K12 (ATCC 29425) were thawed from frozen stock and cultivated overnight at 37°C on separate tryptone soya broth agar slants which were stored at 4°C and used for up to 2 weeks. Artificial urine media was prepared as described previously [121], sterilized and then supplemented with 1.0 g/L tryptone soya broth prepared separately to make the total artificial urine media (AUM) [14, 121]. Colonies of *P. mirabilis* and *E. coli* were each inoculated into separate flasks of 75 mLs of AUM and grown for 4 hours at 37°C on a shaker at 240 rpm.

3.3.4 Biofilm growth in catheter prototypes

We grew biofilms with a co-community of *P. mirabilis* and *E. coli* on the main drainage lumen of catheter prototypes using a continuous flow method as established by Stickler et al. [14], but modified to accommodate a manifold of four 50 mL artificial bladders in a vertical orientation (example artificial bladder shown Figure 25).

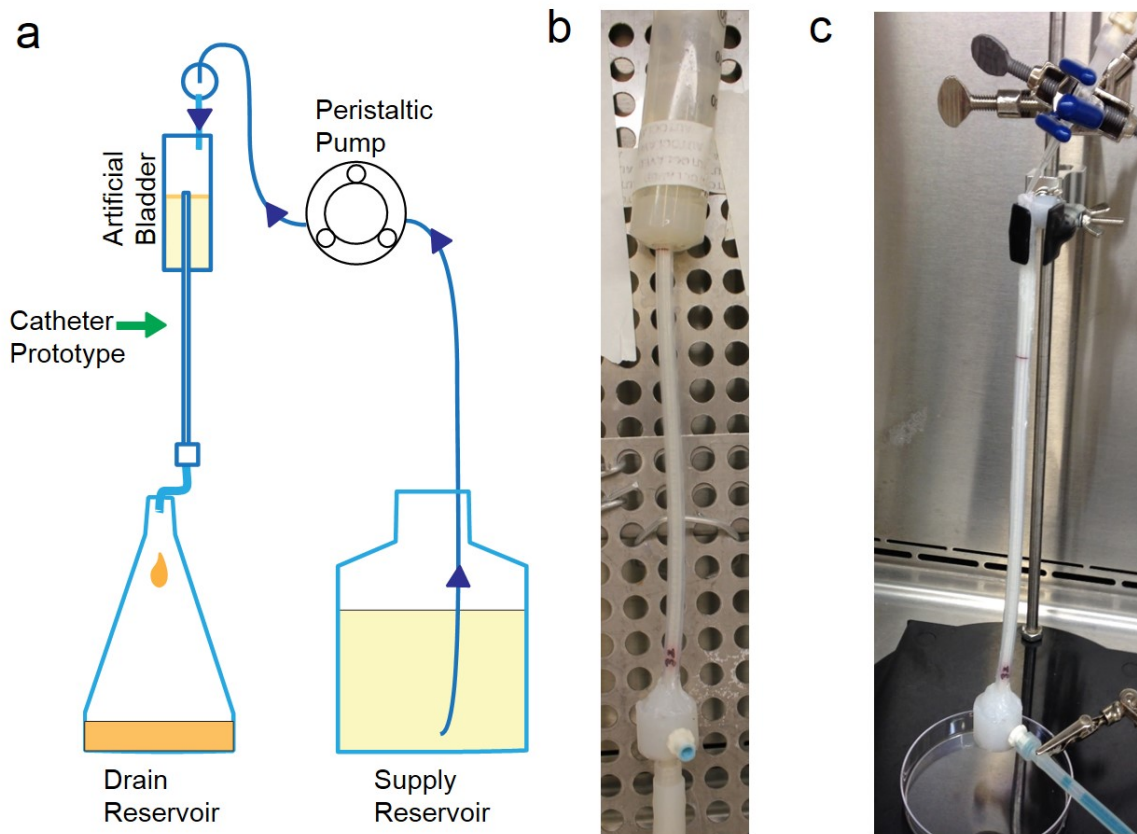


Figure 25:The setup for biofilm-growth and debonding in urinary catheter prototypes. (a) Schematic of biofilm-growth system that uses an “artificial bladder” to supply infected urine to the catheter. The artificial bladder is a vessel modified to accept the distal, top tip of a catheter prototype penetrating the bottom and extending approximately 4 cm into the vessel, which thereby maintains a residual volume of 30 mL in the artificial bladder. (b) Optical image of artificial bladder with catheter prototype; the main urine drainage lumen of the catheter prototype drains into a collection manifold on the bottom end. The diameter of the catheter prototype shaft is 6.7 mm. The artificial bladder and prototypes were inoculated with 4 hour-cultures of *P. mirabilis* and *E. coli*. After allowing the bacteria to adhere for 1 hour, artificial urine media was pumped at 0.5 mL min^{-1} into the artificial bladder and through the prototypes. The bladder and prototypes were maintained at 37°C in a mini-incubator. A mature biofilm grew over approximately 30 hours. (c) Setup for rinsing setup for testing debonding after biofilm growth. Artificial urine media supplied at 4 mL min^{-1} flowed downward through the prototype’s main urine drainage lumen for 1 minute. Prototypes designated for actuation were hydraulically inflated through a hub port 10 times approximately 20 seconds into the rinse. Rinse effluent was collected, and the

debonded biofilm (the white matter in the petri dish) was weighed. The prototype was then removed for inspection.

The distal (non-hub) tips of the prototype catheters were inserted through a pressure-fit seal in the bottom of the artificial bladders; they were inserted approximately 4 cm into the bladder to ensure the bladder would hold 30 mL before draining through the catheter. The catheter prototypes, artificial bladders, and all associated supply and drain tubing were sterilized and placed in a Class II biosafety cabinet. The bladders and prototypes were maintained at 37°C in a mini-incubator. The bladders each held a 30 mL reservoir of infected media that would overflow into the distal tip of the catheter prototype and then drip-feed through the main drainage lumen of the prototypes as fresh media was added to the bladder. The system was primed with AUM, and then inoculated with 4 hour cultures of 5 mL of *P. mirabilis* and *E. coli*, each introduced into the artificial bladder. The bacteria were left for 1 hour to allow attachment and infection of the bladders and catheters. The model was then run continuously at a flow rate of 0.5 mL min⁻¹ supplied via peristaltic pumping until the desired time point when a thick biofilm was visible through the walls of the prototype, or a system blockage occurred. All biofilm growth was conducted in a sterile biosafety cabinet. The sterility of the artificial bladder growth system was confirmed by control runs without bacterial inoculation; no deposition was observed and no biofilm was formed on control samples.

3.3.5 Actuation testing

For the samples undergoing only one round of biofilm removal, the prototypes were gently removed from the artificial bladders and kept covered in a hydrated state. The samples were suspended vertically, and artificial urine media was introduced into the upper end at a flow rate of 4 mL min^{-1} for 1 minute (Figure 25). Samples designated for inflation were rapidly inflated to a pressure of 80 kPa and then deflated 10 times at 0.6 s^{-1} to achieve 35% average strain, each inflate/deflate cycle taking less than one second, approximately 20 seconds into the 1 minute rinse. Inflation was conducted hydraulically using a syringe-delivered, pre-determined volume of water. Prototype samples were weighed before biofilm growth, before rinse, and after the rinse in order to assess the weight of biofilm grown and removed. The effluent from each sample's rinse was also collected. We centrifuged the effluent, removed the liquid supernatant, and weighed the remaining biofilm as another measure of biofilm removal. Samples were then dissected into tip, top, middle and bottom sections. 1 mm thick sections for cross-sectional views of the main lumen and 1 cm long sections that were filleted in half for longitudinal views of the main lumen were sliced from the top, middle, and bottom sections. Those sections, in addition to cross sectional views of the tip, were then optically photographed. Additional pieces from the top, middle, and bottom were stained with 0.01% crystal violet for 10 minutes and rinsed 2 times with DI water before similar slicing for cross sectional and longitudinal views. Representative longitudinal,

crystal violet stained samples were carefully cut to excise the main lumen from the catheter shaft to allow flattened views of the biofilm coverage of the main lumen. Stained sections were also optically photographed, and selected sections were examined on the phase microscope at 10x magnification.

Fresh prototype catheter samples were fabricated to undergo two rounds of biofilm removal. The co-community biofilm of *P. mirabilis* and *E. coli* was grown on the main drainage lumen of catheter prototypes using the same continuous flow method described above. We utilized inflation actuation as described above to remove the biofilm from all samples once the biofilm formed. We then replaced the consumed supply of AUM with a fresh supply of AUM, and emptied the drainage collection flask before re-starting the peristaltic pump at the same flow rate of 0.5 mL min^{-1} . Once the co-community biofilm regrew (after approximately 24 hours), we stopped the flow. The artificial bladders and the catheter samples were carefully removed from the flow loop and all catheters were rinsed with AUM supplied into the artificial bladder at a flow rate of 4 mL min^{-1} for 1 minute. Samples designated for inflation were rapidly inflated to a pressure of 100 kPa and deflated 10 times to achieve 40% strain approximately 20 seconds into the 1 minute rinse. The effluent from each sample's rinse was collected and samples were then dissected as described above.

3.3.6 Preparation of flat silicone coupons:

We poured two-part silicone (Dragon Skin 0020®, Smooth-On Inc., USA) and allowed it to set to generate flat silicone samples that we then trimmed to 24 mm x 75mm to fit in a drip flow reactor; the method is documented in detail in our previous work [121]. The flat samples were sterilized in the biosafety cabinet by rinsing with 95% ethanol and sterilized water.

3.3.7 Biofilm growth on flat silicone coupons:

The drain of a drip flow reactor (BioSurface Technologies Corporation) was modified to keep flat silicone coupons submerged in 0.3 – 0.6 cm media while under flow. The reactor was maintained at 37°C by placing it in a mini-incubator. AUM was introduced using a peristaltic pump to prime the flow system. The samples in the reactor were infected with 4 hour cultures of 5 mL each of *P. mirabilis* and *E. coli*, and the infected culture was left for 1 hour to allow bacterial attachment before the media supply was resumed. The model was run continuously at a flow rate of 0.5 mL min⁻¹ until the desired time point, or until a system blockage occurred.

3.3.7 Rheology of biofilms and substrates:

Silicone samples (10 x 10 mm) covered by a thin layer of biofilm were used to perform a frequency-sweep oscillation test at room temperature in a mechanical rheometer (AR-G2, Rheology Advantage Instrument, USA). We assumed that the biofilm did not slip during the testing process. Bare silicone samples (without biofilm

attached) were measured as controls. The applied strain amplitude for the testing was 0.5%, and the frequency was swept from 0.1 to 10 Hz [122]. The measured storage and loss moduli for the biofilm and the substrate are presented in Figure 35.

3.3.8 Adhesion testing of biofilms:

Biofilm adhesion was tested using the method reported by Chen et al. [123]. The adhesive strength between the biofilms and the silicone substrate is defined as the work per unit area required to remove the biofilms from the surface [124, 125]. As shown in Figure 26, a rake-shaped probe with a width of 1 cm was fabricated for the scratch testing with a MSA tester (TA Instruments, USA). The adhesion strength between the biofilm and the silicone substrate can be calculated as

$$\Gamma = \left(\int_L F_{biofilm} dl - \int_L F_{control} dl \right) / (WL)$$

using the measured forces and sample dimensions [123], where W is the sample width and L is the moving displacement of the probe.

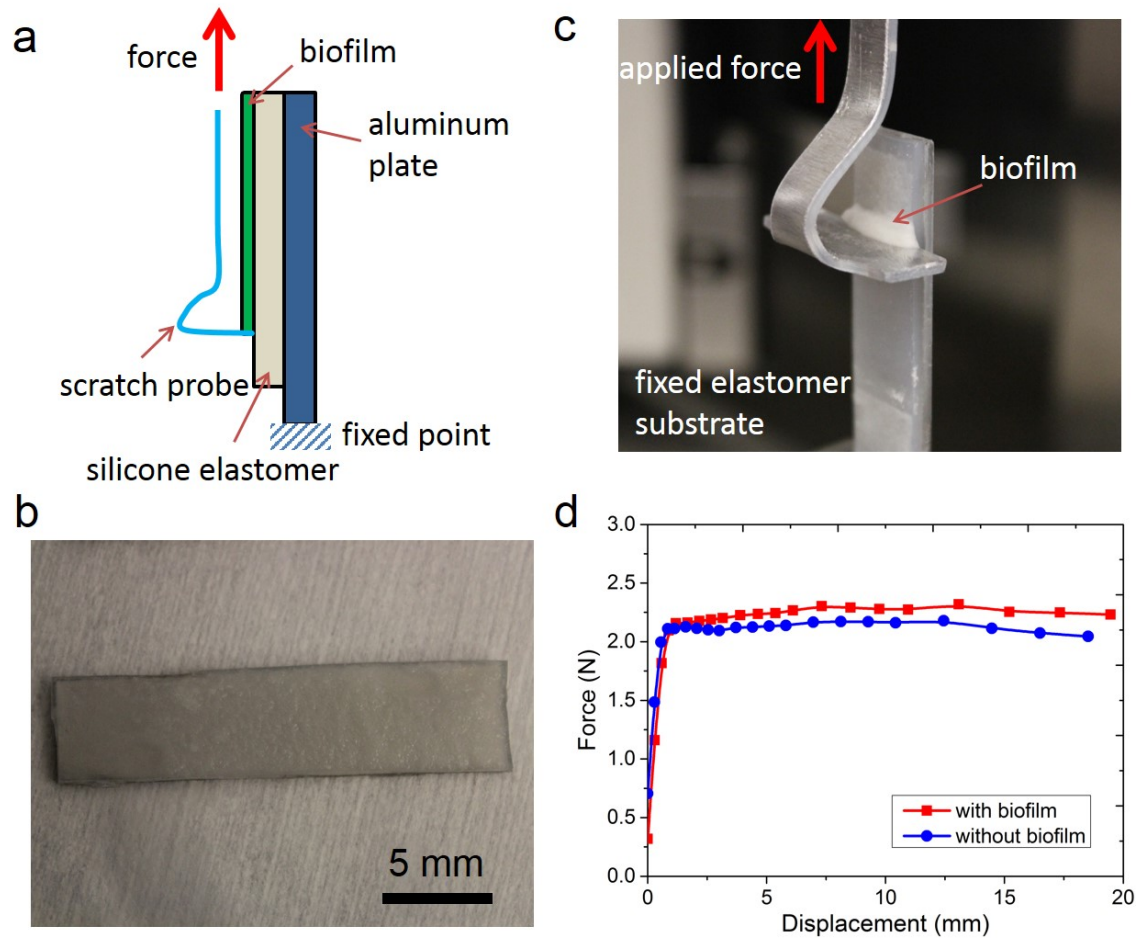


Figure 26: Adhesion strength testing for the mixed community biofilm of *P. mirabilis* and *E. coli* biofilms. (a) Schematic of the experimental set-up for the adhesion testing using a custom designed scratch probe. (b) Sample of biofilms grown on the surface of silicone (Dragon Skin 0020®, Smooth-On Inc., USA) attached on an aluminum strip. (c) Optical image of the testing set-up. (d) Representative force-displacement curves obtained from the scratch tests. Rate=0.5mm/s.

The biofilm-covered silicone sample (silicone was Dragon Skin 0020®, Smooth-On Inc., USA) was affixed at the bottom with the grip. The probe was carefully adjusted to penetrate into the biofilm and slightly touch the silicone substrate. The probe was

then moved at a controlled rate (0.5 mm/s) to scrape the surface of the biofilm-covered sample. Thereafter, a second run on a biofilm-free substrate was performed as a control. Figure 26 shows the shear forces measured for a control and an experiment. The difference between the two measurements was used to calculate the adhesion strength (based on the obtained force and sample dimensions) between the biofilm and the substrate [123].

3.3.9 Statistical analysis

Statistical comparisons were conducted using GraphPad Prism 5 (USA). Group means were compared by two-tailed, unpaired *t*- tests with Welch's correction to account for potentially unequal variances. "****" denotes $P < 0.001$ where shown in figures. Data are presented as mean +/- standard deviation in bar and line graphs.

3.4 Results

3.4.1 Concept for urinary catheter with active fouling-release

As depicted in Figure 27, we have proposed a simple but new concept for a urinary catheter prototype capable of releasing biofilms by means of active actuation of elastomers [121]. The design is based on equipping the catheter with inflation lumens between the inner main lumen and outer catheter wall (Figure 27a). After infectious biofilms form on the surface of the main drainage lumen (Figure 27b), we can pneumatically or hydraulically actuate the inflation lumens to a controlled level of strain

for multiple inflate/deflate cycles (Figure 27c). As a consequence, the biofilm is debonded from the surface of the main lumen and then can be easily removed by a minimal flow of liquid (e.g., urine generated by a patient, Figure 27d), thereby clearing the urine drainage lumen for continued use.

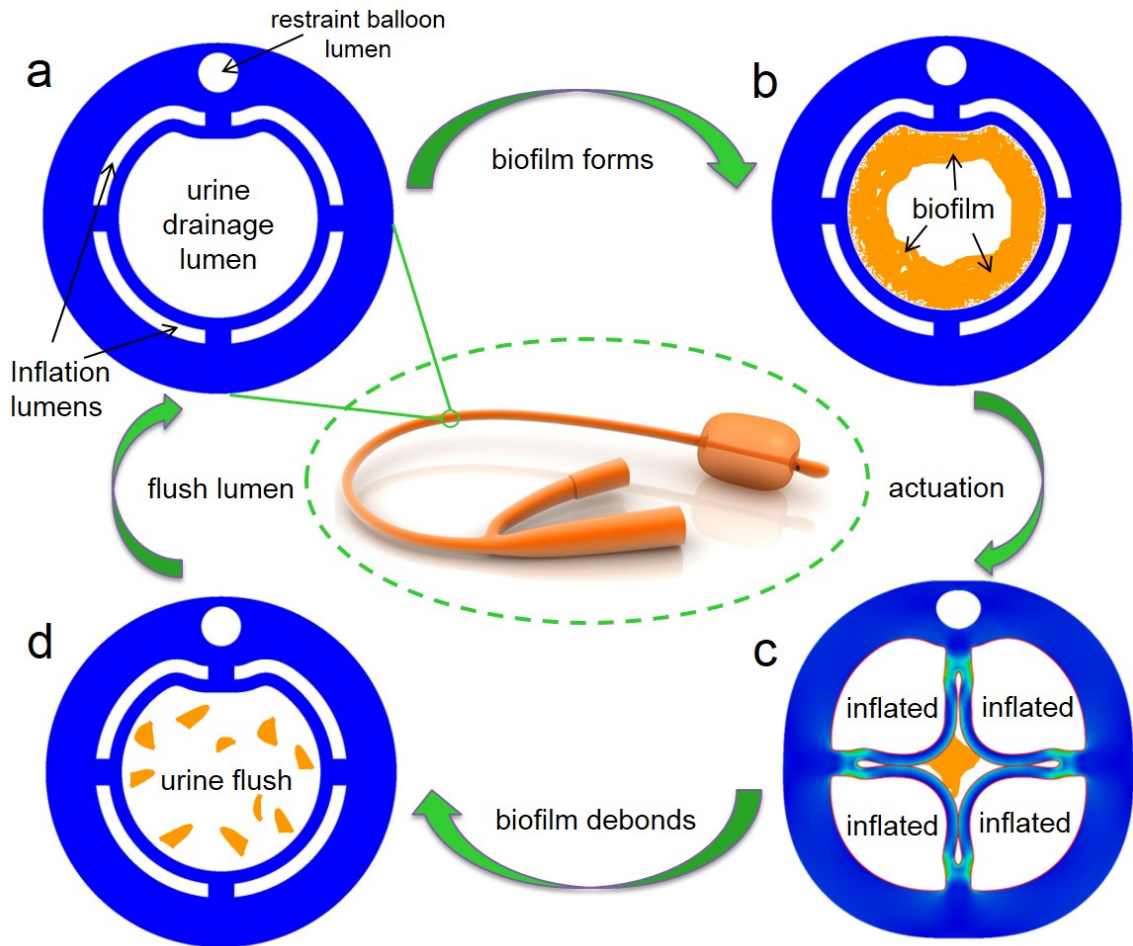


Figure 27: Schematic of a urinary catheter capable of on-demand removal of infectious biofilms via active deformation. (a) Cross-section of a conceptual design for a urinary catheter shaft with intra-wall inflation lumens. (b) Biofilm forms on the surface of urine drainage lumen after 1-2 days. (c) Actuation of inflation lumens by pumping air or water to generate large mismatched strains between biofilm and the surface of main lumen to debond the biofilm from the urine drainage lumen. (d) The detached biofilm is removed by the flow of urine once the inflation lumens are deflated. Therefore, the catheter can be maintained free of mature biofilms for long-term use and thereby may reduce the risk of catheter-associated urinary tract infections.

In our previous work, we found that active surface deformation can effectively detach mature crystalline urinary biofilms from flat and curved surfaces of silicone elastomers. We also showed that both the strain rate and strain level generated by actuation can have a significant influence on biofilm debonding [121]. The biofilm debonds once the energy release rate exceeds the adhesion strength between the biofilm and the substrate. Since this validation of the general concept for biofilm release, we have focused, and report herein, the development of designs for a new generation of urinary catheters with the ability of on-demand biofilm release. The small cross section of the catheter and the limitations of the manufacturer's capabilities required us to carefully optimize the design, while the design process itself revealed new and fundamental insights about inflation and biofilm debonding performance in constrained regions.

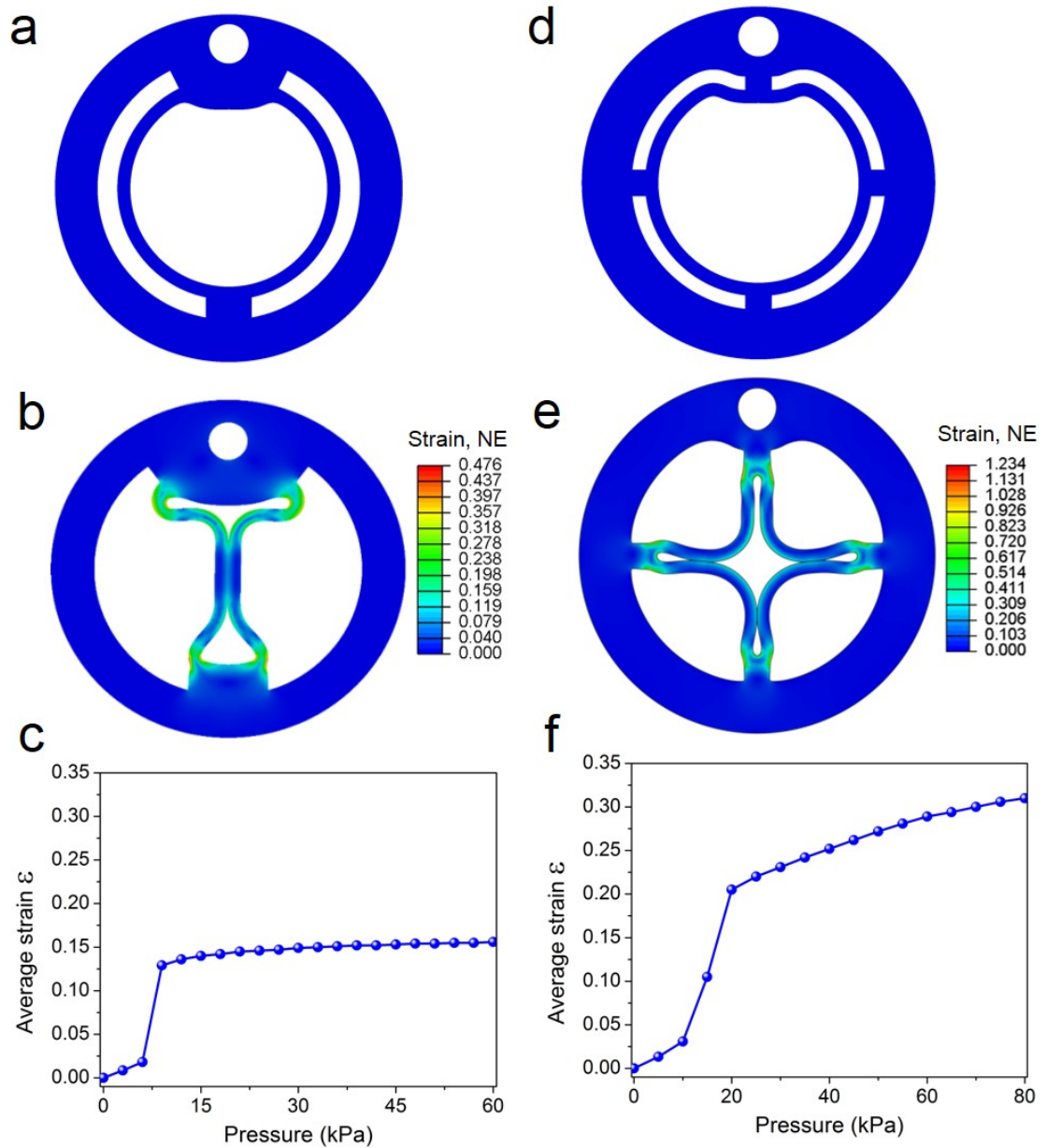


Figure 28: Finite element models show that a four-inflation-lumen design for a urinary catheter shaft achieves higher levels of tensile strains along the urine luminal surface than a two-inflation-lumen design at the same inflation pressure. (a) Cross-section of catheter shaft with two intra-wall inflation lumens. (b) Predicted strain distribution over the cross section of the two-lumen catheter from finite element model when both inflation lumens are simultaneously inflated by a pressure of 60 kPa. (c) Predicted average strain along the urine luminal surface for the two-inflation-

lumen configuration reaches a plateau after the inflation walls interact with each other. (d) Cross-section of catheter shaft with four inflation lumens. (e) Strain distribution of the four-lumen catheter when inflation pressure is 80 kPa. (f) Predicted average strain along the luminal surface of the four-lumen configuration; 30% strain is achieved at approximately 70 kPa.

In order to actuate the maximum area of the drainage lumen's surface within the catheter, we designed the inflation lumens to underlie as much of the perimeter as possible. We used the finite element models to predict inflation performance and the resultant strains in the wall of the main lumen. We first designed a two-inflation-lumen catheter, in which each inflation lumen takes up almost half of the perimeter of the catheter (see Figure 28a). The finite element model clearly demonstrated that, after an initial increase of the surface strain on the surface of main drainage lumen, as inflation pressure increased, the surface strain stops increasing at ~15% due to the interfering contact of the two walls in the confined space of the drainage lumen (Figure 28c). From our previous study, we know that the biofilm debonds once the energy release rate, G , exceeds the adhesion strength between the biofilm and the substrate due to applied strain, and $G \propto \mu_f \varepsilon^2 H$ (where μ_f is the storage modulus of the biofilm, ε is the applied strain in the substrate, and H is the biofilm thickness) [69]. We found that the majority (i.e. >70%) of the biofilm debonds once the applied strain in the substrate reaches a "critical" value, ε_c [69]. For instance, in mucoid biofilms such as *E. coli*, the majority of the biofilm debonds at a critical strain of 15% (although critical strain can be lower

depending upon biofilm thickness [69] and substrate modulus [126]); and in crystalline biofilms such as *P. mirabilis*, the critical strain is approximately 25% [121]. We desired to exceed 30% strain as a conservative design goal [121]. We considered programmed, sequential inflation of the two-inflation-lumen design to achieve the desired critical strains, but this caused large distortion of the cross-section outer diameter (Figure 29).

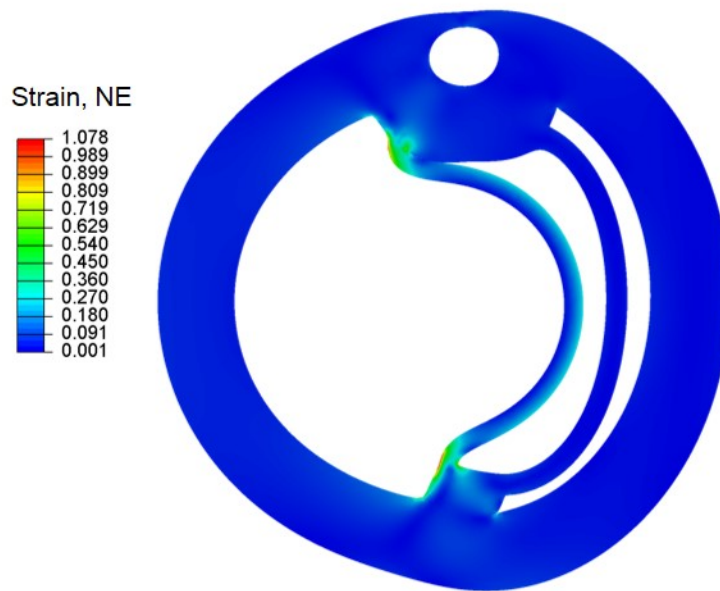


Figure 29: Contour plot of nominal strains, and the resultant deformation profile, of the cross-section of a catheter with two lumens when one lumen is actuated to achieve an average strain of 30%.

Therefore, to limit interference between inflated lumens, we reduced the perimeter length of the individual inflation lumens while increasing the number of inflation lumens to four (Figure 28d). Using finite element models (Figure 28e), we predicted that the strains along the internal surface of the drainage lumen can reach greater than the desired 30% strain at a pressure load of approximate 70 kPa. Clinicians

can easily achieve 70 kPa (assuming silicone with a shear modulus of 0.69 MPa) using off-the-shelf syringes commonly used in hospitals, so we moved forward with a four-inflation-lumen design. It was also readily apparent that the luminal surface overlying the walls between the inflation lumens cannot be inflated during the actuation process. However, high compressive strains in these regions are expected due to the inflation on either side of these regions (i.e. inflation on either side “squeezes” the in-between wall area) (Figure 28e). We thus hypothesized that the biofilm overlying the wall area would also debond from the substrate surface due to the large mismatched strain introduced by compression.

3.4.2 Catheter fabrication

We contracted with Vesta Inc. (Lanham, Maryland, USA) (which routinely extruded silicones for the medical industry) to produce a series of iterations of the multi-lumen catheter shafts for our prototypes. Based on manufacturing limitations in fabricating high-aspect-ratio inflation lumens, we optimized the shape of cross sections of the inflation lumens for manufacturing using both finite element model predictions and experiments with fabricated prototypes (see Figure 30, and Figure 31). The optimization and fabrication of the catheter prototypes required several versions of the catheter be generated. We first modeled, and then fabricated, catheter prototypes using a 50 durometer silicone (Dow Corning two-part, platinum-catalyzed Class VI silicone feedstock; 50 durometer extrusion from Vesta Inc.). we experimentally characterized the

shafts' strain upon hydraulic actuation. Due to the slight variation between the real inflation lumens' configuration and the original design, especially an increase in inflation wall thickness to 0.27 mm, the experimental inflation pressure had to be higher than the predicted pressure to achieve a satisfactory strain level. We found the inflation required a higher inflation pressure than was manually achievable (Figure 30).

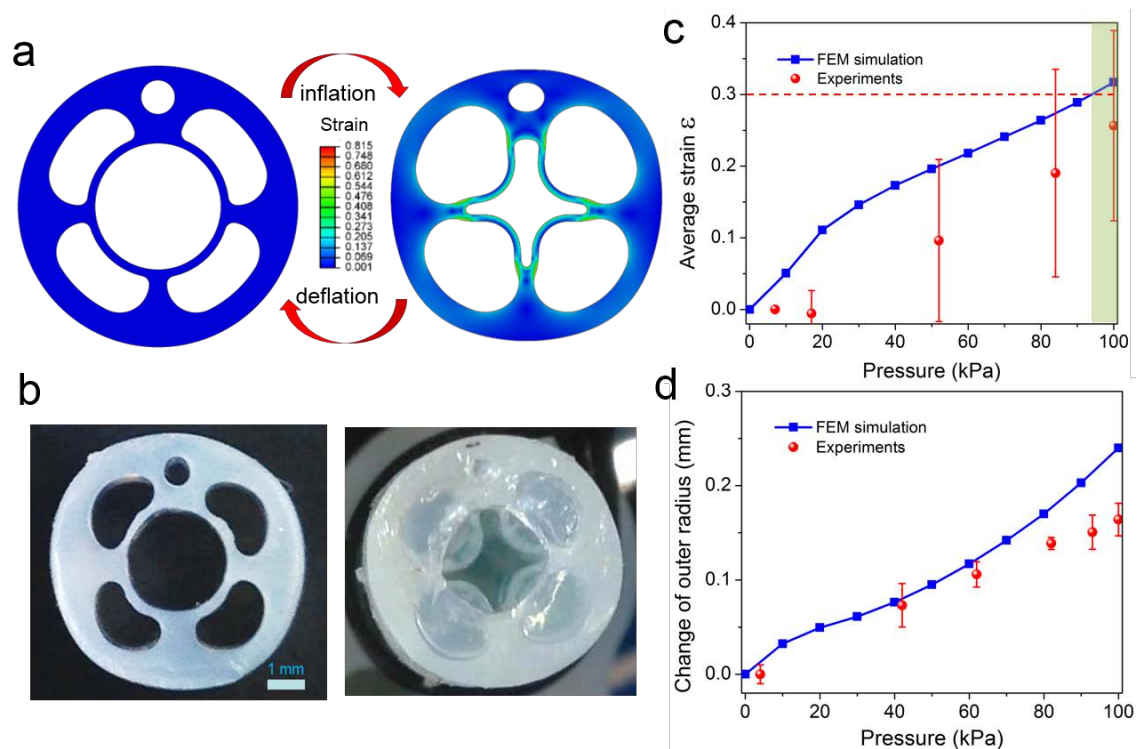


Figure 30: FEM simulation and experimental data of a four-lumen catheter shaft made of 50 durometer silicone elastomer. (a) Schematic of cross section and FEM model (100kPa) of extruded silicone urinary catheter shaft. (b) Photographs of the cross-section and the inflated four-lumen catheter at 80 kPa inflation pressure. Scale bar indicates 1 mm. (c) The average strain of the urine luminal surface for the four-lumen configuration; 30% strain is achieved at approximately 93 kPa. (d) The change of the outer radius of the shaft as a function of applied pressure.

Catheter prototypes constructed using the 50 durometer silicone shaft required inflation to >100 kPa to achieve the desired substrate strain. Since exceeding 90–100 kPa was challenging using manual inflation using a 10 cc syringe, we improved our design to reduce the inflation pressure needed. We conducted another extrusion with a “softer” 35 durometer silicone feedstock (shear modulus of 0.52MPa) instead of the 50 durometer feedstock. Figure 31 presents the average strain of the 35 durometer catheters obtained under various inflation pressures. It was found that the pressure to achieve 30% average strain became now only 70 kPa. However, the increase in outer radius from both simulations and experiments becomes much larger (as compared to the catheter with 50 durometer elastomer, see Figure 30 and Figure 31) and rose to an unacceptable level. The FDA guidelines related to urinary catheters dictate no change in diameter greater than 0.33 mm (1 Fr on the French catheter scale).

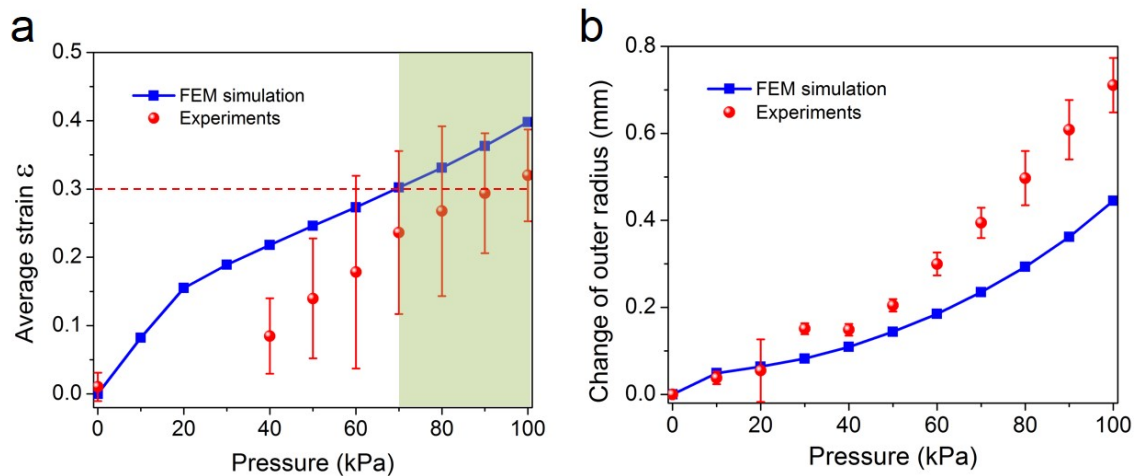


Figure 31: FEM simulation and experimental data of an extruded four-lumen catheter shaft made of 35 durometer silicone elastomer. (a) The average strain of the luminal surface for the four-lumen configuration; 30% strain is achieved at

approximately 70 kPa. (d) The change of the outer radius of the shaft as a function of applied pressure.

Therefore, we finally added a thin-walled, higher-modulus (65 durometer) “sheath” to the outside of the catheter to constrain the deformation of the outer surface (Figure 32b).

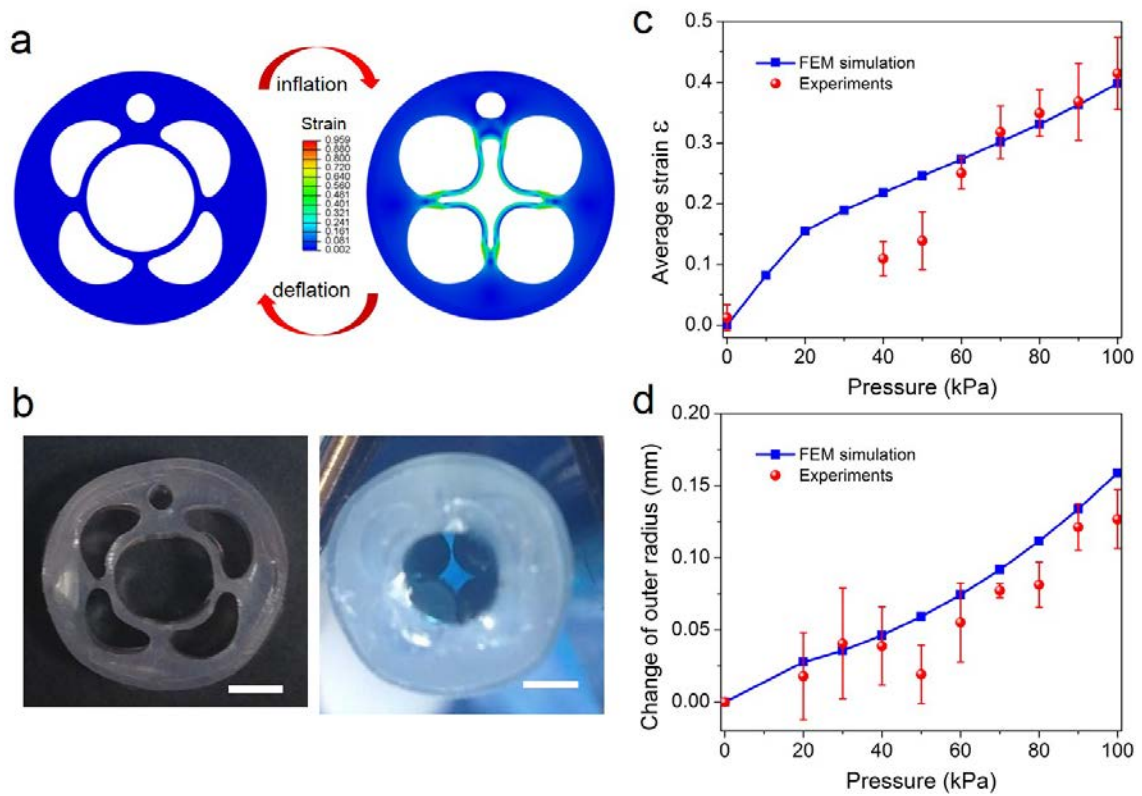


Figure 32: Experimental testing of a catheter shaft agrees well with the numerical prediction of strain of the central luminal surface as a function of inflation pressure. (a) Cross-section and FEM model for a silicone urinary catheter shaft with four inflation lumens. Strain contour plot from FEM model subjected to an inflation pressure of 80 kPa. (b) Digital photograph of the cross-section of a catheter shaft made of 35 durometer, low modulus silicone and constrained with a 65 durometer, high-modulus silicone sheath; and a representative image of its profile when inflated to 80 kPa. Scale bar indicates 1 mm. (c) Calculated and experimental average strain of the central luminal surface. 30% strain is achieved at approximately 70 kPa. (d) The increase in the outer radius of the shaft as a function of applied inflation pressure.

We again employed finite element models to estimate the strains under different inflation pressures of the cross-section of the optimized, final version of the urinary catheter shaft, which has four inflation lumens and is made of low modulus silicone (35 durometer) and constrained with a high-modulus (65 durometer) silicone sheath. Figure 32c shows the average strains obtained as a function of the applied hydraulic pressure. The elastomer for the sheath was assumed to be a Neo-Hookean material with a shear modulus of 2.44 MPa (Figure 23b).

Simulation results confirmed that the inflated wall can easily achieve substrate strains sufficient to debond crystalline biofilms (e.g., greater than 30% strain) over most of the surface (Figure 32c). As shown in Figure 32d, the change in the outer radius of the shaft at higher pressure was dramatically reduced with the added sheath. We experimentally actuated the catheter with sheath using colored water and verified that the numerical results agree well with experimental data in the relevant range (Figure 32c and d) and exhibited similar appearance during the inflation process (Figure 33 and Video of the inflation). Figure 32b shows the final deformation profile of the four inflation lumen catheter, which is similar to the profile predicted by the strain contour plot at 80 kPa as shown in and Figure 32a.

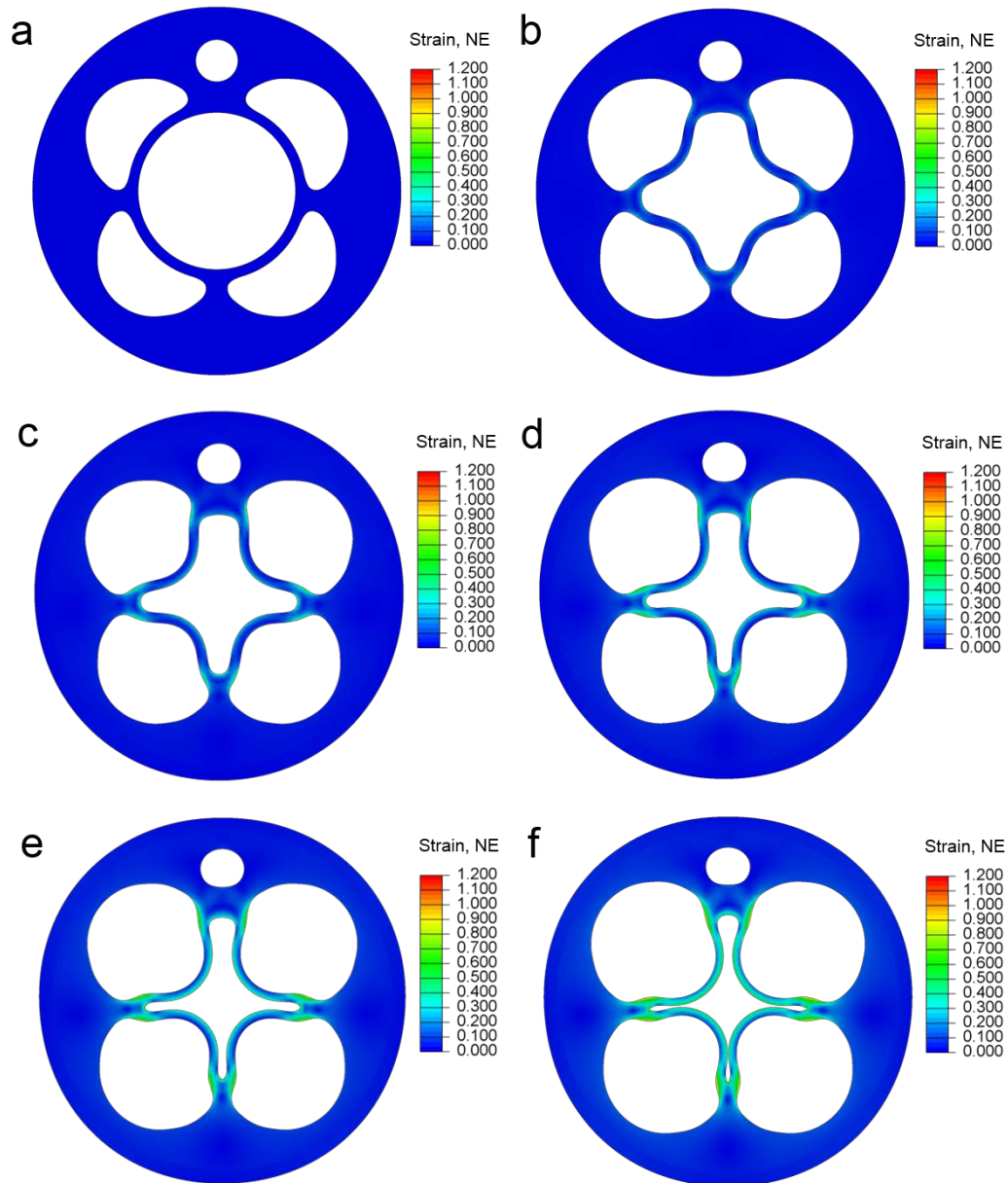


Figure 33: Deformation profiles from FEM simulation of an extruded four-lumen catheter shaft made of 35 durometer silicone shaft and with a 65 durometer silicone sheath when it is subjected to a range of pressures. Deformation profiles predicted at the following pressures: (a) 0 kPa, (b) 20 kPa, (c) 40 kPa, (d) 60 kPa, (e) 80 kPa and (f) 100 kPa.

3.4.3 Biofilm debonding

We next experimentally demonstrated the efficacy of the new catheter in debonding a mixed community biofilm of *P. mirabilis* and *E. coli* from the main drainage lumen surface of the catheter prototype in an *in vitro* biofilm model. *E. coli* is present in up to 90% of diagnosed urinary tract infections, and *P. mirabilis* is another frequent infecting bacterium that can accumulate in thickness sufficiently to block the urinary catheter causing trauma, leakage, pyelonephritis, and septicemia while overall being very difficult to treat [41, 104]. We chose *P. mirabilis* and *E. coli* to represent a challenging-to-remove and yet typical mixed community biofilm. Additionally, the two species have been shown to be non-interfering in a urinary catheter model, so we hypothesized that they would form a robust mixed-community biofilm [41, 104]. We employed an artificial bladder biofilm growth model modified to fit our prototypes. The model fed infected artificial urine downward through prototypes (Figure 25) at a rate of 0.5 mL min^{-1} , and after approximately 30 hours achieved uniform biofilm distribution around the perimeter and down the length of the main lumen (see Figure 34a for uninflated control sample). Our previous experiment with a similar biofilm growth model with only *P. mirabilis* had required approximately 42 hours to achieve a mature biofilm [121], and after accounting for the differences in geometry and dimensions it appears that the two bacterial strains exhibited a mild synergistic influence on biofilm growth.

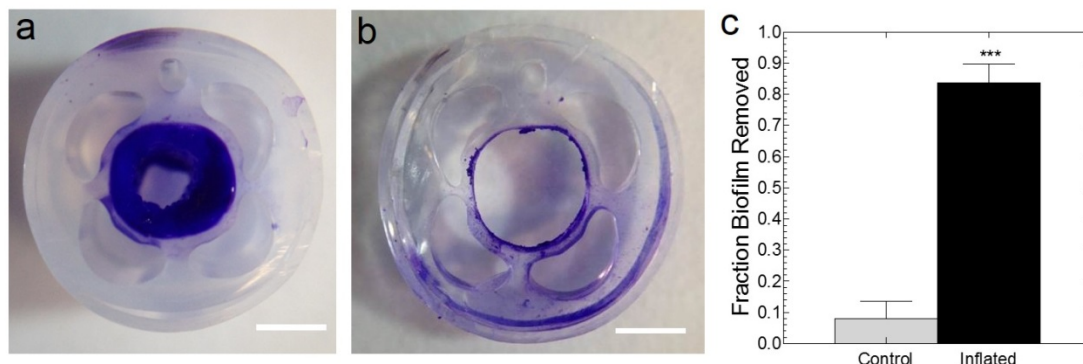


Figure 34: Prototype fouling-release urinary catheter debonds mixed community *P. mirabilis* and *E. coli* biofilm. Representative optical images of the cross sections of urinary catheter shafts with biofilm intact on main lumen of (a) control (uninflated) and removed from the main lumen of (b) inflated prototypes. All catheters were rinsed at 4 mL min^{-1} with artificial urine for 1 minute. Catheters designated for inflation were inflated to 80 kPa (approximately 35% strain) 10 times. Sections of the catheter shaft were removed and stained with crystal violet to enhance biofilm visualization. (c) Inflation removed a significant fraction of *P. mirabilis* and *E. coli* biofilm mass as determined by weight of biofilm in the rinse effluent normalized to the weight of biofilm grown in each run. N=3 replicates, “*” indicates $p < 0.005$. Scale bar indicates 1 mm.**

Once a mature biofilm was clearly visible covering the interior of the catheter, we gently removed the catheters from the artificial bladders and mounted them vertically for rinsing and testing (see Figure 34c). Each catheter was rinsed with artificial urine media supplied at 4 mLmin^{-1} for 1 min. Catheters that we designated for inflation/actuation were rapidly inflated to 80kPa and deflated 10 times, achieving an average of approximately 30% strain, at 20 s into the rinse (see supplemental videos). The debonding of the biofilm due to the actuation and the subsequent removal of the biofilm in the effluent was visually observed through the walls of the catheter. In cases

where the catheter was almost clogged with biofilm, the debonded biofilm would flow downward and then re-clog at the hub. We realized that imperfections in the hub region were creating a choke point and used a plastic tube inserted into the main lumen to shunt past the hub, which allowed the biofilm to flow out from the catheter in subsequent runs. We collected the effluent, centrifuged it, removed the supernatant, and then weighed the remaining biofilm in order to quantify the biofilm detachment using biofilm mass removed normalized to the biofilm mass grown for a particular run of four samples.

Finally the catheter was removed and sectioned to facilitate observation of the biofilm on the main drainage lumen surface. Sections from the top, middle, and bottom of the catheter shaft were also stained with 0.1% crystal violet to enhance biofilm visualization. Figure 34 shows representative optical images of the cross sections of control urinary catheter shaft with mixed community *P. mirabilis* and *E. coli* biofilm intact on the main lumen of a control vs. an actuated catheter. As shown in the representative images, the majority of the biofilm accumulated in the main lumen was clearly removed by inflation. We statistically analyzed the normalized biofilm mass removed and confirmed that the inflation removed a large fraction ($\approx 80\%$) of *P. mirabilis* and *E. coli* biofilm mass ($p < 0.005$ for $N=3$ replicates).

We visually observed that the biofilm exhibited a predominantly crystal composition as is typical with mixed community biofilms containing urease-producing

strains such as *P. mirabilis*. [23] In order to analyze the mechanical properties of the co-biofilm, we grew the mixed community biofilm on flat silicone samples as previously described [121]. We tested the complex visco-elastic modulus of the biofilms using an AR G-2 Rheometer and found that the mixed community biofilms demonstrated properties similar to our previous results for single-strain *P. mirabilis* biofilms [121]. The mixed community biofilms of *P. mirabilis* and *E. coli* were predominantly elastic with a storage modulus, G' , of $\sim 2.5 \times 10^4$ Pa and loss modulus, G'' , of $\sim 3.9 \times 10^3$ Pa for the scanned frequencies (Figure 35). We also carefully tested the adhesion strength of the biofilm based on a modified scratch test [123] and found that the co-biofilm exhibited an adhesion strength of approximately $\sim 8 \text{ Jm}^{-2}$.

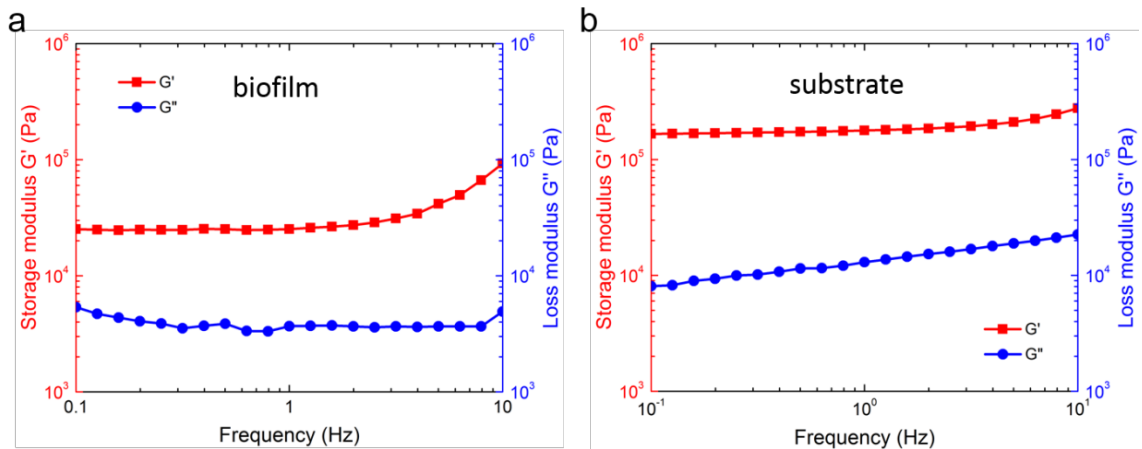


Figure 35: Storage modulus, G' , and loss modulus, G'' , of the co-biofilm of *P. mirabilis* and *E. coli* and the silicone substrate as a function of frequency. Moduli of (a) the co-biofilm of *P. mirabilis* and *E. coli* and (b) the silicone substrate. In both cases, the storage modulus is much higher than the loss modulus. Thus, these two kinds of materials are both apparently elastic dominant [127].

3.4.4 Repeated biofilm debonding

To assess the performance of the catheter in repetitive debonding of the biofilm for long term use, we regrew biofilm using the artificial bladder system for 24h after initially debonding the biofilm from all of the sample catheters after ≈ 30 hours of biofilm growth. We chose to leave the catheter prototypes “in situ” in the artificial bladders during the rinse and debonding steps to more closely simulate clinical conditions. Artificial urine media accumulated in the artificial bladders before flowing into the distal tip of the catheter, instead of being fed directly into the distal, top tip of the catheter. Catheters designated for inflation after the second round of biofilm growth were rapidly inflated to 100kPa (approximately 40% strain) and deflated 10 times approximately 20 seconds into the rinse. We again observed biofilm debonding from the main drainage lumen upon inflation actuation, and collected and weighed biofilm mass in the rinse effluent. Figure 36c describes the performance of the second run of debonding after re-growing the biofilm; actuation again removed the majority of the mixed community biofilm ($83.6 \pm 6.2\%$ N=4) at a statistically significant level ($p < 0.001$). The prototypes were removed, sectioned, and optically imaged. Figure 36a and Figure 36b show the representative optical images from cross sections that were crystal violet stained to enhance visualization. Control samples show thick biofilm coverage and inflated samples confirm substantial biofilm removal.

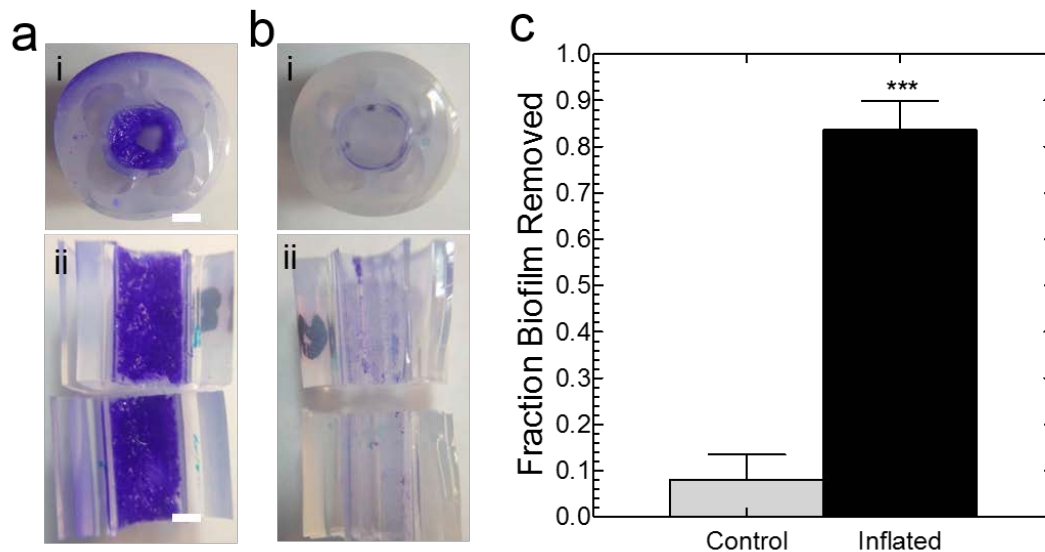


Figure 36: Prototype urinary catheter repeatedly debonded biofilms with mixed communities of *P. mirabilis* and *E. coli*. Biofilms were re-grown on samples that had undergone actuation. Samples were rinsed at 4 mL min^{-1} of artificial urine for 1 minute. Catheters designated for inflation were inflated to 100 kPa (approximately 40% average strain) for 10 times. Sections of the catheter shaft were removed and imaged, and select sections were crystal violet stained to enhance biofilm visualization. (a) Representative optical images from control samples (no inflation); both (i) cross section and (ii) sliced open samples show thorough biofilm coverage. Scale bar indicates 1 mm. (b) Representative optical images from inflated samples; (i) both cross section and (ii) sliced open samples show substantial biofilm removal. (c) Inflation removed a significant fraction of re-grown *P. mirabilis* and *E. coli* biofilm mass as determined by weight of biofilm in the rinse effluent normalized to the weight of biofilm grown in each run. $N=4$ replicates, “*” indicates $p<0.001$.**

Figure 37 shows optical images of cross sections along the length of three representative urinary catheters' shafts; a control, a catheter that underwent one round of biofilm debonding, and a catheter that underwent two rounds of biofilm debonding. We show the unstained cross sections since the distal tips (the end without a hub) were not stained, but the stained cross sections had similar results. Biofilm removal clearly occurs along the length of the catheter, thereby confirming our hypothesis that the intrawall actuation would work along the length of the catheter. Additionally, the second round of biofilm removal appears to be as successful at removing biofilm as the first actuation. If we compare the fraction of biofilm removed for the first round of biofilm removal against the second, we find no statistical difference between the data sets (N=4).

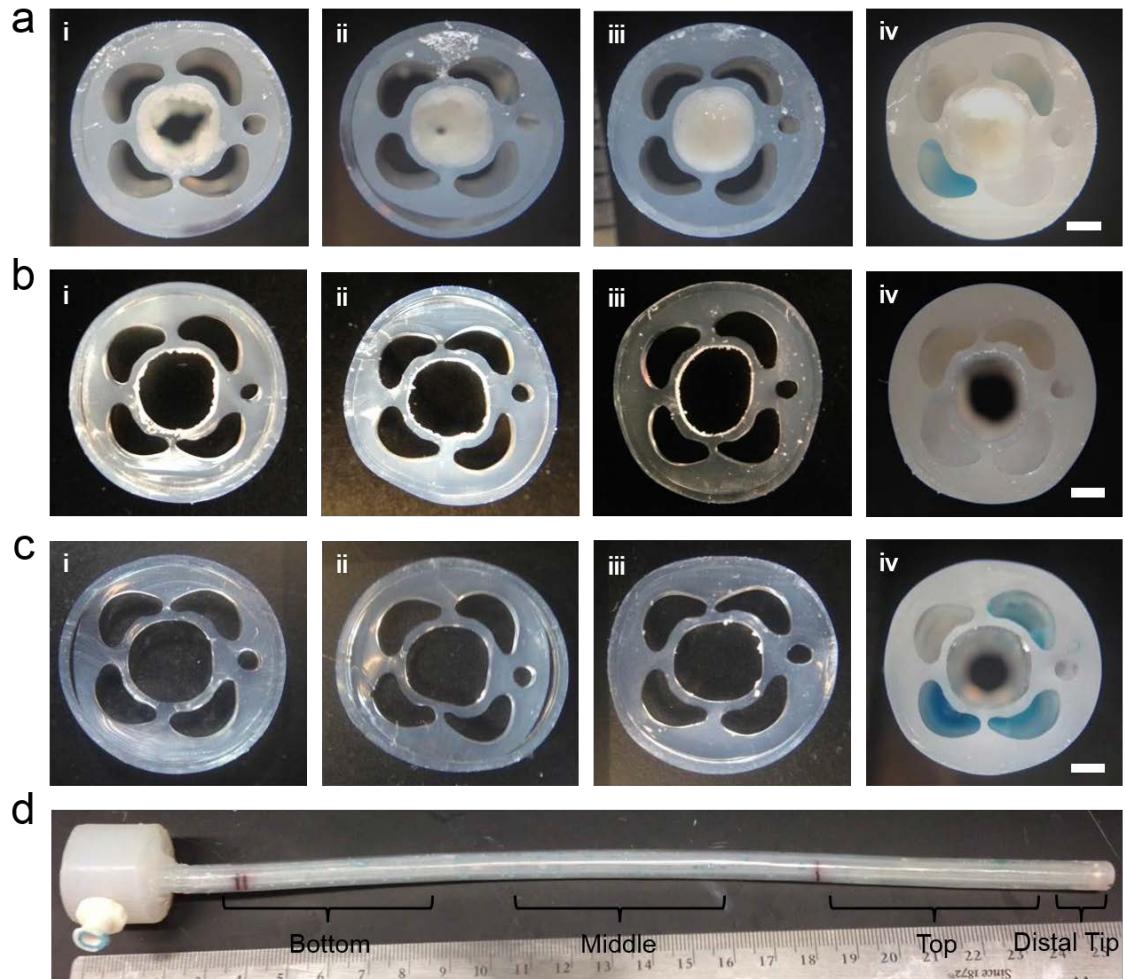


Figure 37: Prototype urinary catheters debond biofilms with mixed communities of *P. mirabilis* and *E. coli* along the full length of the catheter shaft. Representative optical images of the cross sections from (a) control catheter (no inflation), (b) first round of inflation after 30 h of growth of biofilm, and (c) second round of debonding after re-growing the biofilm for another 24 h. (d) Sections were taken from the prototypes at the following locations: (i) bottom, (ii) middle, (iii) top, and (iv) distal tip. Blue coloring in intra-wall inflation lumens is an artifact of residual colored water used for inflation. Scale bars indicate 1 mm.

3.4.5 Compressive strain of the substrate to debond biofilms

Previous studies have shown in several milieus that tensile strain to the substrate can debond overlying biofilm from the substrate [69, 121]. However, the shafts of these prototype catheters represent the first opportunity to evaluate the impact of compressive strain on biofilm debonding. Figure 38a shows the strain predicted by finite element modeling using ABAQUS to have occurred in a catheter inflated to 100 kPa, and maps the absolute value of the strain onto the surface of the catheter after deflation.

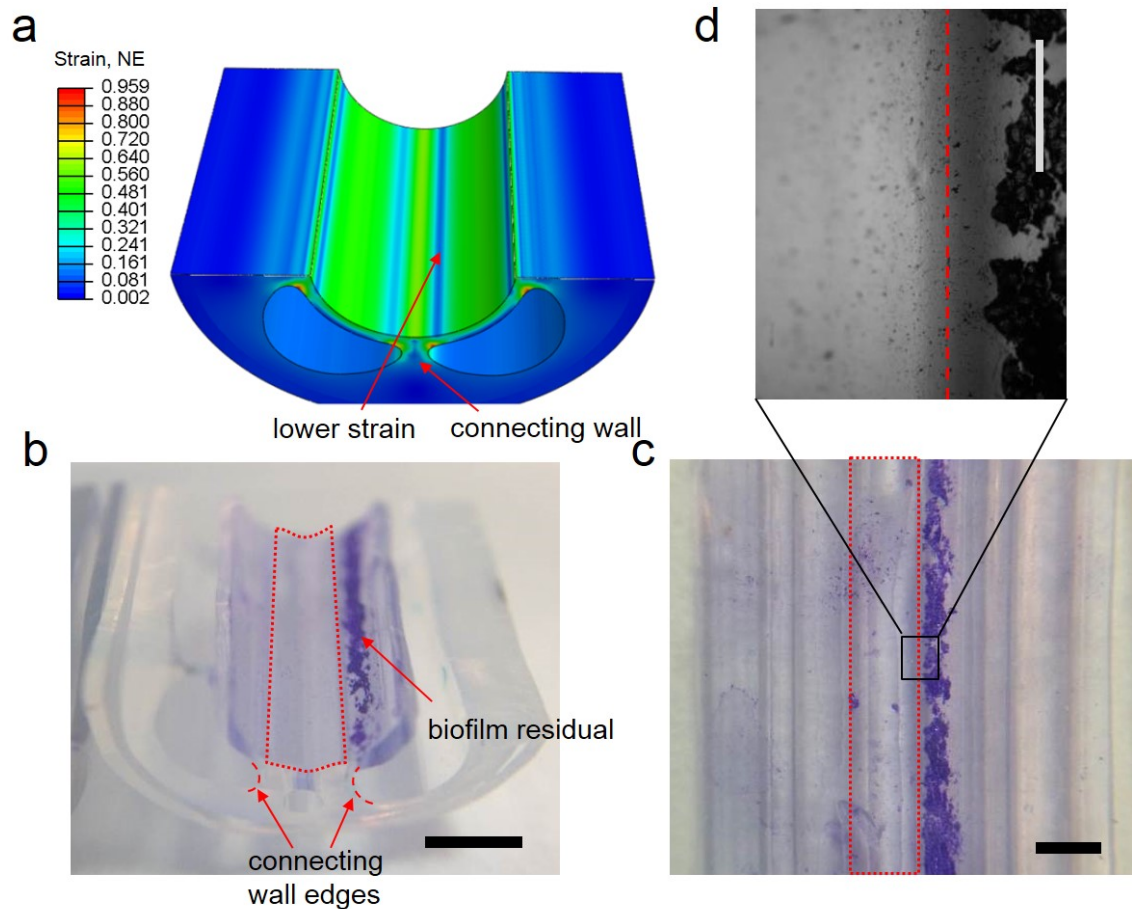


Figure 38: Compressive strain along luminal surface also debonds biofilm. (a) Contour plot of FEM-calculated nominal strains (absolute values of compressive and tensile strains) along luminal surface during inflation mapped onto undeformed surface. Compressive strain is generated in the luminal surface over the connecting walls due to the compression derived from the squeezing of adjacent inflation lumens during inflation. Lower absolute values of strain appear at the edge of inflation lumens due to the transition from tensile to compressive strain at the connecting walls. **(b)** Optical image of sliced-open crystal violet stained section of a catheter shaft that experienced two rounds of biofilm growth and debonding. Red, dashed box highlights the region on the luminal surface overlying a connecting wall between inflation lumens that has substantial biofilm removal due to compressive strain. **(c)** Optical image of luminal surface excised from catheter and flattened. Scale bars indicate 1 mm. **(d)** Optical microscopic image of luminal surface overlying the boundary between the wall and the inflation lumen. Dashed line shows area

overlying connection wall. Biofilm is visible at edge of inflation area, where low levels of strain were predicted by FEM calculations. Scale bar indicates 500 μm .

The area of the luminal surface overlying the wall between intrawall inflation lumens (i.e., the connecting wall) does not undergo tensile strain, but does undergo a significant amount of compressive strain. Interestingly, the area of the luminal surface that undergoes the least strain is the very edge of the intrawall inflation lumen, where the strain transitions from tensile to compressive and presents as an area of low absolute strain. When we examined longitudinal sections of catheters that had undergone actuation to debond biofilm (see representative section Figure 38b), it appeared that areas of the luminal surface that we predicted had undergone compressive strain still had debonded the majority of the biofilm. We carefully excised the luminal surface from the rest of the catheter shaft in representative samples and took optical images (Figure 38c) and microscope images (Figure 38d) and confirmed that the biofilm was removed in areas of high compressive strain, and residual biofilm was at the predicted edge of the inflation area where we predicted the low strain values.

3.5 Chapter conclusions

Active surface deformation is an efficient but simple method for detaching biofilm from a silicone substrate. We demonstrated a prototype of a multi-inflation-lumen urinary catheter with the ability to debond biofilms from the previously-

inaccessible main drainage lumen to keep its functionality. With the guidance of finite element analysis and experimental testing, we developed a design of an extrudable catheter shaft with four intra-wall inflation lumens that can apply sufficient strains around the majority of the perimeter. We further characterized the performance of the catheters by growing mixed community biofilms of *E. coli* and *P. mirabilis* on the main drainage lumen of the prototypes. The catheter prototypes were able to remove the biofilm on-demand repeatedly. We believe the design could be even further optimized in the future with the use in conjunction of other methods to reduce the adhesion of the main luminal surface [59, 116-119]. The ability to repeatedly remove biofilm suggests the real-world applicability of our catheter design for use in the challenging area of long term care. Upon close inspection of the interior of the catheter, we also discovered the first demonstration of compressive strain in the substrate debonding the overlying biofilm. The new prototype fouling-release catheter was made using readily-available techniques suitable to cost-effective, large-scale medical device manufacture. Our design offers a potential non-antibiotic, non-biologic approach to controlling symptomatic and asymptomatic biofilms and thereby reducing the persistent burden of catheter-associated urinary tract infections.

3.6 Chapter acknowledgements

V.L. and C.C. contributed equally to this work. This work was financially supported by the NSF's Research Triangle Materials Research Science and Engineering Center (DMR-1121107), the Office of Naval Research (N0014-13-1-0828), and the Duke-Coulter Translational Partnership Grant Program. Catheter image from Figure 27 licensed from Shutterstock Inc.

4. Chapter 4: Anti-fouling urinary catheters: Conclusions and Future Directions

4.1 Summary

The results of this work demonstrated that anti-fouling urinary catheters offer a promising non-biologic, non-antibiotic method to remove biofilms and thereby impact the thus far intractable problem of catheter-associated infections. The catheters utilize pressure-actuated chambers in the walls of the catheter to generate regio-selective strain and thereby remove biofilms from the main lumen. The urinary catheter prototypes are capable of on-demand removal of biofilms from the previously-inaccessible main drainage lumen of catheters. As a first step towards the design of the anti-fouling catheter, in Chapter 2 we demonstrated that sufficient strain applied to a flat silicone elastomer substrate would debond mature *Proteus mirabilis* crystalline biofilms. We examined the influence of strain rate and found that decreasing the applied strain rate would decrease the debonding. Proof-of-concept prototypes of sections of shafts of anti-fouling catheters constructed to incorporate a single intra-wall inflation chamber were able to inflate and induce substrate deformation as predicted by finite element modeling. The proof of concept prototypes were then able to debond mature crystalline biofilm from their strained surfaces.

Adjusting the number and position of intra-wall inflation lumens facilitated the design of an anti-fouling catheter shaft in Chapter 3. The shaft incorporated four intra-wall inflation lumens that could generate strain over the majority of the luminal surface

upon inflation-induced actuation. That multi-lumen catheter shaft was manufactured using techniques standard to the catheter industry. Catheter prototypes constructed using that shaft were able to generate greater than 30% strain on the majority of the luminal surface as predicted by finite element modeling, which indicates the potential for finite element modeling as a tool for future catheter design. Those multi-lumen anti-fouling catheter prototypes were able to on-demand remove greater than 80% of a mixed community biofilm of *P. mirabilis* and *E. coli*. In addition, detailed observation of the luminal surface revealed biofilm debonding due to application of compressive strain to the substrate. Finally, the anti-fouling catheter prototypes were able to debond and remove a mixed community biofilm of *P. mirabilis* and *E. coli* regrown on the luminal surface, thereby demonstrating the promise of repeated use of the anti-fouling approach. Biofilms on urinary catheters are critical to the progression of symptomatic CAUTIs, and the anti-fouling catheter technology demonstrated in this study provides a powerful option for on-demand removing biofilms and potentially stopping the progression of symptomatic infections.

4.2 Future directions

The future directions describe proposed collaborative work with individuals both at the Duke University School of Medicine and within the Lopez lab.

4.2.1 Coulter Translational Project Partnership

A Coulter Translational Project proposal was submitted March 2014, and that proposal went to the final, competitive presentation round in May 2014. The proposal was approved for the 2014-2015 cycle starting October 2014. The project involves collaboration with the Duke School of Medicine (SOM), as represented by Howard Levinson from the SOM Department of Plastic Surgery. Gabriel P. Lopez, Xuanhe Zhao, and Vrad Levering represent the Duke Department of Biomedical Engineering. The team supporting the project grew once it received funding, and future work conducted after the filing of this dissertation will involve collaboration between Vrad Levering and members of the Duke SOM such as Mohammed Ibrahim, MD. The following sections related to the Coulter summarize the proposal, planned efforts, and the progress made toward each Coulter project-specific aim.

4.2.1.1 Coulter project summary

The need to control the urinary stream is ubiquitous in healthcare with over 30 million Foley urinary catheters sold annually. The greatest problem with Foley catheters today is catheter-associated urinary tract infections (CAUTIs), however hospitals bear additional concerns about the financial implications of CAUTI's since each CAUTI directly increases the cost of patient care. CAUTIs require treatment with antibiotics and are on the Center of Medicare Services list of "never events". Thus, hospitals do not

receive payments for treating hospital acquired CAUTIs [5]. CAUTIs are caused by biofilm formation within the catheter lumen [128].

As described in this document, the anti-fouling technology uses a mechanical approach to actively deform the intraluminal surface of the Foley catheter and physically detach the biofilm. In addition to potentially reducing the risk of CAUTIs, the ability to repeatedly remove the biofilm and keep the catheter main lumen clear could also possibly extend the indwelling catheter life and thereby reduce catheter-related costs in another way [121]. We filed a patent application through Duke OLV that describes both the platform technology for biofouling mitigation, and specifically a urinary catheter configuration based on this technology. We constructed and tested proof-of-concept prototypes of catheter shafts that debonded greater than 90% of a biofilm, a revolutionary breakthrough in catheter design [121].

The proposed technology utilizes existing materials and manufacturing processes, increasing cost of manufacturing approximately 16%. This is pivotally important since urinary catheters are a low-cost, high-volume product covered by 6 HCSPS reimbursement codes. Using silver-eluting anti-biofouling catheters as a basis for financial modeling, an estimated \$0.50 increase in manufacturing cost of our Foley would generate a \$3.35 increase in profit per catheter. Cardinal Health, a catheter manufacturer and potential licensee that we are currently in dialog with, said that if the catheter were clinically effective, the technology would reduce the total cost of home

care and be a “big win” for acute care. As such, it would allow a manufacturer to increase sales in an ever-growing market. We won Coulter funding for the next critical steps in product development; fabricating a fully functional medical grade catheter for confirmatory *in vitro* testing followed by a phase I clinical study.

The work conducted towards Aims 2 and 3 of this thesis helped simultaneously advance and answer questions related to the Coulter project. We assessed many of the responses for the Coulter project using just the shaft tubing. During the course of our studies described within this document, we evaluated a variety of factors that determine the inflation performance of the device. The shaft’s geometry and modulus (moduli if made of multiple components) dictate the direction and degree of inflation and thereby influence the substrate strain achieved, which then determines the biofilm removal. We used multiple moduli of silicone and components for developing the proof-of-concept prototypes in Chapter 2, and developed a knowledge of the minimum ratio of external to internal thickness to prevent external inflation in urinary catheters. However, we also realized that a high durometer or inelastic sheath significantly helped the design to force inward inflation. This allowed the catheter to use a low durometer inner shaft to keep the inflation pressure sufficiently low, while the outer sheath helped prevent external inflation. The patent application was written to anticipate multiple techniques for mechanical detachment of the biofilm and provides many options beyond those

described in this document, so the use of multiple materials or components is covered by the intellectual property.

The work described in Chapter 3 to develop a multi-lumen, extruded catheter shaft composed of silicone and at clinically relevant dimensions (6.7 mm in diameter) was fundamental for continuing to advance the Coulter project goals. The catheter shaft design work conducted by the Lopez lab team addressed multiple significant questions that were ancillary to the scientific discussion of Chapter 3 but important to the device design; and which will be useful for developing the complete functional prototypes.

The most obvious and crucial question addressed was that the anti-fouling catheter shaft indeed debonded biofilm, and could debond biofilm repeatedly. We felt that demonstrating mixed community biofilm release at 2 and 4 days was a conservative *in vitro* model system for the *in vivo* pilot clinical study. Demonstrating repeated release provided initial evidence confirming this system's clinical relevance for reducing biofilm coverage while assisting in preparing protocols for a pilot clinical trial.

We initiated collaborations and completed an agreement with a third-party catheter manufacturer to design, build, and document "complete" prototypes (with hubs and bladder restraint balloons) for the clinical trial. Figure 39 shows the designed catheter, but until the complete prototype is fabricated we will continue to assess the shaft's performance through evaluations of the inflation reliability, consistency of dimensions post-inflation, and overall inflation durability.

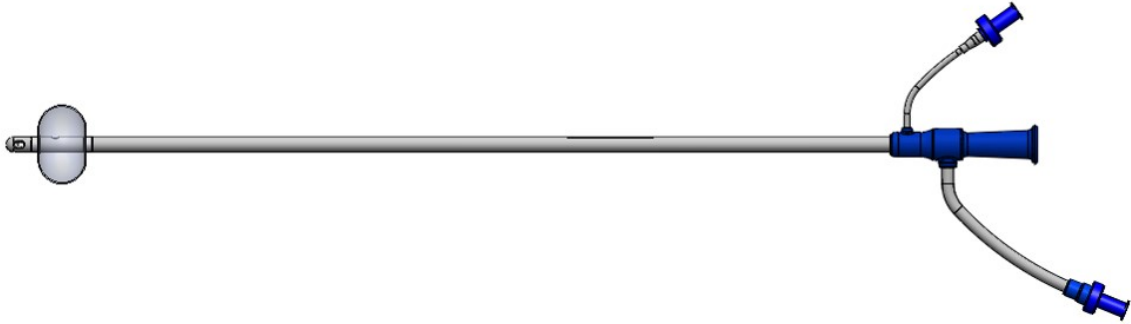


Figure 39: Side view of the prototype anti-fouling urinary catheter designed in collaboration with the third-party catheter manufacturer.

4.3 Conclusions and implications of this research

The results of this work demonstrated that anti-biofouling urinary catheters can serve as potential, compelling options for reducing and preventing long-term biofilm buildup on the inner surfaces of indwelling urinary catheters. Biofilm formation on urinary catheters is critical to the progression of catheter associated urinary tract infections, which are the number one source of nosocomial infections in the USA. Although directly testing the reduction in catheter associated urinary tract infections was beyond the scope of this dissertation, the *in vitro* demonstration of biofilm removal and prevention of biofilm buildup has profound implications for the potential to transform the long-stagnant urinary catheter standard of care. The design for urinary catheters has changed little in the last 50 years, and the work documented in this dissertation presents a practical and imminently implementable design change that can potentially reduce the infection rate without requiring new materials or drugs. Due to

the practical and presumably low-cost potential addition of the technology to current manufacturing practices, the catheter project team is currently investigating licensing and startup next-steps to facilitate implementing the technology in the commercial arena.

The anti-fouling design and technology has potential for use in other applications beside the urinary catheter covered in this document (typically called “Foley’s”). Suprapubic urinary catheters are inserted through the anterior abdominal wall and directly into the bladder (instead of up the urethra). Suprapubic catheters are left indwelling and require a retention balloon similar to Foley urinary catheters, but are much shorter than Foley’s (approximately 25 cm vs 42 cm). Suprapubic urinary catheters use a substantially similar design to the “Foley” urinary catheters we worked with, and although they were long considered less prone to infection than Foley’s, suprapubic catheters unfortunately suffer similar issues with biofilm build-up and have indistinguishable rates of infection [129]. As such, suprapubic catheters would likely benefit from the anti-fouling methods deployed in the anti-fouling Foley urinary catheters described in this document.

Other catheters, such as central venous catheters, also suffer from biofilm infections and indeed in these catheters the consequences of infection are often more severe than infections associated with urinary catheters [102] due to the central venous catheters’ location within the vasculature. Additionally, these catheters can suffer

biofilm-like formation of undesirable proteinaceous layers [102] that would potentially debond in a similar fashion to biofilms upon application of active surface deformation.

Overall, the anti-fouling methods used to remove biofilms from the previously-inaccessible main lumen of urinary catheters provide a potential boon to the future use of urinary catheters, as well as presenting a promising platform technology that could be applicable in anti-fouling use in other medical device applications.

Appendix A

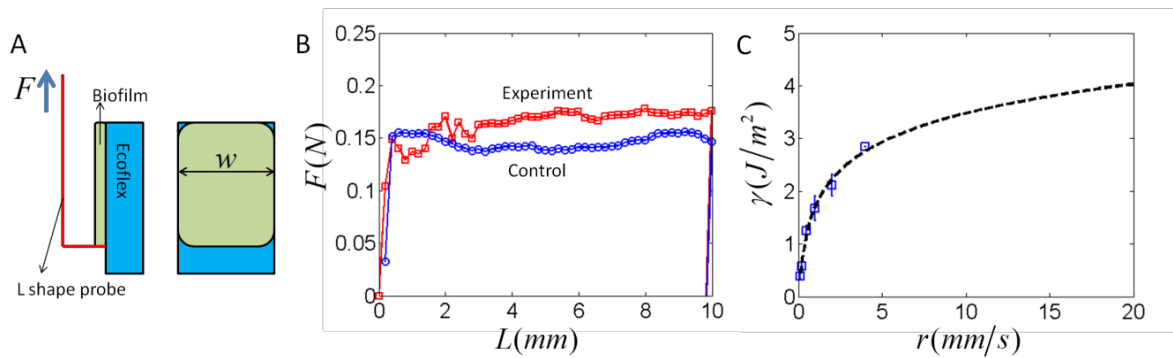


Figure 40: Adhesion force of mature *P. mirabilis* crystalline biofilm measured via modified scratch test A) Diagram of scratch test B) Representative run of scratch test. Rate=0.5mm/s. We measured the bulk adhesion using a method established in Chen *et al.* [123], to measure an adhesion strength ranging from 1.25 to 4 $J m^{-2}$ for stretching rates 0.5 – 20 mm/s. Mature *P. mirabilis* crystalline biofilm was grown on flat silicone elastomer substrate using the methods described in Chapter 2.

References

1. (CDC), C.f.D.C.a.P. *Catheter - associated Urinary Tract Infections (CAUTI)*. Available from: http://www.cdc.gov/HAI/ca_uti/uti.html.
2. Donlan, R.M., *Biofilm formation: a clinically relevant microbiological process*. Clin Infect Dis, 2001. **33**(8): p. 1387-92.
3. Pace, J., M. Rupp, and R. Finch, , ed. *Biofilms, Infection and Antimicrobial Therapy*. 2006, Taylor and Francis Group, CRC Press: London.
4. Stickler, D.J., *Bacterial biofilms in patients with indwelling urinary catheters*. Nat Clin Pract Urol, 2008. **5**(11): p. 598-608.
5. Scott, R. *CDC: Direct Medical Costs of Healthcare Acquired Infections and Benefits of Prevention*. 2009.
6. Hooton, T.M., et al., *Diagnosis, prevention, and treatment of catheter-associated urinary tract infection in adults: 2009 International Clinical Practice Guidelines from the Infectious Diseases Society of America*. Clin Infect Dis, 2010. **50**(5): p. 625-63.
7. Siddiq, D.M. and R.O. Darouiche, *New strategies to prevent catheter-associated urinary tract infections*. Nat Rev Urol, 2012. **9**(6): p. 305-14.
8. Matsukawa, M., et al., *Bacterial colonization on intraluminal surface of urethral catheter*. Urology, 2005. **65**(3): p. 440-4.
9. Morris, N.S., D.J. Stickler, and R.J. McLean, *The development of bacterial biofilms on indwelling urethral catheters*. World J Urol, 1999. **17**(6): p. 345-50.
10. Roberts, A.P., et al., *Transfer of a conjugative transposon, Tn5397 in a model oral biofilm*. FEMS Microbiol Lett, 1999. **177**(1): p. 63-6.
11. Saint, S., et al., *Risk factors for nosocomial urinary tract-related bacteremia: a case-control study*. Am J Infect Control, 2006. **34**(7): p. 401-7.
12. Costerton, J.W., et al., *Bacterial biofilms in nature and disease*. Annu Rev Microbiol, 1987. **41**: p. 435-64.

13. Stickler, D.J., et al., *Blockage of urethral catheters by bacterial biofilms*. J Infect, 1993. **27**(2): p. 133-5.
14. Stickler, D.J., N.S. Morris, and C. Winters, *Simple physical model to study formation and physiology of biofilms on urethral catheters*. Methods Enzymol, 1999. **310**: p. 494-501.
15. Jones, B.V., et al., *Ultrastructure of Proteus mirabilis swarmer cell rafts and role of swarming in catheter-associated urinary tract infection*. Infect Immun, 2004. **72**(7): p. 3941-50.
16. Zhao, H., et al., *In vivo phase variation of MR/P fimbrial gene expression in Proteus mirabilis infecting the urinary tract*. Mol Microbiol, 1997. **23**(5): p. 1009-19.
17. Chavan, R.R., et al., *Characterization of the complete genome of a novel citrivirus infecting Actinidia chinensis*. Arch Virol, 2013.
18. Morita, T., et al., *Effects of noradrenaline and acetylcholine on ureteral peristalsis*. Tohoku J Exp Med, 1983. **141**(4): p. 489-90.
19. Suzuki, T., [*Experimental and physiological study on the effects of autonomic drugs upon the pacemaker activity of pelviureteral peristalsis*]. Nihon Heikatsukin Gakkai Zasshi, 1983. **19**(2): p. 123-38.
20. Kosaka, R., et al., *Effect of a bearing gap on hemolytic property in a hydrodynamically levitated centrifugal blood pump with a semi-open impeller*. Biomed Mater Eng, 2013. **23**(1-2): p. 37-47.
21. Kim, S.H., et al., *Preliminary Validation of a New Magnetic Wireless Blood Pump*. Artif Organs, 2013.
22. Koyama, T., et al., *Evaluation of esophageal peristalsis in patients with esophageal tumors: initial experience with cine MR imaging*. Magn Reson Med Sci, 2005. **4**(3): p. 109-14.
23. Macleod, S.M. and D.J. Stickler, *Species interactions in mixed-community crystalline biofilms on urinary catheters*. J Med Microbiol, 2007. **56**(Pt 11): p. 1549-57.
24. Yoshimura, N. and M.B. Chancellor, *Differential diagnosis and treatment of impaired bladder emptying*. Rev Urol, 2004. **6 Suppl 1**: p. S24-31.

25. Wang, Z.Y., et al., [*Proteus syndrome with a giant hemangiomas in the spleen associated with chronic DIC--two case report and literature review*]. *Zhonghua Xue Ye Xue Za Zhi*, 2007. **28**(3): p. 152-5.
26. Stickler, D.J. and G.L. Jones, *Reduced Susceptibility of Proteus mirabilis to triclosan*. *Antimicrob Agents Chemother*, 2008. **52**(3): p. 991-4.
27. Jones, G.L., et al., *A strategy for the control of catheter blockage by crystalline Proteus mirabilis biofilm using the antibacterial agent triclosan*. *Eur Urol*, 2005. **48**(5): p. 838-45.
28. Lemack, G.E., A.G. Baseman, and P.E. Zimmern, *Voiding dynamics in women: a comparison of pressure-flow studies between asymptomatic and incontinent women*. *Urology*, 2002. **59**(1): p. 42-6.
29. Ceri, H., et al., *The Calgary Biofilm Device: new technology for rapid determination of antibiotic susceptibilities of bacterial biofilms*. *J Clin Microbiol*, 1999. **37**(6): p. 1771-6.
30. Jones, B.D. and H.L. Mobley, *Proteus mirabilis urease: nucleotide sequence determination and comparison with jack bean urease*. *J Bacteriol*, 1989. **171**(12): p. 6414-22.
31. Cox, A.J. and D.W. Hukins, *Morphology of mineral deposits on encrusted urinary catheters investigated by scanning electron microscopy*. *J Urol*, 1989. **142**(5): p. 1347-50.
32. Armbruster, C.E. and H.L. Mobley, *Merging mythology and morphology: the multifaceted lifestyle of Proteus mirabilis*. *Nat Rev Microbiol*, 2012. **10**(11): p. 743-54.
33. Pearson, M.M., et al., *Complete genome sequence of uropathogenic Proteus mirabilis, a master of both adherence and motility*. *J Bacteriol*, 2008. **190**(11): p. 4027-37.
34. Hoeniger, J.F., *Cellular changes accompanying the swarming of Proteus mirabilis. II. Observations of stained organisms*. *Can J Microbiol*, 1966. **12**(1): p. 113-23.
35. Jones, S.M., et al., *Structure of Proteus mirabilis biofilms grown in artificial urine and standard laboratory media*. *FEMS Microbiol Lett*, 2007. **268**(1): p. 16-21.
36. Morgan, S.D., D. Rigby, and D.J. Stickler, *A study of the structure of the crystalline bacterial biofilms that can encrust and block silver Foley catheters*. *Urol Res*, 2009. **37**(2): p. 89-93.

37. Sabbuba, N., G. Hughes, and D.J. Stickler, *The migration of Proteus mirabilis and other urinary tract pathogens over Foley catheters*. BJU Int, 2002. **89**(1): p. 55-60.
38. Stickler, D., et al., *Why are Foley catheters so vulnerable to encrustation and blockage by crystalline bacterial biofilm?* Urol Res, 2003. **31**(5): p. 306-11.
39. Stickler, D.J. and S.D. Morgan, *Observations on the development of the crystalline bacterial biofilms that encrust and block Foley catheters*. J Hosp Infect, 2008. **69**(4): p. 350-60.
40. Coker, C., H. Zhao, and H.L. Mobley, *Green fluorescent protein urea sensors. Uropathogenic Proteus mirabilis*. Methods Mol Biol, 2002. **183**: p. 287-93.
41. Williams, G.J. and D.J. Stickler, *Effect of triclosan on the formation of crystalline biofilms by mixed communities of urinary tract pathogens on urinary catheters*. J Med Microbiol, 2008. **57**(Pt 9): p. 1135-40.
42. Trevisani, F., et al., *Surveillance for hepatocellular carcinoma in elderly Italian patients with cirrhosis: effects on cancer staging and patient survival*. Am J Gastroenterol, 2004. **99**(8): p. 1470-6.
43. Hunt, J.T., et al., *Discovery of the pyrrolo[2,1-f][1,2,4]triazine nucleus as a new kinase inhibitor template*. J Med Chem, 2004. **47**(16): p. 4054-9.
44. Borzini, P., et al., *Regarding "Randomized trial and local biological effect of autologous platelets used as adjuvant therapy for chronic venous leg ulcers"*. J Vasc Surg, 2004. **39**(5): p. 1146-7; author reply 1147.
45. Sergiacomi, G., et al., *Non-invasive diagnostic and functional evaluation of cardiac and pulmonary involvement in systemic sclerosis*. In Vivo, 2004. **18**(2): p. 229-35.
46. Babic-Erceg, A., et al., *Dermatophytoses in Split and Dalmatia, Croatia, 1996-2002*. Mycoses, 2004. **47**(7): p. 297-9.
47. Dror, N., et al., *Advances in microbial biofilm prevention on indwelling medical devices with emphasis on usage of acoustic energy*. Sensors (Basel), 2009. **9**(4): p. 2538-54.
48. Cleasby, G.W., W.E. Fung, and J.V. Fiore, Jr., *Photocoagulation of exudative senile maculopathy*. Trans Pac Coast Otoophthalmol Soc Annu Meet, 1970. **51**: p. 233-58.
49. Lew, H.S. and Y.C. Fung, *Plug effect of erythrocytes in capillary blood vessels*. Biophys J, 1970. **10**(1): p. 80-99.

50. Mazzetti, I., et al., *A role for chemokines in the induction of chondrocyte phenotype modulation*. *Arthritis Rheum*, 2004. **50**(1): p. 112-22.
51. Fung, Y.C., *Mathematical representation of the mechanical properties of the heart muscle*. *J Biomech*, 1970. **3**(4): p. 381-404.
52. Kakol, Z., et al., *Effect of low-level titanium(IV) doping on the resistivity of magnetite near the Verwey transition*. *Phys Rev B Condens Matter*, 1992. **46**(4): p. 1975-1978.
53. Glied, S.A. and P.C. Borzi, *The current state of employment-based health coverage*. *J Law Med Ethics*, 2004. **32**(3): p. 404-9.
54. Lombardo, L.J., et al., *Discovery of N-(2-chloro-6-methyl-phenyl)-2-(6-(4-(2-hydroxyethyl)-piperazin-1-yl)-2-methylpyrimidin-4-ylamino)thiazole-5-carboxamide (BMS-354825), a dual Src/Abl kinase inhibitor with potent antitumor activity in preclinical assays*. *J Med Chem*, 2004. **47**(27): p. 6658-61.
55. Ista, L.K., S. Mendez, and G.P. Lopez, *Attachment and detachment of bacteria on surfaces with tunable and switchable wettability*. *Biofouling*, 2010. **26**(1): p. 111-8.
56. Ista, L.K., V.H. Perez-Luna, and G.P. Lopez, *Surface-grafted, environmentally sensitive polymers for biofilm release*. *Appl Environ Microbiol*, 1999. **65**(4): p. 1603-9.
57. Shivapooja, P., et al., *ARGET-ATRP synthesis and characterization of PNIPAAm brushes for quantitative cell detachment studies*. *Biointerphases*, 2012. **7**(1-4): p. 32.
58. Stickler, D.J., et al., *A sensor to detect the early stages in the development of crystalline *Proteus mirabilis* biofilm on indwelling bladder catheters*. *J Clin Microbiol*, 2006. **44**(4): p. 1540-2.
59. Reddy, S.T., et al., *Micropatterned surfaces for reducing the risk of catheter-associated urinary tract infection: an in vitro study on the effect of sharklet micropatterned surfaces to inhibit bacterial colonization and migration of uropathogenic *Escherichia coli**. *J Endourol*, 2011. **25**(9): p. 1547-52.
60. Cerca, N., R. Oliveira, and J. Azeredo, *Susceptibility of *Staphylococcus epidermidis* planktonic cells and biofilms to the lytic action of *staphylococcus bacteriophage K**. *Lett Appl Microbiol*, 2007. **45**(3): p. 313-7.
61. Kelly, D., et al., *Prevention of *Staphylococcus aureus* biofilm formation and reduction in established biofilm density using a combination of phage K and modified derivatives*. *Lett Appl Microbiol*, 2012. **54**(4): p. 286-91.

62. Schmidt, J.C., et al., *Brushing without brushing?--a review of the efficacy of powered toothbrushes in noncontact biofilm removal*. Clin Oral Investig, 2013. **17**(3): p. 687-709.
63. Xu, J., et al., *Minimization of treatment time for in vitro 1.1 MHz destruction of Pseudomonas aeruginosa biofilms by high-intensity focused ultrasound*. Ultrasonics, 2012. **52**(5): p. 668-75.
64. Hazan, Z., et al., *Effective prevention of microbial biofilm formation on medical devices by low-energy surface acoustic waves*. Antimicrob Agents Chemother, 2006. **50**(12): p. 4144-52.
65. Falagas, M.E., et al., *Outcome of antimicrobial therapy in documented biofilm-associated infections: a review of the available clinical evidence*. Drugs, 2009. **69**(10): p. 1351-61.
66. Ha, S.K., et al., *Successful use of cytology brush in the treatment of relapsing CAPD peritonitis*. Nephrol Dial Transplant, 1997. **12**(9): p. 1997-9.
67. Raz, R., D. Schiller, and L.E. Nicolle, *Chronic indwelling catheter replacement before antimicrobial therapy for symptomatic urinary tract infection*. J Urol, 2000. **164**(4): p. 1254-8.
68. Phanindhar Shivapooja, Q.W., Beatriz Orihuela, Daniel Rittschof, Gabriel P. López and Xuanhe Zhao *Bioinspired Surfaces with Dynamic Topography for Active Control of Biofouling*. Advanced Materials, 2013. DOI: 10.1002/adma.201203374.
69. Shivapooja, P., et al., *Bioinspired surfaces with dynamic topography for active control of biofouling*. Adv Mater, 2013. **25**(10): p. 1430-4.
70. Lahaye, E., et al., *Does water activity rule P. mirabilis periodic swarming? I. Biochemical and functional properties of the extracellular matrix*. Biomacromolecules, 2007. **8**(4): p. 1218-27.
71. Paradzik, M.T., B. Levojevic, and A. Gabric, *[Decrease of urinary tract infections following catheterization after the education of health care workers, introduction of protocols and surveillance lists]*. Lijec Vjesn, 2011. **133**(1-2): p. 15-9.
72. Jones, B.D. and H.L. Mobley, *Proteus mirabilis urease: genetic organization, regulation, and expression of structural genes*. J Bacteriol, 1988. **170**(8): p. 3342-9.

73. Morris, N.S., D.J. Stickler, and C. Winters, *Which indwelling urethral catheters resist encrustation by Proteus mirabilis biofilms?* Br J Urol, 1997. **80**(1): p. 58-63.
74. Morris, N.S. and D.J. Stickler, *Encrustation of indwelling urethral catheters by Proteus mirabilis biofilms growing in human urine.* J Hosp Infect, 1998. **39**(3): p. 227-34.
75. Pickard, R., et al., *Antimicrobial catheters for reduction of symptomatic urinary tract infection in adults requiring short-term catheterisation in hospital: a multicentre randomised controlled trial.* Lancet, 2012. **380**(9857): p. 1927-35.
76. Ilievski, F., et al., *Soft robotics for chemists.* Angew Chem Int Ed Engl, 2011. **50**(8): p. 1890-5.
77. Majidi, L. and M. Zareyan, *Quantum transport of pseudospin-polarized Dirac fermions in gapped graphene nanostructures.* Journal of Computational Electronics, 2013. **12**(2): p. 134-144.
78. Shepherd, R.F., et al., *Multigait soft robot.* Proc Natl Acad Sci U S A, 2011. **108**(51): p. 20400-3.
79. Villanueva, C., S.G. Hossain, and C.A. Nelson, *Silicone catheters may be superior to latex catheters in difficult urethral catheterization after urethral dilation.* J Endourol, 2011. **25**(5): p. 841-4.
80. Goeres, D.M., et al., *Statistical assessment of a laboratory method for growing biofilms.* Microbiology, 2005. **151**(Pt 3): p. 757-62.
81. Goeres, D.M., et al., *A method for growing a biofilm under low shear at the air-liquid interface using the drip flow biofilm reactor.* Nat Protoc, 2009. **4**(5): p. 783-8.
82. Kazmierska, K.A., et al., *In vitro multicompartmental bladder model for assessing blockage of urinary catheters: effect of hydrogel coating on dynamics of Proteus mirabilis growth.* Urology, 2010. **76**(2): p. 515 e15-20.
83. Malic, S., et al., *Development of an "early warning" sensor for encrustation of urinary catheters following Proteus infection.* J Biomed Mater Res B Appl Biomater, 2012. **100**(1): p. 133-7.
84. Croes, S., et al., *Staphylococcus aureus biofilm formation at the physiologic glucose concentration depends on the S. aureus lineage.* BMC Microbiol, 2009. **9**: p. 229.

85. Favre-Bonte, S., T. Kohler, and C. Van Delden, *Biofilm formation by Pseudomonas aeruginosa: role of the C4-HSL cell-to-cell signal and inhibition by azithromycin*. J Antimicrob Chemother, 2003. **52**(4): p. 598-604.
86. Limbert, G., et al., *On the mechanics of bacterial biofilms on non-dissolvable surgical sutures: A laser scanning confocal microscopy-based finite element study*. Acta Biomater, 2013.
87. Aggarwal, S. and R.M. Hozalski, *Effect of strain rate on the mechanical properties of Staphylococcus epidermidis biofilms*. Langmuir, 2012. **28**(5): p. 2812-6.
88. Hall-Stoodley, L., J.W. Costerton, and P. Stoodley, *Bacterial biofilms: from the natural environment to infectious diseases*. Nat Rev Microbiol, 2004. **2**(2): p. 95-108.
89. Ehret, A.E. and M. Bol, *Modelling mechanical characteristics of microbial biofilms by network theory*. J R Soc Interface, 2012.
90. Bol, M., et al., *Recent advances in mechanical characterisation of biofilm and their significance for material modelling*. Crit Rev Biotechnol, 2013. **33**(2): p. 145-71.
91. Lieleg, O., et al., *Mechanical robustness of Pseudomonas aeruginosa biofilms*. Soft Matter, 2011. **7**(7): p. 3307-3314.
92. Lahaye, E., et al., *Does water activity rule P. mirabilis periodic swarming? II. Viscoelasticity and water balance during swarming*. Biomacromolecules, 2007. **8**(4): p. 1228-35.
93. Stankovich, S., et al., *Graphene-based composite materials*. Nature, 2006. **442**(7100): p. 282-286.
94. Bergstrom, J.S. and M.C. Boyce, *Mechanical behavior of particle filled elastomers*. Rubber Chemistry and Technology, 1999. **72**(4): p. 633-656.
95. Lau, P.C., et al., *Absolute quantitation of bacterial biofilm adhesion and viscoelasticity by microbead force spectroscopy*. Biophys J, 2009. **96**(7): p. 2935-48.
96. Xia, Z.C. and J.W. Hutchinson, *Crack patterns in thin films*. Journal of the Mechanics and Physics of Solids, 2000. **48**(6-7): p. 1107-1131.
97. Wang, Q. and X. Zhao, *Creasing-wrinkling transition in elastomer films under electric fields*. Phys Rev E Stat Nonlin Soft Matter Phys, 2013. **88**(4 Pt 1): p. 042403.

98. Hutchinson, J.W. and Z. Suo, *Mixed-Mode Cracking in Layered Materials*. Advances in Applied Mechanics, Vol 29, 1992. **29**: p. 63-191.
99. Thalladi, V.R., et al., *Simulation of indentation fracture in crystalline materials using mesoscale self-assembly*. J Am Chem Soc, 2002. **124**(33): p. 9912-7.
100. Lu, N.S., J.I. Yoon, and Z.G. Suo, *Delamination of stiff islands patterned on stretchable substrates*. International Journal of Materials Research, 2007. **98**(8): p. 717-722.
101. Burnier, M., et al., *Salt-dependent renal effects of an angiotensin II antagonist in healthy subjects*. Hypertension, 1993. **22**(3): p. 339-47.
102. Sousa, C., M. Henriques, and R. Oliveira, *Mini-review: Antimicrobial central venous catheters--recent advances and strategies*. Biofouling, 2011. **27**(6): p. 609-20.
103. Kambal, C., et al., *Catheter-associated UTIs in patients after major gynaecological surgery*. Prof Nurse, 2004. **19**(9): p. 515-8.
104. Jacobsen, S.M., et al., *Complicated catheter-associated urinary tract infections due to Escherichia coli and Proteus mirabilis*. Clin Microbiol Rev, 2008. **21**(1): p. 26-59.
105. Wang, R., et al., *Inhibition of Escherichia coli and Proteus mirabilis adhesion and biofilm formation on medical grade silicone surface*. Biotechnol Bioeng, 2012. **109**(2): p. 336-45.
106. Mulla, S.A. and S. Revdiwala, *Assessment of biofilm formation in device-associated clinical bacterial isolates in a tertiary level hospital*. Indian J Pathol Microbiol, 2011. **54**(3): p. 561-4.
107. Ahimou, F., et al., *Biofilm cohesiveness measurement using a novel atomic force microscopy methodology*. Appl Environ Microbiol, 2007. **73**(9): p. 2897-904.
108. Pavithra, D. and M. Doble, *Biofilm formation, bacterial adhesion and host response on polymeric implants--issues and prevention*. Biomed Mater, 2008. **3**(3): p. 034003.
109. Costerton, J.W., L. Montanaro, and C.R. Arciola, *Biofilm in implant infections: its production and regulation*. Int J Artif Organs, 2005. **28**(11): p. 1062-8.
110. Campoccia, D., L. Montanaro, and C.R. Arciola, *A review of the clinical implications of anti-infective biomaterials and infection-resistant surfaces*. Biomaterials, 2013. **34**(33): p. 8018-29.

111. Davey, P., et al., *Systematic review of antimicrobial drug prescribing in hospitals*. *Emerg Infect Dis*, 2006. **12**(2): p. 211-6.
112. Dellit, T.H., et al., *Infectious Diseases Society of America and the Society for Healthcare Epidemiology of America guidelines for developing an institutional program to enhance antimicrobial stewardship*. *Clin Infect Dis*, 2007. **44**(2): p. 159-77.
113. Epstein, A.K., et al., *Control of bacterial biofilm growth on surfaces by nanostructural mechanics and geometry*. *Nanotechnology*, 2011. **22**(49): p. 494007.
114. Flores-Mireles, A.L., et al., *EbpA vaccine antibodies block binding of Enterococcus faecalis to fibrinogen to prevent catheter-associated bladder infection in mice*. *Sci Transl Med*, 2014. **6**(254): p. 254ra127.
115. Ling, L.L., et al., *A new antibiotic kills pathogens without detectable resistance*. *Nature*, 2015.
116. Chung, K.K., et al., *Impact of engineered surface microtopography on biofilm formation of Staphylococcus aureus*. *Biointerphases*, 2007. **2**(2): p. 89-94.
117. Epstein, A.K., et al., *Biofilm attachment reduction on bioinspired, dynamic, micro-wrinkling surfaces*. *New Journal of Physics*, 2013. **15**.
118. Leslie, D.C., et al., *A bioinspired omniphobic surface coating on medical devices prevents thrombosis and biofouling*. *Nat Biotechnol*, 2014. **32**(11): p. 1134-40.
119. Wong, T.S., et al., *Bioinspired self-repairing slippery surfaces with pressure-stable omniphobicity*. *Nature*, 2011. **477**(7365): p. 443-7.
120. Yang, W.J., et al., *Polymer brush coatings for combating marine biofouling*. *Progress in Polymer Science*, 2014. **39**(5): p. 1017-1042.
121. Levering, V., et al., *Soft robotic concepts in catheter design: an on-demand fouling-release urinary catheter*. *Adv Healthc Mater*, 2014. **3**(10): p. 1588-96.
122. Pavlovsky, L., et al., *Effects of Temperature on the Morphological, Polymeric, and Mechanical Properties of Staphylococcus epidermidis Bacterial Biofilms*. *Langmuir*, 2015. **31**(6): p. 2036-2042.
123. Chen, M.J., Z. Zhang, and T.R. Bott, *Direct measurement of the adhesive strength of biofilms in pipes by micromanipulation*. *Biotechnology Techniques*, 1998. **12**(12): p. 875-880.

124. Chen, M.J., Z. Zhang, and T.R. Bott, *Effects of operating conditions on the adhesive strength of Pseudomonas fluorescens biofilms in tubes*. Colloids and Surfaces B: Biointerfaces, 2005. **43**(2): p. 61-71.
125. Garrett, T., M. Bhakoo, and Z. Zhang, *Characterisation of bacterial adhesion and removal in a flow chamber by micromanipulation measurements*. Biotechnology Letters, 2008. **30**(3): p. 427-433.
126. Phanindhar Shivapooja, Q.W., Lizzy M. Szott, Beatriz Orihuela, Daniel Rittschof, Gabriel P. López and Xuanhe Zhao, *Dynamic surface deformation of silicone elastomers for management of marine biofouling: laboratory and field studies using pneumatic actuation*. Biofouling, *In press* 2015.
127. Meyers, M. and K. Chawla, *Mechanical Behavior of Materials*, 1999. Prentice-Hall, Upper Saddle River.
128. Trautner, B.W. and R.O. Darouiche, *Role of biofilm in catheter-associated urinary tract infection*. Am J Infect Control, 2004. **32**(3): p. 177-83.
129. Bonkat, G., et al., *Microbial biofilm formation and catheter-associated bacteriuria in patients with suprapubic catheterisation*. World J Urol, 2013. **31**(3): p. 565-71.

Biography

Vrad Levering was born in Bastrop, Texas in 1975. He graduated as co-valedictorian from Bastrop High School in 1993. Vrad received his Honors Chemical Engineering B.S. from the University of Texas at Austin in 1998 where he also performed research in Dr. C. Grant Willson's lab (recipient of the National Medal of Technology and Innovation). His education at the University of Texas was paid for by the Hoechst Celanese Outstanding Sophomore in Chemical Engineering and the Ernest and Virginia Cockrell Engineering Scholarships. He was also in Tau Beta Pi and was a co-op intern at IBM. After UT, he worked as a medical device engineer at W.L. Gore. for nine years where he worked on products including vascular grafts, pacing leads, stents, delivery catheters, balloon catheters, and shunts. Vrad started the PhD Biomedical Engineering program at Duke in 2009 and received a M.S. while researching cardiovascular cell therapies with Dr. George Truskey, and joined the Lopez lab in 2012 after excitement about the research and translational opportunities. His research interests include biofilms, cell therapies, and translational medical device development. His specific research project developed novel techniques for the controlled detachment of the biofilm using active soft materials. Vrad is a Duke CBTE Fellow, Morton H. Freedman Fellowship Winner, Research Triangle Materials Research Science and Engineering Center former fellow, and member of the PhD Plus Certificate program. Vrad has traveled to 25+ countries and enjoys backpacking, kickboxing, and salsa dancing.

Publications

- Soft Robotic Concepts in Catheter Design: an On-demand Fouling-release Urinary Catheter: **Vrad Levering**, Qiming Wang, Phanindhar Shivapooja, Xuanhe Zhao, and Gabriel P. López; *Advanced Healthcare Materials*, 2014, **3**(10): p. 1588-96.

- Endothelial Colony Forming Cells (ECFCs) as a Model for Studying Effects of Low Dose Ionizing Radiation: a Cytostatic Effect of a Single Dose: Alexander V Kinev, **Vrad Levering**, Kenneth Young, Francis Ali-Osman, George A Truskey, Mark W Dewhirst, Dora Il'yasova; *Cancer Investigation*. 2013 Apr 26.

- Human Umbilical Cord Blood-derived Endothelial Cells Re-endothelialize Vein Grafts and Prevent Thrombosis: Melissa A. Brown, Lisheng Zhang, **Vrad W. Levering**, Lisa L. Satterwhite, Jiao Wui, Leigh Brian, Neil J. Freedman, and George A. Truskey; *Arterioscler Thromb Vasc Biol*, 2010. **30**(11): p. 2150-5.

- Dynamic Adhesion of Umbilical Cord Blood Endothelial Progenitor Cells Under Laminar Shear Stress: Mathew G. Angelos, Melissa A. Brown, Lisa L. Satterwhite, **Vrad W. Levering**, Natan T. Shaked, and George A. Truskey; *Biophys J*, 2010. **99**(11): p. 3545-54.

- Tailoring of a photoactive compound for non-chemically amplified 248-nm resist formulations: M. Leeson, A. Pawloski, **Vrad Levering**, W. Yueh, and C. Grant Willson; *Advances in Resist Technology and Processing*, 1998; *Proc. SPIE Vol. 3049*, p. 861-870.

Publications in Preparation

- Optimization of a design for a urinary catheter capable of repeated on-demand removal of infectious biofilms via active deformation: **Vrad Levering**, Changyong Cao, Phanindhar Shivapooja, Howard Levinson, Xuanhe Zhao, and Gabriel P. López; (In final review for submittal to *Biomaterials*)

- Human Umbilical Cord Blood-derived Endothelial Cells and Human Aortic Endothelial Cells Influence Re-endothelialization in Murine Vein Grafts: **Vrad W. Levering**, Lisheng Zhang, Leigh Brian, Neil J. Freedman, and George A. Truskey; (In preparation for submittal to *Cardiovascular Research*)

- Novel Gene Expression Patterns of Endothelial Cell Networks Reveal Targets for New Proangiogenic Therapies: Howard C. Ray, Lisa L. Satterwhite, Derek D. Cyr, **Vrad W. Levering**, Cristina E. Fernandez, Joseph E. Lucas, George A. Truskey, William M. Reichert; (In preparation for submittal to *PLoS One*)